Field and Laboratory Observations of Small-scale Dispersion in Wetlands

by

Anne F. Lightbody

B.S./M.S. Biology (1999)
Yale University

Submitted to the Department of Civil and Environmental Engineering
in Partial Fulfillment of the Requirements for the Degree of

Master of Science in Civil and Environmental Engineering

at the

Massachusetts Institute of Technology

June 2004

Signature of Author . . . . . .
Department of Civil and Environmental Engineering
May 7, 2004

Certified by . . . . . .
Professor Heidi M. Nepf
Thesis Supervisor

Accepted by . . . . . .
Professor Heidi M. Nepf
Chairman, Departmental Committee on Graduate Studies

Field and Laboratory Observations of Small-scale Dispersion in Wetlands

by

Anne F. Lightbody

Submitted to the Department of Civil and Environmental Engineering
on May 7, 2004, in Partial Fulfillment of the
Requirements for the Degree of Master of Science in
Civil and Environmental Engineering

Abstract

Estimating longitudinal dispersion in wetlands is a necessary first step in predicting the behavior of dissolved species and suspended particles. However, many processes are involved, and they can interact in nonlinear ways. Relevant processes include turbulent diffusion, which describes net solute flux created by turbulent eddies. Other dispersive processes result from the retardation of a portion of the solute relative to the rest of a cloud. This retardation can be provided by trapping in the vortex structure behind stems (hold-up dispersion), velocity deficits well downstream of stems (stem-wake dispersion), or transverse gradients in longitudinal velocity (shear dispersion).

To better understand the relative magnitude of these various dispersive processes, measurements were taken of velocity, vertical diffusion, and longitudinal dispersion in both the laboratory and the field. Laboratory flume experiments were conducted using an emergent canopy of rigid cylinders with different cylinder densities over depth. Field experiments were conducted in a natural salt marsh.

Drag due to local stem density was found to control horizontal velocity in both the lab and field studies over most of the depth. The resulting non-uniform velocity profile generated shear dispersion, which controlled dispersion at longer distances (> 250 cm) downstream of a slug release. For distances < 250 cm downstream, wake shear dispersion was found to be most important.

Thesis Supervisor: Heidi M. Nepf

Title: Associate Professor of Civil and Environmental Engineering

Acknowledgements

This work was supported by a National Defense Science and Engineering Graduate Fellowship.

This research would not have been possible without the help of Heidi Nepf, who has been a better advisor, teacher, mentor, and cheerleader than I could ever have imagined. I sincerely thank her for her willingness to take on a reformed biologist and let me learn so much about fluid mechanics.

I am indebted to my undergraduate research assistants Priyanka Sundareshan, Nan Yang, Alessandro Papa, and especially Amanda Sorenson for their help with both field and laboratory research. Marco Ghisalberti, Brian White, Yukie Tanino, and Aaron Chow were instrumental in my development of appropriate techniques in the laboratory. I am also grateful that the Plum Island Ecosystem Long Term Ecological Research program and the Ecosystems Center at the Marine Biological Laboratory allowed me the use of their field house, boat dock, and expertise.

Thanks also to my parents, whose love has always been permanent and unconditional; to my sister, Lisa, who told me to go into environmental engineering in the first place; to Elbert Lin, who helped me make the decision to do so; and to all my other friends and family who have put up with me over the last two years.

Table of Contents

List of Figures

List of Tables

Chapter 1

Introduction

1.1 The importance of wetlands

Wetlands play many important roles in a larger ecosystem (Mitsch and Gosselink, 1986). They provide habitat for a diverse range of species, ranging from dragonfly larvae to striped bass to night herons to mink. They assist in flood control, shoreline protection, and groundwater recharge. They also play a purification role, removing sediment and contaminants from polluted waters. Dissolved species, fine organic particles, and small neutrally buoyant organisms are strongly affected by fluid motion. Understanding transport processes in wetland environments is therefore crucial to understanding the behavior of nutrients, contaminants, and suspended particles moving through these systems.

Transport processes have a wide range of important impacts on wetland ecology. A variety of organisms in both fresh and salt water rely on transport by water currents for passive dispersal of larval stages (Butman, 1987; Fonseca and Hart, 1996; Peterson, 1996). Understanding patterns of benthic recruitment therefore requires determining how these organisms are transported. In addition, benthic community composition may be related to overlying water composition, including organic matter, nutrients, and pollution. Transport and mixing within that layer may also control survivorship of underlying macrofauna (Pearson et al., 1983; Finelli et al., 2002; Ramey and Snelgrove, 2003). Larger organisms, particularly in marine systems, may rely on chemical signals in the water column for information on foraging and mating (e.g., Finelli, 2000). Wetland macrophytes may also rely on water currents for seed dispersal (Middleton, 2000).

Physical processes are also central to water quality improvement in wetlands. Both constructed and natural wetlands have a well-documented ability to remove contaminants from input water (Tilley and Brown, 1998). For example, some wetlands have been shown to remove over 80% of nitrogen and over 90% of total phosphorus, total suspended solids, biochemical oxygen demand, heavy metals, and pathogens (Sundaravadivel and Vigneswaran, 2001). Constructed treatment wetlands, which exploit wetlands' natural purification ability, are increasingly used for water quality improvement. There are numerous types of constructed wetlands, with surface flow systems the most analogous to natural open water wetlands (Kadlec and Knight, 1996).

Contaminants that enter a wetland, either natural or constructed, are removed through a combination of chemical, biological, and physical mechanisms, which act to consume, break down, bury, or volatize contaminants. Many of the most important mechanisms are chemical and biological. For example, *Nitrosomonas* and *Nitrobacter* bacteria catalyze the biological oxidation of ammonium to nitrate, and facultative microorganisms such as *Pseudomonas* and *Vibrio* catalyze the denitrification of nitrate to nitrogen gas (Sundaravadivel and Vigneswaran, 2001).

Sedimentation is one of the most important physical removal processes in a wetland. Suspended sediments can clog pipes and interfere with water clarity so are themselves a form of pollution. In addition, many pollutants adsorb readily to suspended particles in a waste stream. For some contaminants, such as phosphorus, sedimentation is the most important removal mechanism (Braskerud, 2002). When the particles settle out of the waste stream, which they tend to do in the low velocities present in a wetland, the pollutants bound to them also settle out. Gleason et al. (1979) planted natural *Spartina alterniflora* stems in densities of 27, 54, and 108 stems/m^2 on a sloping sand beach subject to mechanically generated waves. The greatest deposition and least erosion were observed for the highest plant density, suggesting that the vegetation dissipates wave energy and supports sediment deposition. Hosokawa and Horie (1992) observed sediment settling in a bed of emergent vegetation mimics (5-mm-diameter acrylic pipe) of unknown density in a 24-m by 0.8-m flume. Sediment was observed to settle

more quickly in the presence of vegetation. In addition, they performed a field investigation in a natural reed field using pumped water at constant head and marsh silt and found that again the presence of vegetation enhances settling (Hosokawa and Horie, 1992). Shi et al. (2000) reported that suspended sediment concentrations are lower inside a salt marsh canopy, suggesting that sediments settle out in response to passing through the canopy. Yang (1998) found that marsh vegetation, in addition to increasing overall accretion, can even increase the deposition of fine silts and clays, which settle more slowly and are therefore more difficult to remove from the water column. By reducing near-bottom shear stresses, wetland vegetation can also prevent sediment resuspension (Christiansen et al., 2000; Vermaat et al., 2000), further contributing to net deposition of sediments.

1.2 Residence times and residence time distributions

The longer water remains in the wetland, the more time it interacts with the wetland and its myriad chemical, biological, and physical processes. The residence time of a wetland, τ, is defined as the average length of time that a parcel of water spends in the wetland, and it is usually strongly correlated with the ability of the wetland to remove contaminants. For example, Tilley and Brown (1998) reported that a constructed wetland removed 8% of total phosphorus with a residence time of 3.3 hours but removed 82% with a residence time of 20 hours.

The residence time distribution (RTD) is the probability density function for residence times; it describes the amount of time various fractions of water spend in the wetland. If the wetland is at steady state, the RTD is both the distribution of times that fluid entering the wetland will stay in the system and the distribution of times that fluid leaving the wetland has spent in it (Werner and Kadlec, 1996). The RTD is typically on a continuum between two extremes. A continuously stirred reactor is produced if mixing in the wetland is complete and instantaneous, which implies that longitudinal dispersion is much more important than advection (Figure 1-1). At the other extreme, absolutely no longitudinal mixing but complete lateral and vertical mixing produces plug flow, in which advection dominates and dispersion is negligible. Theoretically, in a wetland with volume V and flow rate Q, both a continuously stirred reactor and plug flow

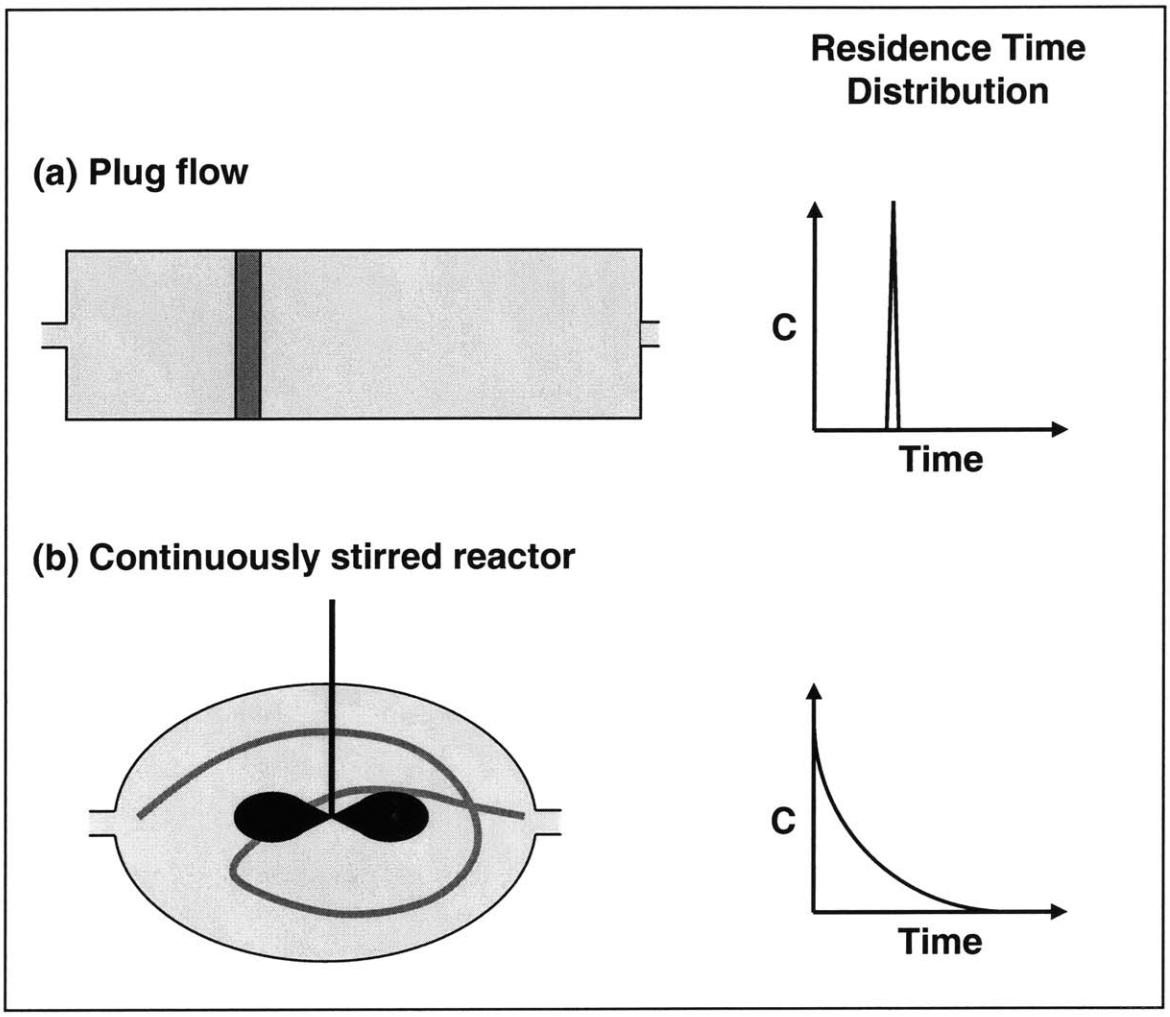

Figure 1-1. Cartoons of simple reactor models. The graphs on the right show the associated residence time distributions, which would result when a slug of tracer was introduced into the volume. The plots show the concentration of tracer remaining in the volume as a function of time. (a) Plug flow is created when longitudinal mixing is much less important than advection, so that fluid moves through the system in discrete slabs. The associated residence time distribution is a spike, with all fluid exiting at exactly its residence time. (b) Fluid in a stirred reactor is assumed to be instantaneously mixed throughout the volume of the wetland or other container. This situation is created when advection is much less important than longitudinal mixing. The associated residence time distribution is an exponential decay, with most parcels exiting soon after entering but some persisting for a much longer time.

should produce a mean residence time, $\tau = V/Q$, although excluded zones in the flow typically make the measured mean residence time less than V/Q.

When removal processes are non-linear, removal is maximized for plug flow behavior (Werner and Kadlec, 1996; Persson et al., 1999). In general, wetlands that are long and thin promote plug flow behavior. If the length to width ratio is less than ideal, which has been suggested to be 4:1, good hydraulic efficiency can be promoted by bathymetric features that act to elongate the effective flow path and distribute the inflow across the width of the pond, such as baffles, small islands, berms, and aquatic benches (Persson et al., 1999). Islands and baffles both reduce the volume of the wetland, but by altering flow paths and increasing the effective wetland volume, their enhancement of plug flow conditions may overcome this inherent reduction in nominal residence time (Koskiaho, 2003).

True plug flow does not exist in either natural or constructed wetlands (Werner and Kadlec, 1996; Persson et al., 1999). Perfect plug flow is never obtained because some dispersion is always present. Mixing can result from turbulence generated by wind waves, biological organisms, flow around submerged stems or clumps of vegetation, or bottom shear (Werner and Kadlec, 1996; Kadlec, 2000). Wind can create recirculation by driving surface waters to one side of the wetland, setting up pressure-driven return currents near the bed, although dense plant canopies can block much of the wind and eliminate surface wind stress (Werner and Kadlec, 1996; Kadlec, 1990). Deeper and less vegetated channels can move some water faster than other (Kadlec and Knight, 1996). Dead zone dispersion can result if water is entrained in litter or dense vegetation (Werner and Kadlec, 1996). However, mixing rates are rarely high enough to generate continuously stirred behavior. Intermediate residence time distributions therefore result (Persson et al., 1999), and dispersive processes are important.

Understanding and predicting these dispersive processes are vital to understanding and predicting the transport of all dissolved and suspended species through the wetland. This project focuses on transport, in particular dispersion, within the vegetated canopy of a free surface wetland.

1.3 Dispersion at different length scales

Consider a cloud of scalars that are simultaneously introduced into a wetland (i.e., a slug release). The dispersion constant, K [units of L^2/T], is a measure of the rate of spatial growth of the cloud per unit time. If the particles move at different velocities, they will become spread out longitudinally over time, and the cloud will grow. Dispersion is thus intimately related to the presence of different velocities in different parts of the flow, which can affect different particles in different ways.

Previous field studies in wetlands have estimated K from experiments done at a variety of scales. Saiers et al. (2003) measured dispersion in a wetland in the Florida Everglades by releasing small particles into the vegetation and measuring their concentration 6.8 m downstream. The best-fit estimate of longitudinal dispersion was determined to be $K = 0.42$ cm^2/s. In a separate experiment, Chendorain et al. (1998) calculated that $K = 14.0$ cm^2/s over the length of a 70-m long continuously vegetated constructed wetland. In a third experiment, Kadlec (1994) injected a dye tracer at the inlet of a 2-ha wetland that was 175 m long. Measurements of the tracer at the outlet led to the estimation that $K = 169$ cm^2/s over the whole wetland.

The largest and smallest of these estimates of K differ by a factor of 400. The difference is undoubtedly partial due to the slightly different shape, vegetation, and depth of each wetland. The largest difference between the studies, however, is the issue of scale. A simple scaling argument holds that:

$$K \sim \sigma_u \, l \tag{1-1}$$

where σ_u [L/T] is the spatial variability in velocity and l is the length scale over which it varies. This equation makes intuitive sense. Increasing the difference in velocity between two particles will cause them to become more spread out. Similarly, increasing the distance between regions of different velocities will decrease the ability of particles to move between these regions, so

differences in velocity can be maintained over a longer period of time and particles can become more separated.

Figure 1-2 shows a plan view of an idealized wetland, which consists of patches of average width A of different types of vegetation (e.g., Kadlec, 1994). If all the stems within each stand of vegetation are identical and velocity does not change over depth, then within each patch the stems themselves, of diameter d, will set the scale over which velocity can change. A cloud of particles much smaller than A will be located within only one of the vegetation patches. Dispersion of that cloud will be influenced only by stem-scale velocity gradients, so $K_{small} \sim \sigma_u d$.

Once the cloud grows to a size much greater than A, it will stretch over several different vegetation patches. The velocity experienced by the particles will therefore change over a length scale of A, so $K_{large} \sim \sigma_u A$. Since $A >> d$, assuming σ_u is constant (the same range of velocities is present) implies that $K_{large} >> K_{small}$. (A cloud much larger than A will actually experience both K_{large} and K_{small}. K_{large} will overwhelm the contribution of K_{small}, however, and will control the overall observed dispersion.) Because the cloud has grown in size, the dispersion controlling its behavior has also increased.

The increase can be augmented if the additional heterogeneity in regions increases the size of σ_u by introducing a wider ranger of velocities into the flow. Most wetlands contain some channels of open water. When the cloud has spread over the entire wetland, it will be affected by flow through and around clumps of vegetation (Kadlec, 1994). The presence of fast-moving currents and nearly stationary (or even backward) flow in dense wrack (dead stems and leaves caught in the live canopy) will add even more heterogeneity to the system.

Thus, scale analysis predicts that, as the length scale of interest continues to increase, the magnitude of the dispersion it experiences will also increase. This effect explains why, for the example data presented above, the dispersion constant measured in a whole wetland is so much larger than the constant measured over several meters of homogeneous grasses.

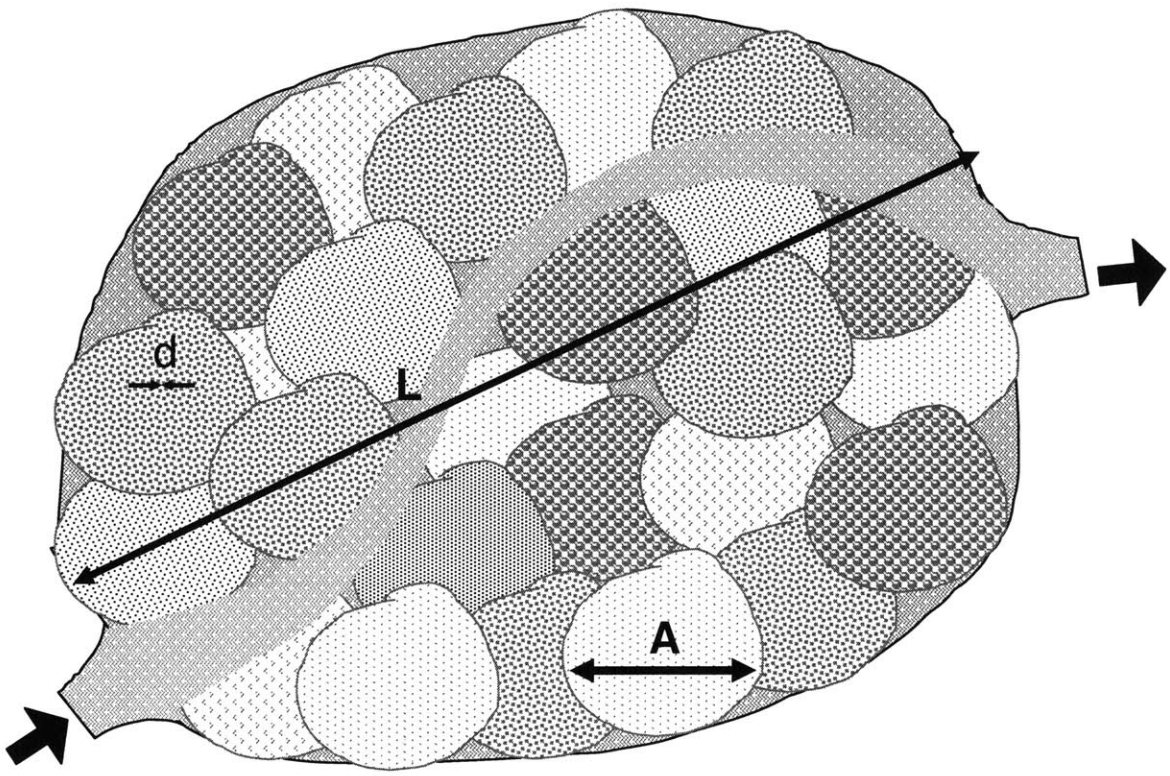

Figure 1-2. Idealized plan view of a wetland. Spatial heterogeneity exists on at least three scales: the diameter of the individual plant stems (*d*), the width of each patch of homogeneous vegetation (*A*), and the length of the whole wetland (*L*).

Dispersion increases also with length scale in the vertical. Figure 1-3 shows a longitudinal velocity profile that varies over depth, which may be found in a wetland (e.g., Gambi et al., 1990; Leonard and Luther, 1995; Shi et al., 1995; Shi et al., 1996; Nepf and Vivoni, 2000; Vermaat et al., 2000). A scalar cloud that does not extend very far over depth will not experience very large velocity deviations from the mean. A cloud that is well mixed over depth will experience both larger deviations from the mean (greater σ_u) over a larger length scale (larger l), so it will exhibit much larger dispersion. Again, a larger length scale leads to larger dispersion.

Currently, the mechanics of dispersion at the scale of the stem are fairly well understood (White and Nepf, 2003). Dispersion at the scale of the wetland has also been measured in numerous empirical studies (cf. Kadlec and Knight, 1996). Less is known about the processes underlying dispersion at intermediate length scales and the magnitude of the resulting dispersion constants. In this realm, it is expected that velocity variations over depth will play a role in observed longitudinal dispersion. This paper explores the effect of these velocity variations on dispersion in a salt marsh on a length scale between 50 cm and 5 m.

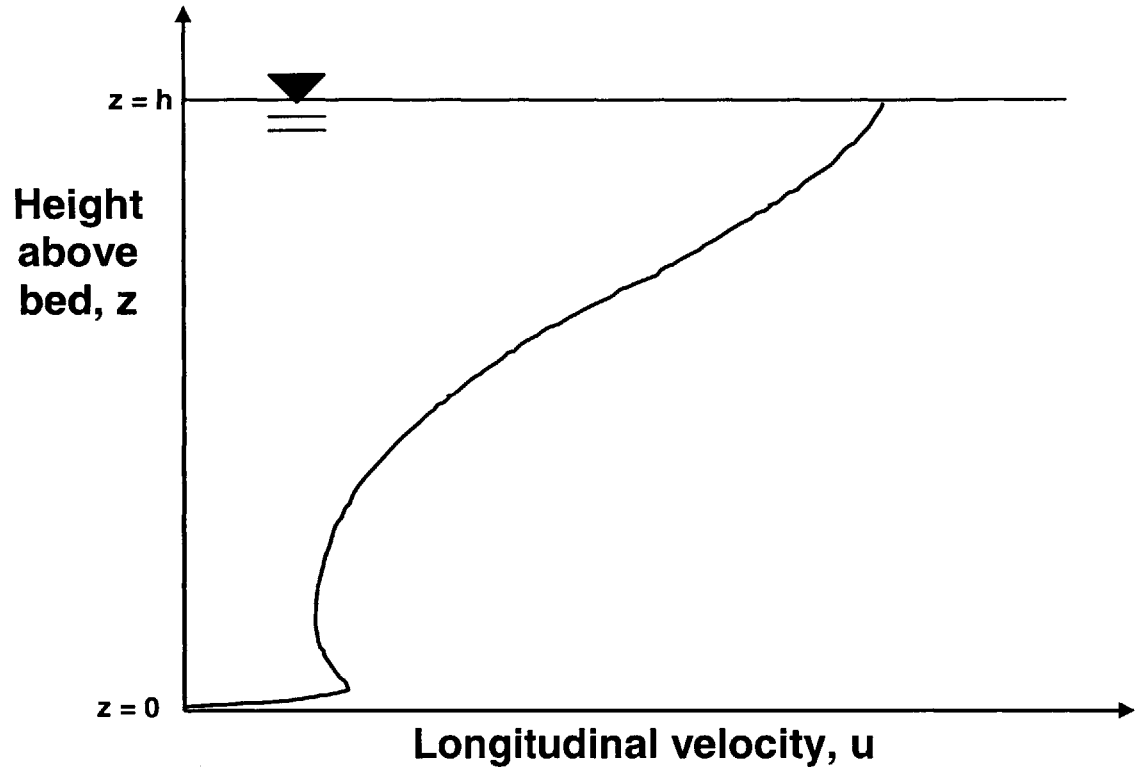

Figure 1-3. Example of a velocity profile with vertical variation. Longitudinal velocity will typically change over depth. This type of profile could be created as a result of drag due to vegetation, if stems are thicker and more numerous near the bottom. The jet near the bottom could be created if leaves emerge from the stem at some distance above the bottom.

Chapter 2

Theory

Freshwater and saltwater surface flow wetlands are physically similar in that they consist of shallow water moving through a canopy of vegetation. In many situations, the canopy is emergent: the vegetation is longer than the water is deep, so it extends above the water surface. Many marsh grasses, including *S. alterniflora* and *Juncus roemerianus* (needle rush), are roughly cylindrical, and their bending is minimal in low velocity flow. Although *S. alterniflora* propagates vegetatively and therefore tends to grow in clumps, when averaged over a scale much larger than that of the individual stem, the stems can be considered to be random. There is precedent for modeling marsh grass such as these species as randomly distributed, emergent, rigid, vertical circular cylinders (Lopez and Garcia, 2001; Nepf, 1999; White and Nepf, 2003). Such an approximation greatly simplifies the theoretical analysis. However, it makes many assumptions. One of the largest assumptions is that stem diameter is constant and that stem frontal area is uniform over depth. It is known, however, that frontal area may change dramatically over the plant height (Leonard and Luther, 1995). This paper explores how this assumption may be relaxed.

2.1 A simple model for transport through homogeneous emergent vegetation

For now, consider a model plant canopy in which emergent circular cylinders of equal and constant diameter, d, are distributed randomly with some uniform stem density, n [L^{-2}], over a planar bed (Figure 2-1). For continuous stands of *S. alterniflora*, stem density is in the range of 150 to 1100 stems per square meter (Valiela et al., 1978; Leonard and Luther, 1995;

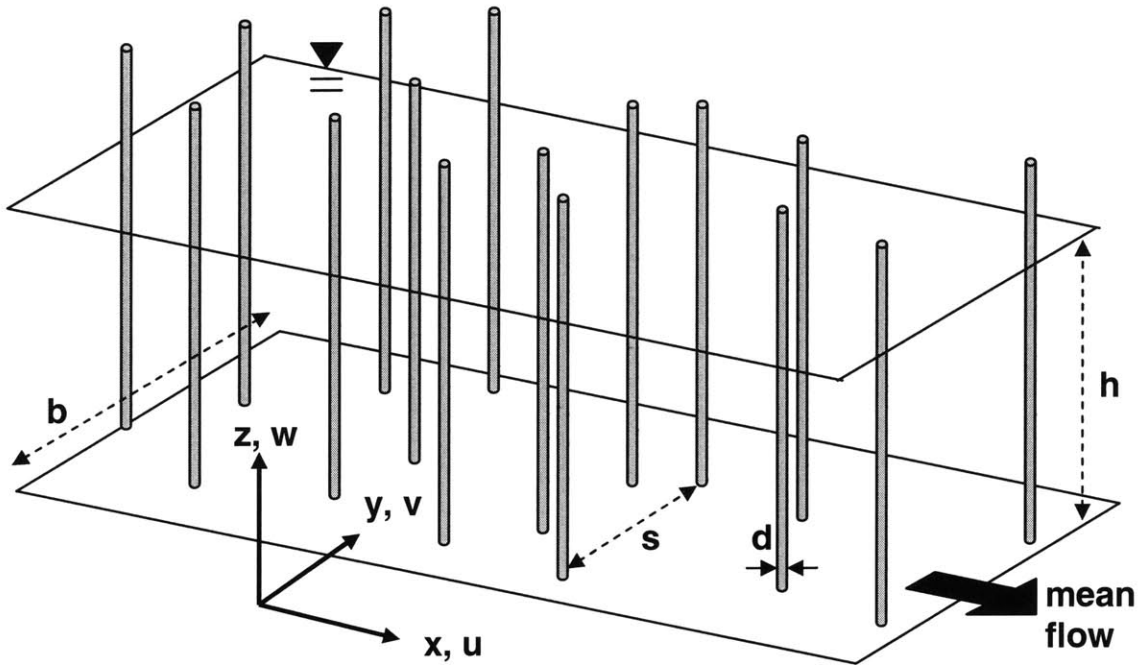

Figure 2-1. Definition sketch for the model canopy. Emergent circular cylinders are placed randomly on a plane bed with average spacing s. The axes are oriented so that the x-direction is in the direction of mean surface slope, which is the direction of mean flow. The canopy may or may not have a finite width, b.

Christiansen et al., 2000; Shi et al., 2000). The frontal area of the stems per unit area of bed is *nhd*, where *h* is the water depth. The stem frontal area per unit flow volume, *a* [L^{-1}], can be denoted by:

$$a = \frac{stem\ frontal\ area}{flow\ volume} = nd \tag{2-1}$$

This variable is a measure of the vegetation density. The volume of cylinders per unit area bed is given by $\alpha\frac{\pi}{4}ad$, where α is a constant that reflects the geometry of the plant distribution. For a random distribution of stems, Serra et al. (2004) determined that $\alpha \approx 3.4$. Since it differs by an 0(1) constant, for order of magnitude analysis *ad* will be used here to represent the vegetation density. The effective porosity of the canopy is then equal to 1 – *ad*. The mean center-to-center spacing between cylinders, *s*, is related to the average number of stems per unit bed area. For a random array,

$$s = \sqrt{\frac{1}{n}} = \sqrt{\frac{d}{a}} = \sqrt{\frac{d}{a}} \tag{2-2}$$

2.2 Governing equations

The water flowing through a canopy of vegetation can be described by the governing equations for incompressible viscous fluid flows. Consider a parcel of water, which is a collection of many molecules yet few enough so that its constituent molecules behave as a unit. Each parcel of water in the flow follows the equations of motion and the continuity equation:

$$\rho\frac{Du_i}{Dt} + \rho F_{c,i} = -\frac{\partial P}{\partial x_i} + \rho g_i + \frac{\partial \tau_{ji}}{\partial x_j} \tag{2-3}$$

$$\frac{\partial u_i}{\partial x_i} = 0 \tag{2-4}$$

where $i = 1, 2, 3$ and $j = 1, 2, 3$ refer to the x, y, and z directions, respectively; u is the fluid velocity; ρ is the fluid density; P is the fluid pressure, $F_{c,i}$ is the Coriolis acceleration in the i direction, and τ_{ji} is the shear stress in the i direction on the j face. Since water is a Newtonian fluid, $\tau_{ji} = \mu\left(\frac{\partial u_i}{\partial x_j} + \frac{\partial u_j}{\partial x_i}\right)$, where μ is the viscosity of water.

Many environmental flows are turbulent. The flow is characterized by complex, three-dimensional fluid motions that are difficult to predict. Unlike laminar flow, parcel motions are unsteady, and the velocity is not constant. The flow contains an appreciable amount of vorticity. Vortex structures called eddies exist in a large range of sizes, from as large as the flow boundaries themselves to so small that they are dissipated by viscosity. The effect of these eddies is to create apparently random fluctuations on a wide range of scales in the velocity and pressure records. Although the governing equations still describe the flow, they become extremely unwieldy and ultimately intractable due to the complicated nature of the turbulent fluctuations.

The solution is to apply a process known as Reynolds decomposition, in which the velocity and pressure variables, such as the longitudinal velocity $u(t)$, are expressed as the sum of a temporal average, $\overline{u}$, and the fluctuations from the average, $u'(t)$ (e.g., Lopez and Garcia, 2001). The averaging process occurs over a time period longer than the timescale of the fluctuations but still shorter than the timescale for change in the system mean, such as diurnal or tidal variation. The equations of motion are then Reynolds-averaged by substituting in the Reynolds decompositions and averaging over that same time period. This process removes turbulent fluctuations but generates additional cross-correlation terms, called Reynolds stresses, in the governing equations.

The presence of stems throughout the flow creates spatial heterogeneity in the velocity field. Again, the Reynolds-averaged equations of motion describe the flow exactly, but in general it is unnecessary to resolve the flow at this length scale. Therefore, the equations are

also averaged spatially over a horizontal scale much larger than that of the individual stems. This process removes the effect on the velocity field of individual stem wakes. In the averaged equations, the effect of the individual stems appears in the generation of a drag force per unit volume, F_d, which results from the net effect of these obstacles in the flow. After these averages are taken and assuming that the volume fraction of the stems is small ($ad << 1$), the equations of motion become:

$$\rho\frac{Du_i}{Dt}+\rho F_{c,i}=-\frac{\partial P}{\partial x_i}+\rho g_i+\frac{\partial}{\partial x_j}\left[\mu\left(\frac{\partial u_i}{\partial u_j}+\frac{\partial u_j}{\partial u_i}\right)-\rho\overline{u_i'u_j'}\right]-F_{d,i} \tag{2-5}$$

where all variables represent temporally and spatially averaged quantities, u is the average velocity in the fluid only (the pore velocity), and u_i' and u_j' represent deviations from the average velocity.

In a natural system the water depth, h, is much smaller than the canopy width, B, and length, L, so the mean vertical velocity component may be assumed small compared with the horizontal components and the vertical stress variations may be assumed large compared with the horizontal components. The vertical momentum equation (z-direction) then reduces to a statement of hydrostatic pressure:

$$P=\rho g(\eta-z) \tag{2-6}$$

where η is the local free surface elevation above a datum (Figure 2-2). Further, with $w \approx 0$ and $\partial/\partial z \approx 0$, the equation for flow in the longitudinal direction (parallel to the surface slope) reduces to:

$$\rho\left(\frac{\partial u}{\partial t}+v\frac{\partial u}{\partial y}\right)+\rho F_{c,x}=-\rho g\frac{\partial \eta}{\partial x}+\frac{\partial}{\partial y}\left(\mu\frac{\partial u}{\partial y}-\rho\overline{u'v'}\right)+\frac{\partial}{\partial z}\left(\mu\frac{\partial u}{\partial z}-\rho\overline{u'w'}\right)-F_d \tag{2-7}$$

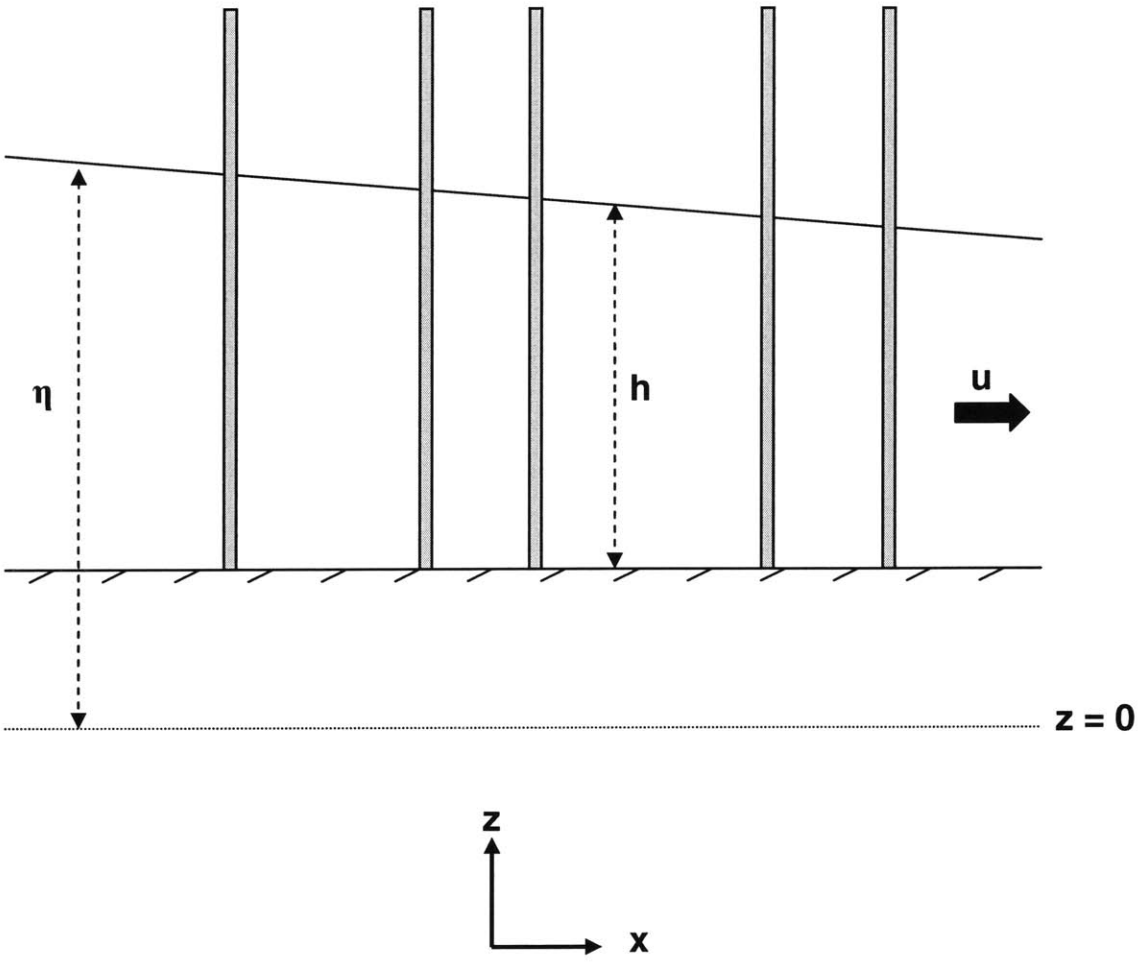

Figure 2-2. Side view of the model canopy. The surface elevation is measured in reference to a fixed datum at $z = 0$. The x-axis is oriented in the direction of mean surface slope, $\partial\eta / \partial x$, so mean flow is in the x direction. The illustration is not to scale, and the magnitude of the surface slope is increased over what would be expected in flow through a canopy of widely spaced cylinders. In such a canopy, the water depth, h, is approximately constant over short horizontal distances.

Under conditions typical for a salt marsh, or for a freshwater wetland if the timescale for wind setup is much less than that for changes in wind speed, the local acceleration and Coriolis terms are generally negligible (Burke and Stolzenbach, 1983). In these situations, the equation for flow in the longitudinal direction reduces to a balance between the pressure force, shear stresses, and drag force. Introducing the kinematic viscosity, $\upsilon = \frac{\mu}{\rho}$, and dropping the Coriolis and convective acceleration terms,

$$\frac{\partial u}{\partial t} + \frac{\partial}{\partial z}\left(\upsilon \frac{\partial u}{\partial z} - \overline{u'w'}\right) + \frac{\partial}{\partial y}\left(\upsilon \frac{\partial u}{\partial y} - \overline{u'v'}\right) = -g\frac{\partial \eta}{\partial x} + \frac{1}{\rho}F_d \tag{2-8}$$

To solve this equation, the Reynolds stresses $\overline{u'w'}$ and $\overline{u'v'}$ must be related to mean flow quantities, a process known as turbulence closure. The eddy viscosity model is one of the most common methods of turbulence closure. This model asserts that turbulent eddies behave like diffusive agents, transporting momentum from high to low velocity regions. When the eddies are much smaller than the velocity gradient, their action can be parameterized by an effective turbulent viscosity, υ_t, which is analogous to the molecular viscosity. The x-direction momentum equation can then be written:

$$\frac{\partial u}{\partial t} + g\frac{\partial \eta}{\partial x} + \frac{\partial}{\partial z}\left((\upsilon + \upsilon_t)\frac{\partial u}{\partial z}\right) + \frac{\partial}{\partial y}\left((\upsilon + \upsilon_t)\frac{\partial u}{\partial y}\right) = \frac{1}{\rho}F_d \tag{2-9}$$

The turbulent viscosity constants change throughout the flow field, depending on eddy size and strength. Typical values are $\upsilon_t >> 1$ cm^2/s. The molecular viscosity $\upsilon \sim 10^{-2}$ cm^2/s. Therefore, in almost all situations where turbulence is present, $\upsilon_t >> \upsilon$, turbulent shear stresses dominate viscous stresses, and molecular viscosity may be neglected.

Note that, if the flow is steady, then the time-dependent terms drop out. If it is further assumed that the turbulent and molecular stress terms are small compared to the vegetative drag, then the nonlinear viscous terms are also negligible. In a homogeneous canopy, vegetative drag

dominates the flow except within one stem diameter of the bed (Nepf et al., 1997b), and this equation reduces to a balance between pressure and drag forcing:

$$\rho g \frac{\partial \eta}{\partial x} = F_d \tag{2-10}$$

2.3 Reynolds number

Fluid flows have different characteristics depending on which terms dominate in the equation of motion. Flow conditions can be described by the Reynolds number, a non-dimensional variable that is the ratio of the inertial and the viscous forces in the flow. The x-direction momentum equation can be non-dimensionalized as follows. Let the velocity scale on a characteristic horizontal velocity, U, such that a non-dimensional velocity u^* can be written $u^* = u/U$. Let L denote a length scale over which this velocity changes, so the non-dimensional position $x^* = x/L$. The steady-state one-dimensional momentum equation can then be rewritten in terms of the dimensionless variables u^* and x^*. The inertial terms, such as $\rho u \frac{\partial u}{\partial x}$, can all be written $\frac{\rho U^2}{L} \frac{\partial u^{*2}}{\partial x^*}$. The viscous terms, such as $\frac{\partial}{\partial x}\left(\mu \frac{\partial u}{\partial x}\right)$, can all be written $\frac{\mu U}{L^2} \frac{\partial u^*}{\partial x^{*2}}$. The ratio of these two groups of scaled terms is called the Reynolds number (Re) and can be written:

$$\mathrm{Re} = \frac{inertial\ forces}{viscous\ forces} = \frac{\mu UL}{\rho} = \frac{UL}{\nu} \tag{2-11}$$

The Reynolds number determines many flow characteristics. The Reynolds number based on the entire flow depth, for which the representative length scale $L = h$, determines whether large-scale turbulence will be present in the flow:

$$\mathrm{Re}_h = \frac{Uh}{\nu} \tag{2-12}$$

where the subscript denotes that the Reynolds number is based on water depth. For $Re_h < 2000$, the flow is usually laminar. For $Re_h > 4000$, the flow is fully turbulent. Intermediate Reynolds number values suggest transitional flows. Flows within natural emergent canopies can vary over several orders of magnitude, from meters per day in some freshwater systems to over 10 cm/s during peak tidal flows in a saltwater marsh (Leonard and Luther, 1995; Leonard and Reed, 2002). Water depths in typical systems range from several centimeters to over a meter. The Reynolds number based on depth can therefore range from O(1) to O(100,000), so either laminar or turbulent conditions may exist in natural vegetation.

The length scale over which the velocity changes near each stem is the stem diameter. The relevant measure of the local flow conditions is:

$$\mathrm{Re}_d = \frac{Ud}{\nu} \tag{2-13}$$

where the subscript denotes that the Reynolds number is based on stem diameter. The characteristics of flow around a circular cylinder change dramatically as Re_d increases. At low Reynolds numbers, $Re_d << 1$, the viscous terms dominate and the streamlines around the cylinder are symmetric. This condition is known as Stokes flow. For an isolated cylinder, as the Reynolds number increases to about 10, a recirculating wake or vortex forms behind the cylinder. Above $Re_d \approx 35$, unsteadiness is present in the wake, and convective currents begin to play a role. Above $55 < Re_d < 70$, vortices are regularly shed into the flow (Gerrard, 1978). Observations have indicated that Re_d ranges from O(1) to O(1000) in coastal and freshwater systems (Leonard and Luther, 1995), so vortex shedding may be present.

2.4 Vegetation drag

The primary hydrodynamic effect of the vegetation is to create drag in the flow (equation 2-10; Hosokawa and Horie, 1992). Turbulent kinetic energy decays exponentially with increasing distance into a stand of marsh vegetation, with increased dissipation occurring in denser canopies (Leonard and Luther, 1995; Nepf, 1999). There are several possible

formulations for this drag force. The Manning equation is the traditional approach to describing flow in open channels. The formula is based on the assumption of incompressible, turbulent, steady flow at constant depth in a prismatic open channel in which flow is controlled by a balance between gravity and drag. The equation includes a roughness coefficient that reflects the roughness of the channel bottom and side walls. This coefficient has been tabulated for many surfaces (e.g., Streeter et al., 1998, p. 285) and has been used to describe flow through emergent vegetation (Petryk and Bosmajian, 1975; Hosokawa and Horie, 1992). Alternatively, a Darcy-Weisbach friction factor can be used to describe flows in streams in which the flow is controlled by gravity. This formulation has also been applied to shallow vegetated flows (e.g., Darby, 1999). These hydraulic models best describe situations in which vegetation is not emergent and so can be captured as a form of bed friction or hydraulic roughness. In addition, they rely on fully developed turbulence, a condition that is often not met in wetlands (Kadlec, 1990). Although they can be applied in wetland situations, they fail to retain physical significance and must be carefully calibrated for each implementation.

An alternative method of specifying drag is to introduce a non-dimensional drag coefficient, C_d. This coefficient is defined such that the drag force per unit length on an isolated infinitely long cylinder is:

$$F_{d,ind} = \tfrac{1}{2} C_d \rho U^2 A \tag{2-14}$$

where A is the frontal area per unit length of this one stem and U is the depth-averaged free-stream flow velocity. For rigid vegetation, the drag coefficient, but not A, changes based on the flow conditions. The drag coefficient on an isolated cylinder is well known (e.g., Streeter et al., 1998, p. 334). For Stokes flow ($Re_d < 1$), $C_d = 24/Re_d$. For $1 < Re_d < 1000$, the drag coefficient on a single cylinder is O(1) and can be approximated by (White, 1991):

$$C_d = 1 + 10 Re_d^{-0.66} \tag{2-15}$$

When multiple cylinders are present, the simplest form of the drag force would simply be to multiply the drag force on an individual cylinder by the number of cylinders present:

$$F_{d,tot} = \tfrac{1}{2} C_d \rho n U^2 A \qquad (2\text{-}16)$$

However, the response of the drag force is actually more complicated. At high stem densities the cylinders will significantly reduce the flow area, and the effective porosity of the canopy must be included in the formulation of the drag force (Jadhav and Buchberger, 1995). In addition, the velocity vortex shedding may be suppressed at downstream cylinders, due both to a reduction in the local free-stream velocity impinging on the downstream cylinder and to a delay in the point of separation on the downstream cylinder (Nepf, 1999). These sheltering effects reduce the C_d for each cylinder in an array from that observed for an isolated cylinder. Nepf (1999) performed numerical simulations and experimental trials to explore the variation in C_d with ad in a random array of circular cylinders over the range $200 < Re_d < 10{,}000$ and determined that $C_d \approx 1.0$ and is approximately constant for $ad < 0.1$. Numerical simulations have also shown that, for $Re_d << 1$, C_d is only a weak function of ad (Koch and Ladd, 1997). In their study of flow through submerged vegetation, Gambi et al. (1990) found that differences in velocity profiles between different stem densities (n = 400-1200 m^{-2}; $ad \approx 0.01$-0.2) in a *Zostera marina* (eel grass) canopy only became evident at high flow velocities. Fischer-Antze et al. (2001) were able to successfully model a moderate Reynolds number flow over a bed of submerged circular cylinders at $Re_d = 50 - 300$ using a C_d model with a constant $C_d = 1.0$, so there is precedent for modeling flow through a bed of cylinders using a simple drag law. In this analysis, equation 2-15 will be used for $F_{d,tot}$ with C_d given by equation 2-14.

Although it is currently assumed that the bed consists of identical cylinders, it is possible that not all stems will have the same diameter. Their diameters are likely to be distributed around a mean value, which could be considered a representative diameter for the entire population (White, 2002). Re_d values will then also be distributed around a mean value. Note that drag around cylindrical objects depends only on the projection of the frontal area, A and is not directly dependent on the diameter. As long as the change in diameter is not so dramatic that

differences in Re_d affect C_d, the mean diameter will accurately characterize the total drag as long as the stems are cylindrical and do not interact with each other.

Under steady, uniform, two-dimensional conditions, when it is assumed that the stress term is small compared to vegetative drag, the momentum equation reduces to a balance between the pressure and drag forces (equation 2-10). The total drag force present in the flow is the sum of the bed drag and the vegetation drag. For a relatively smooth bottom, bed drag is much smaller than vegetation drag (Zavistoski, 1994). Bed drag will therefore be neglected here, and the pressure forcing due to the stems will be assumed to balance the vegetation drag:

$$\rho g \frac{\partial \eta}{\partial x} = \frac{1}{2} \rho C_d A U^2 \tag{2-17}$$

Note that this equation describes depth-averaged pressure forces and flow. However, in a real canopy velocity may not be constant over depth.

2.5 Transport equation

Modeling wetland mixing processes is most important in describing the motion of species dissolved or suspended in the water. In wetland environments, all such species are governed by conservation of mass. The differential form of the conservation of mass equation for an incompressible flow is known as the transport equation:

$$\frac{\partial C}{\partial t} + u \frac{\partial C}{\partial z} + v \frac{\partial C}{\partial y} + w \frac{\partial C}{\partial z} = \frac{\partial}{\partial x}\left(D_{m,x} \frac{\partial C}{\partial x} \right) + \frac{\partial}{\partial y}\left(D_{m,y} \frac{\partial C}{\partial y} \right) + \frac{\partial}{\partial z}\left(D_{m,z} \frac{\partial C}{\partial z} \right) \pm S \tag{2-18}$$

where S indicates sources and sinks and $D_{m,x}$, $D_{m,y}$, and $D_{m,z}$ are the molecular diffusion coefficients in the x, y, and z directions, respectively. In general, molecular diffusion is both homogeneous (spatially constant) and isotropic (equivalent in all three directions), so $D_{m,x} = D_{m,y} = D_{m,z} = D_m$ = constant.

Like the equations of motion, the transport equation can be Reynolds-averaged and then averaged over a spatial scale larger than that of the stem spacing (cf. Section 2-2). The resulting equation describes the motion of assemblages of many scalar particles and contains cross-correlation terms. If the turbulence is homogeneous, then these fluxes can be described by a Fickian diffusion coefficient, which relates the mass rate of flux of a solute to the gradient of the solute concentration (see Section 2.6.1). The result is the three-dimensional averaged transport equation:

$$\frac{\partial C}{\partial t} + u\frac{\partial C}{\partial x} + v\frac{\partial C}{\partial y} + w\frac{\partial C}{\partial z} = (D_m + D_x)\frac{\partial^2 C}{\partial x^2} + (D_m + D_y)\frac{\partial^2 C}{\partial y^2} + (D_m + D_z)\frac{\partial^2 C}{\partial z^2} \pm S \quad (2\text{-}19)$$

where D_x, D_y, and D_z are diffusion coefficients (due to turbulence or mechanical diffusion) and all values are temporally and spatially averaged. The above assumes that turbulent diffusion is spatially homogeneous. In a canopy dominated by drag due to stems, horizontal turbulence is likely to be homogeneous. Vertical turbulence may be lower than horizontal turbulence, however, especially if the stems shed vortices (Nepf et al., 1997b; Leonard and Reed, 2002). This effect will be ignored here.

Wetlands are almost invariably much wider than they are deep, so average vertical motion can be assumed small relative to horizontal motion. In addition, if a coordinate system is chosen so that x is oriented in the direction of mean surface slope and all flow is in response to the pressure gradient, then average lateral motion will be negligible compared to longitudinal. To simplify the analysis, the three-dimensional transport equation can be integrated laterally and vertically to remove details of motion in these directions. This averaging process creates cross-correlation terms. Noting that the canopy is assumed to be homogeneous and that this formulation was already averaged over stem-scale heterogeneity, the velocity fluctuations are homogeneous [$u' \neq f(x)$]. The cross-correlation terms can then be modeled by a new process, longitudinal dispersion. Substituting in a total longitudinal dispersion constant, K_x, representing

all processes contributing to longitudinal dispersion (including diffusion), and assuming that the species of interest is conservative, the one-dimensional transport equation becomes:

$$\frac{\partial C}{\partial t} + u\frac{\partial C}{\partial x} = K_x \frac{\partial^2 C}{\partial x^2} \tag{2-20}$$

This equation can be non-dimensionalized to compare the relative importance of terms. Over the wetland length, L, longitudinal distance can be written in terms of a non-dimensional length x^*, which scales as x/L. Similarly, a non-dimensional concentration can be written as $C^* = C/C_{max}$, where C_{max} is the maximum observed concentration. A non-dimensional time can be written as $t^* = t/\tau$, where τ is a timescale that describes flow around the stems. The steady-state one-dimensional transport equation can then be rewritten in terms of the dimensionless variables x^*, C^*, and t^*:

$$\frac{L^2}{K_x \tau}\frac{\partial C^*}{\partial t^*} + \frac{uL}{K_x}\frac{\partial C^*}{\partial x^*} = \frac{\partial^2 C^*}{\partial x^{*2}} \tag{2-21}$$

The ratio of advection to dispersion in this system, uL/K_x, is known as the Peclet number, Pe. When $Pe >> 1$, the advection term is much more important than the dispersion term, and fluid travels through the system much more rapidly than it mixes. In the limit as Pe $\rightarrow \infty$, the system approaches plug flow (see Section 1.2). When $Pe << 1$, the dispersion term is much larger. In the limit as Pe $\rightarrow 0$, the fluid is fully mixed and the system approaches a continuously stirred reactor.

2.6 Diffusion processes in a homogeneous canopy

Diffusion is net transport due to random motion. In a canopy where turbulence is present, the diffusion constant in the transport equation (equation 2-18) can result from both molecular and turbulent motion.

2.6.1 Molecular diffusion

Brownian motion causes molecules to continually and randomly bump against each other, sometimes changing places. If the concentration of a molecule is not uniform, then this random motion will result in the net motion of molecules from regions of high concentration to regions of low concentration. This process is known as molecular diffusion. Fick's law for the molecular diffusion process states that the mass rate of flux of a solute, $\dot{m}$, is directly proportional to the gradient of the solute concentration:

$$\dot{m} = -D_m \nabla C \tag{2-22}$$

where the molecular diffusion coefficient $D_m = O(10^{-5}\ cm^2/s)$ and is proportional to the rate of increase in the spatial variance σ^2 of a scalar cloud:

$$D_m = \frac{1}{2}\frac{d\sigma^2}{dt} \tag{2-23}$$

Any process for which the flux is proportional to the gradient of concentration is called Fickian and will cause an evolving cloud to have a Gaussian concentration distribution and a variance that increases linearly with time.

2.6.2 Turbulent diffusion

If turbulence is present, then eddies will result in the bulk motion of larger fluid parcels between different parts of the water column. Scalars dissolved or suspended in this fluid will also move more rapidly than they would in the absence of turbulence. The result is turbulent diffusion, with can be described by a diffusion coefficient, D_t. Turbulent diffusion is Fickian if the turbulence is homogeneous and the scale of the turbulence is smaller than the scale of the

concentration gradient (e.g., Fischer et al., 1979). Nepf (1999) assumes a turbulent Prandtl number of 1 and relates the turbulent diffusivity to the stem geometry and the flow velocity:

$$D_t = \phi U \overline{C_d}^{1/3} A^{1/3} d^{4/3} \tag{2-24}$$

where φ is a constant of proportionality and $\overline{C_d}$ represents the bulk drag coefficient. Note that this formulation assumes isotropic diffusion, even though the highly elongated stem shape is likely to introduce anisotropic turbulence and hence anisotropic turbulent diffusion (Nepf et al., 1997b; Leonard and Reed, 2002).

When turbulence is present ($Re_h > 2000$), molecular diffusion is comparatively unimportant. For example, consider a typical wetland situation in which U = 1 cm/s, $C_d = 1$, A = 0.015 cm^2/cm^3, and d = 0.6 cm, equation 2-24 predicts that D_t = 0.13 cm^2/s. For salt (NaCl) dissolved in water, $D_m = 1.5 \times 10^{-5}$ cm^2/s. Thus, for typical flows, $D_t >> D_m$.

2.7 Longitudinal dispersion processes in a homogeneous canopy

When longitudinal velocity is not uniform over depth (or width), the combination of differential advection and vertical (or lateral) diffusion creates additional mixing when a cloud of scalars is viewed as a whole (Nepf et al., 1997a). Therefore, when the exact three-dimensional transport equation (equation 2-18) is averaged over one or more dimensions, the spatial averaging process introduces cross-correlation terms that represent longitudinal transport. These new dispersive processes can be represented by dispersion coefficients (e.g., K_x in equation 2-20). In general, these processes can be considered Fickian when all particles in the flow have statistically sampled all of the heterogeneity in velocity. Once this condition is met:

$$K_x = \frac{1}{2}\frac{d\sigma^2}{dt} \tag{2-25}$$

There are several mechanisms for longitudinal dispersion in a simple homogeneous system of rigid vertical stems over a flat bed. That is, there are several mechanisms by which a scalar cloud will increase in size due to mixing with the surrounding water as a result of passing through the stems. Diffusion and dispersion processes are additive if they are independent Fickian processes (Nepf, 1999). The overall longitudinal dispersion coefficient, K, is therefore the sum of the contributions from the independent processes:

$$K_x = D_m + D_t + K_w + K_h + K_s \tag{2-26}$$

where the dispersion processes K_w, K_h, and K_s represent the secondary wake dispersion, hold-up dispersion, and shear dispersion, respectively. These processes are described in more detail in the rest of this section.

After dispersion develops, both diffusion and longitudinal dispersion mechanisms are present. Typically, however, dispersion is much larger than both molecular and turbulent diffusion, so in well-mixed systems longitudinal mixing is governed by dispersion. For example, Nepf et al. (1997b) observed that lateral diffusivity (which is likely to be horizontally isotropic) $D_y = 0.70 \pm 0.07$ at a flow speed of 6.5 cm/s for $ad = 0.014$. As was noted above, for a salt solution $D_m = 1.5 \times 10^{-5}$ cm^2/s. In a similar system (flow speed of 5.5 cm/s in a canopy for which $ad = 0.01$), longitudinal dispersion was measured to be $K_x = 2.4 \pm 0.7$ cm^2/s (Nepf et al., 1997a), which is larger than both the molecular and turbulent diffusion constants. Longitudinal dispersion in aquatic canopies is therefore controlled by processes other than diffusion.

2.7.1 Stem-wake dispersion

Stem-wake dispersion results from the spatially heterogeneous velocity field produced by the stems (Figure 2-3). Each stem produces a velocity deficit that has a width of $2d$ and extends a length of $20d$ directly downstream of the stem (Zavistoski, 1994). This variability in velocity means that particles taking different routes through the canopy will move at different speeds, which is a form of mechanical dispersion. White and Nepf (2003) used statistical analysis to

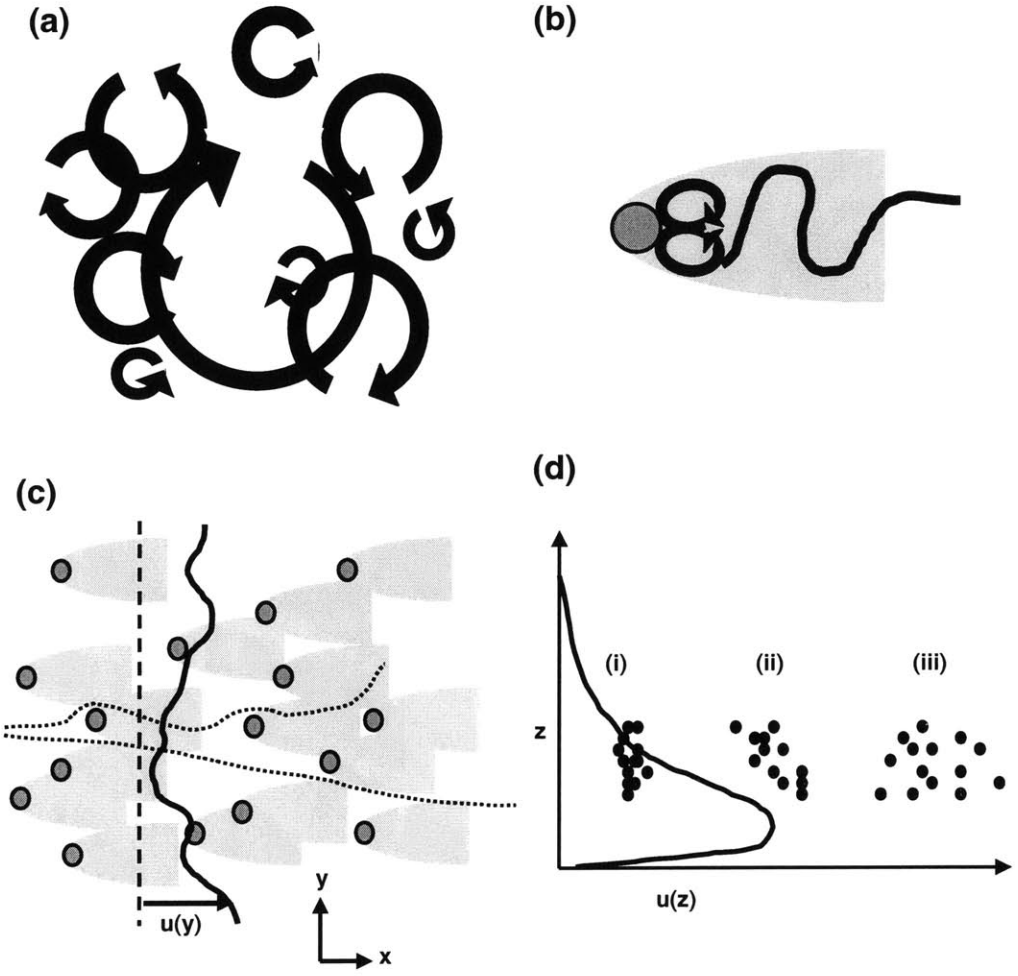

Figure 2-3. Mechanisms of dispersion in a vegetated canopy. (a) Eddies in turbulent flow create turbulent diffusion through random advection of tracer particles. (b) Tracer can become trapped in the primary wake, which is the recirculating zone immediately downstream of a stem. After many particles have become trapped and released, this process becomes a form of mechanical dispersion known as hold-up dispersion. (c) The secondary wakes of cylinders are experienced as velocity deficits by tracer moving downstream. Two particles that start out next to each other will experience different velocity fields and so may become longitudinally separated through the process of stem-wake dispersion. (d) A vertical velocity gradient can create shear dispersion. Tracer particles in different regions of a particle cloud in the shear layer (i) will move at different velocities, so will become longitudinally separated (ii). Vertical diffusion then mixes the cloud over depth, so the entire cloud becomes longer (iii).

estimate the effective longitudinal diffusion constant resulting from secondary wake deficits at low stem density ($ad < 0.1$) and moderate Reynolds number ($10 < Re_d < 650$):

$$K_w = \frac{\gamma}{8} U_o d \sqrt{\overline{C_d}^3 \, \mathrm{Re}_t} \sqrt{\frac{Sc_t}{Sc_t + 1}} \tag{2-27}$$

where γ is weakly proportional to ad and $Re_t = Ud/(\upsilon_t + \upsilon)$. $Re_t \approx 35$ over the range $Re_d = 56$ - 700 (White and Nepf, 2003). This function is only a weak function of the effective turbulent Schmidt number, $Sc_t = (\upsilon_t + \upsilon)/D_t$, and the term $\sqrt{\frac{Sc_t}{Sc_t + 1}} \approx 1$ over the Re_d range 40-160. It is expected that this diffusion process will approach the Fickian limit when each particle has sampled several different wakes, which will occur after a time (White and Nepf, 2003):

$$t_w >> \frac{d}{U\sqrt{ad}} \tag{2-28}$$

Stem secondary wakes may create additional dispersive processes. For example, potential flow theory predicts that streamline curvature around each cylinder will contribute to dispersion (Eames and Bush, 1999). There will also be a contribution by flow accelerating through the gaps between stems, which have an average width s. For a fairly sparse canopy ($ad < 0.1$) at a moderate Reynolds number, however, these contributions are both negligible (White and Nepf, 2003).

2.7.2 Hold-up dispersion

The pair of counter-rotating vortices that appear behind each stem above $Re_d = 10$ (see Section 2.3) can contribute a mechanical dispersion process known as hold-up dispersion. Scalars can get trapped in the recirculation zone while the rest of the scalar cloud advects past, resulting in additional spreading of the scalars. After each particle has become trapped behind

several cylinders, the process becomes Fickian. White and Nepf (2003) show that, in the Fickian limit, the dispersion constant for the trapping process is:

$$K_h = \varepsilon U^2 \bar{\tau} \tag{2-29}$$

where ε is the fraction of fluid volume occupied by the recirculation zones and $\bar{\tau}$ is the mean length of time that each particle remains in a trap. The average volume of recirculation zone within the array is $\varepsilon = \kappa ad$, where the proportionality constant κ reflects the change in wake size with Re_d, cylinder density, and cylinder packing configuration (note the last two dependencies are only important for densely packed arrays, $ad > 0.1$). Simulations have shown that the ratio of the wake area to stem cross-sectional area, which is a measure of ε, is 0.9 for $Re_d = 100$ and 0.68 for $Re_d = 190$ (Duan and Wiggins, 1997).

The mean residence time in an unsteady wake at moderate Re_d is still poorly understood (Gerrard, 1978; White and Nepf, 2003). The residence time is a function of the Reynolds number, since the wake's characteristics change dramatically as Re_d increases. At very low Reynolds number, also known as Stokes flow, the wake is steady, and scalars diffuse in and out through molecular diffusion, D_m. The wake is essentially an extension of the boundary layer around the rest of the cylinder (see Koch and Brady, 1985, for a discussion of diffusion due to a boundary layer). As described in Section 2.3, for $Re_d > 35$, unsteadiness is present in the wake, and convective currents begin to play a role. Above $55 < Re_d < 70$, vortex shedding is present, which provides a regular occurrence of wake turn-over (Gerrard, 1978). Another transition exists at $Re_d \approx 100$. For smaller Re_d, fluid remains in the primary wake long enough for its vorticity to be cancelled by diffusion of opposite-signed vorticity from the opposite side of the wake. The result is that some dye remains close to the cylinder for several oscillation cycles. For $Re_d >> 100$, convective currents are more efficient, and the near wake is almost completely flushed with each vortex shed (Gerrard, 1978).

When the unsteadiness in the wake creates convection currents that sweep through the wake, scalars will be released from the wake on a timescale proportional to the timescale of this unsteadiness, which is $1/f_s$ where f_s is the shedding or unsteadiness frequency. The timescale for

release by convection is then $\bar{\tau}_{conv} = \beta/f_s$, where β is an O(1) constant of proportionality that is a function of Re_d. For $40 < Re_d < 55$, the wake may be unsteady even though vortices are not shed. The unsteadiness will still have a characteristic timescale that can be described by a Strouhal number, $St = f_s d/U$. For a cylinder, the Strouhal number has been found empirically to be determined by the following formula (Fay, 1998, pp. 474-475):

$$St_{cyl} = 0.198\left(1 - \frac{19.7}{\mathrm{Re}_d}\right) \tag{2-30}$$

$St \approx 0.09$ for $Re_d \approx 35$, then approaches a value of 0.2 by $Re_d \approx 200$. Above $Re_d \approx 200$, St is approximately constant over a wide range of Reynolds numbers. The onset of vortex shedding at $55 < Re_d < 70$ does not affect the value of the Strouhal number (Gerrard, 1978).

If the wake size scales on the cylinder diameter, the timescale for release by diffusion is $\bar{\tau}_d = d^2/D_m$. If the timescale for release by diffusion is much greater that the timescale for release by convection, then convection will dominate scalar release. This will occur when $StUd/D_m = StPe >> 1$. Because $Pe = Re_d Sc$, where Sc is the Schmidt number of the solute, $Sc = \upsilon/D_m$, and is typically O(1000), and $St = 0(0.1)$ for moderate Reynolds numbers (Fay, 1998, p. 475), this condition is generally met whenever unsteadiness is present in the wake (White and Nepf, 2003). It is thus expected that convection sets the timescale for scalar release from behind stems at a moderate Reynolds number.

Laboratory experiments have shown that the mean residence time ranges from 40s to 130s for a neutrally buoyant particle in the wake of an emergent circular cylinder with $d = 1.2$ cm, $U = 0.55$ cm/s, and $Re_d = 66$ (Y. Tanino, personal communication). If it is assumed that convection currents dominate the residence time, it would be expected that $\bar{\tau}_{conv} \sim d/StU =$ 16.2s, which is on the same order of magnitude as the experimental observations.

This expression for the mean residence time in the cylinder wake can be substituted into equation 2-29 for the diffusion coefficient for hold-up diffusion. It is expected that when convective processes dominate release,

$$K_h = \frac{\beta\kappa}{St} a d^2 U \tag{2-31}$$

White and Nepf (2003) argue that the timescale to reach the Fickian limit is the timescale for all particles to be trapped exactly once. This timescale is the turnover time for the entire fluid volume to enter a wake, V_f/Q_w, where V_f is the total fluid volume in the array and Q_w is the volumetric flux into all primary wake volume, V_w. Continuity dictates that $Q_w = V_w / \bar{\tau}$. Noting that $\varepsilon = V_w / V_f$, the Fickian limit will be reached when vortex shedding is present if (White and Nepf, 2003):

$$t_h >> \frac{\bar{\tau}}{\varepsilon} = \frac{\beta}{\kappa St a d} \frac{d}{U} \tag{2-32}$$

Before this limit is reached, the scalar concentration leaving the array will exhibit a long tail, corresponding to the slow release of the minority of particles that had been trapped the longest or most frequently.

2.7.3 Shear dispersion

Gradients in longitudinal velocity, called shear, contribute another type of longitudinal dispersion called shear dispersion. In a homogeneous canopy, which has no horizontal gradients, this shear will be vertical, with $u = u(z)$. Following Fischer et al. (1979), the longitudinal shear dispersion coefficient is given by:

$$K_s = -\frac{1}{h}\int_0^h u' \int_0^z \frac{1}{D_z} \int_0^z u' dz\, dz\, dz \tag{2-33}$$

where the vertical diffusion constant, D_z, may be a function of position.

Shear dispersion is Fickian only when a scalar cloud is mixed across the shear. For vertical shear, a slug release requires a certain amount of time to spread vertically. Timescale analysis predicts that the length of time necessary for a slug release to experience shear dispersion is the length of time for it to become fully mixed across the shear layer. This amount of time is given by:

$$t_s = 0.4\frac{h^2}{D_z} \tag{2-34}$$

where h is the width of the velocity gradient and D_z is the diffusion coefficient across the gradient. If U/D_z is constant for a given canopy (cf. equation 2-24, assuming A, d, and C_d are constant), then the distance downstream necessary for the dye to mix across this gradient is $x = Ut_s = 0.4Uh^2/D_z \propto h^2$ and so is independent of the flow velocity. Before reaching the well-mixed limit, dispersion cannot be described by a Fickian relationship (equation 2-25). The longitudinal concentration distribution is skewed, and dispersion processes other than shear dispersion control the rate of longitudinal mixing.

Note that vertical diffusivity plays an important role in shear dispersion. Heuristically, when vertical diffusivity is low, particles that start on different streamlines tend to remain on different streamlines and thus can become spread out longitudinally. Shear dispersion takes a long time to develop under these conditions, however, because particles are not mixed rapidly across the shear layer (cf. equation 2-34). Conversely, when vertical diffusivity is high, shear dispersion develops rapidly but has a lower value.

Exact solutions for the shear dispersion constant (equation 2-33) have been calculated for several relevant situations assuming constant cross-stream diffusivity, D_z, and that the flow is

well mixed over depth (Fischer et al., 1979). Longitudinal dispersion for laminar flow in a linear velocity profile of width h, such that $u(z) = U\frac{z}{h}$, is given by:

$$K_s = \frac{U^2 h^2}{120 D_z} \tag{2-35}$$

Longitudinal dispersion in a step velocity profile, $u(z) = u_1$ for $z < \frac{1}{2}h$ and u(z) = u_2 for $z > \frac{1}{2}h$, is given by:

$$K_s = \frac{(u_1 - u_2)^2 h^2}{48 D_z} \tag{2-36}$$

Finally, longitudinal dispersion in turbulent open-channel flow can be estimated using Elder's formula (Fischer et al., 1979),

$$K_s = 5.93 u_* h \tag{2-37}$$

where u_* is the shear velocity, which is a measure of the shear stress on the bed. As a first approximation, $u_* \approx 0.05U$.

Most environmental flows contain some shear. Even in relatively straight and unobstructed channels, the no-slip condition at the bed creates non-constant longitudinal velocity over depth in a shallow flow, which can result in shear dispersion. In shallow open channel flows, the velocity distribution follows a logarithmic profile, which can result in shear dispersion being much larger than the turbulent diffusion. For example, in a 1-m-deep salt marsh with a longitudinal velocity of 5 cm/s, K_s =148 cm^2/s (Elder, 1959, cited in Fischer et al., 1979), assuming that the shear velocity $u_* \approx 0.05U$. In most flows with emergent vegetation, however, the drag created by the stems limits the bottom boundary layer to within O(d) of the bed (Nepf et al., 1997b). If the stem density is fairly uniform over depth (e.g., in a canopy of reeds), then the longitudinal velocity is approximately constant over depth (White and Nepf, 2003). Under these

conditions shear dispersion is not as important a process as it is in open-channel flow, and dispersion within the canopy will be dominated by the hold-up and stem-wake dispersion mechanisms.

2.8 Extending the model to consider variable stem density over depth

As noted above, the simplified model of randomly-distributed, rigid, vertical circular cylinders deviates from a real plant canopy in many regards. One of these attributes is the assumption that frontal area is uniform over depth. Real vegetation rarely has uniform density over depth (Leonard and Luther, 1995; Shi et al., 1995; Shi et al., 1995; Nepf and Vivoni, 2000). In salt marshes, for example, there is often a litter layer of dead stems and leaves near the bed. The central plant stems rise from this layer. Leaves branch off of this stem above the litter layer. Then, in the upper part of the water column, leaves may end and frontal area may decrease with distance from the bed.

If the drag force is large, then the local velocity at each distance above the bed, $u(z)$, will depend at least in part on the local frontal area, $a(z)$, and the local drag coefficient, $C_d(z)$ (e.g., Nepf and Vivoni, 2000). Assuming that pressure forces balance drag forces at all depths, equation 2-17 can be rewritten in terms of these local variables:

$$\rho g \frac{\partial \eta}{\partial x} = \frac{1}{2} \rho C_d a u^2 \tag{2-38}$$

Rearranging this equation,

$$C_d a u^2 = 2g \frac{\partial \eta}{\partial x} \tag{2-39}$$

If $\partial\eta/\partial x$ is constant for a given flow condition, then $C_d a u^2$ is also a constant, ψ. The velocity profile is therefore dependent on the vertical distribution of frontal area, $u = \sqrt{\psi / C_d a}$. Let $\tilde{u}$ represent the velocity at a particular height above the bed where vegetation drag dominates,

and let $\tilde{a}$ represent the frontal area and $\tilde{C}_d$ the drag coefficient at this same height. Then, if all velocity profiles are normalized by $\tilde{u}$, they collapse into a single profile that depends only on $C_d a(z)$.

$$\frac{u}{\tilde{u}} = \sqrt{\frac{\psi / C_d a(z)}{\psi / \tilde{C}_d \tilde{a}}} = \sqrt{\frac{\tilde{C}_d \tilde{a}}{C_d a(z)}} \tag{2-40}$$

If the depth-averaged velocity does not change so drastically that $C_d(z)$ changes, then normalizing by $\tilde{u}$ can allow the comparison of velocity profiles taken with different depth-averaged velocities.

It was noted in Section 2.4 that the exact behavior of the drag coefficient in obstructed flow at a moderate Reynolds number is still poorly understood. For $ad < 0.10$ it has been suggested that C_d is not a strong function of stem density and is O(1) (Koch and Ladd, 1997; Nepf, 1999). C_d is therefore not likely to vary greatly over depth, and equation 2-40 predicts that $u / \tilde{u}$ will not be strongly dependent on the exact value of C_d.

If the vegetation is submerged, then a goes to zero above the canopy. Ghisalberti (personal communication) has observed that, for a submerged array of circular cylinders in flow at $40 < Re_d < 400$, the difference in velocity between the canopy and the free stream normalized by the free-stream velocity, $\Delta u/U_h$, is a strong function of ad in the canopy. In particular, the best-fit line through zero for flow over a submerged canopy indicates that $\Delta u/U_h \sim a^{0.38}$. It therefore appears that there is some relationship between flow velocity and frontal area density. The relationship between velocity and frontal area has not been previously characterized, however, for an emergent canopy with variable a over depth.

Submerged vegetation creates strong velocity shear and increased turbulence intensities at the top of the canopy (Gambi et al., 1990). The region near the top of the canopy can be considered a free shear layer, which is a region where shear does not arise from boundary conditions (Ghisalberti and Nepf, 2002). The transition between the free stream velocity above

the canopy and the drastically reduced velocity within the canopy creates an inflection point in the velocity profile. When the forcing in the flow is high enough, this inflection point can result in the development of a street of vortices, which will greatly enhance vertical mixing (Ghisalberti and Nepf, 2002).

Frontal area and, as a result, velocity are typically strong functions of depth in emergent vegetation. Pethick et al. (1990) noted that velocity particles in a replicated emergent S. angelica salt marsh were linear below 10 cm from the bed and convex upward at greater distances from the bed. Shi et al. (1995) found that velocity profiles in an emergent *S. angelica* canopy contained a reversal in the flow gradient with a horizontal jet created near the bed. Leonard and Luther (1995) also observed a near-bed jet in a field study of *S. alterniflora.* Similarly, Leonard and Reed (2002) reported that longitudinal velocity in a *S. alterniflora* canopy reaches a minimum 30 cm from the bed. Even if this shear is not high enough to create an inflection point and instability in the flow, its presence may affect mixing processes. In addition, when the canopy generates vertical shear, the assumption that vegetative drag dominates the flow except within one stem diameter of the bed may no longer be correct, and more complex situations may arise.

Differential longitudinal velocities over depth result in the possibility of shear dispersion, which, once it develops, is likely to dominate longitudinal dispersion. The length scale associated with shear dispersion is the canopy height, h, whereas the length scale of stem-wake and hold-up dispersion is the stem diameter, d, or the stem spacing, s. Typical wetland vegetation is relatively thin, with $d < 1$ cm. In a typical canopy, $n = 100 - 500$ stems/m^2, so $s = 1/\sqrt{n} < 1$ cm. If the water depth $h > 10$ cm, and K_x scales on the length scale of the shear (equation 1-1), then shear dispersion is at least an order of magnitude greater than other contributing processes.

To determine the potential role of shear dispersion in an aquatic emergent canopy, longitudinal dispersion was measured in the laboratory in a canopy with varying stem density over depth. A step distribution was chosen, with the stem density twice as high in one layer as the other. This simple arrangement has a more extreme density gradient than stem density

profiles in natural systems, but it offers comparable spatial variance in frontal area density. The velocity spatial variance will be a function of the density variance, so this simplified system and a natural system should produce comparable shear dispersion, assuming that vertical diffusivity is also comparable.

Adapting the model of rigid, circular cylinders to account for variations in stem density over depth does not remove all of the other simplifications made here. For example, real stems are not purely cylindrical. *S. alterniflora* and *Z. marina* leaves are flat, although they may roll slightly (Gambi et al., 1990). The result may affect the drag coefficient. The drag coefficient on a stiff flat plate over the regime of $10 < Re_d < 10^5$ is (Fay, 1998, p. 476):

$$C_d = \frac{1.33}{\sqrt{\mathrm{Re}_d}} \tag{2-41}$$

If this equation is used as an estimate for the drag coefficient in an array, changing the stems in the array from cylindrical to flat plates at $Re_d = 100$ would cause C_d to decrease from 1.5 to 0.13. Other common wetland algae and macrophytes may be highly branched, which would also affect the drag coefficient (Harvey et al., 1995). Changes in the shape of the body cause a change in the Reynolds number at which the transition to vortex shedding occurs (Gerrard, 1978; Luo et al., 2003). Therefore, the shape of the vegetation may play a role in determining wake behavior and possibly dispersion based on vortex trapping. Interactions between two stems will also disturb the wake, and this effect may change depending on the shape of the stems or leaves (Wei and Chang, 2002).

This model also does not account for other complexities inherent in a natural system: dead vegetation (wrack), uneven bed morphology, surface waves, temporal variation due to tidal flow, or many other complicating factors. The model as it exists was therefore tested in the field to gauge its ability to predict actual wetland transport, despite its simplifying assumptions.

Chapter 3

Materials and Methods

Experiments were performed in both the laboratory and the field to assess the ability of the existing theory of flow through emergent aquatic vegetation, presented in Chapter 2, to predict longitudinal mixing over intermediate length scales. In particular the experiment examined the relative roles of turbulent diffusion, stem-wake dispersion, hold-up dispersion, shear dispersion from the bottom boundary layer, and shear dispersion resulting from varying stem density over depth. The laboratory and field setups were designed to compare dispersion over similar length scales, stem densities, and flow speeds.

3.1 Laboratory setup

The laboratory portion of this study was conducted in a 6.7-m-long, 20.3-cm-wide, 30.5-cm-tall plexiglass flume (Figure 3-1). At the inlet, flow was forced into a stilling basin through a sponge to dissipate inlet kinetic energy, and vertical metal screens (hole diameter 6.35 mm, 57% open area) were installed upstream and downstream of the array to straighten the flow. Water depth was maintained at 20 cm ± 1 cm throughout all trials. Depth-averaged flow speeds ranged from 1 to 4 cm/s and were chosen to match velocities observed in stands of the marsh grass *S. alterniflora*. Wooden circular dowels with a diameter of 0.6 cm were used to represent cylindrical marsh grasses. Reynolds numbers based on cylinder diameter (Re_d) ranged from 38 to 193.

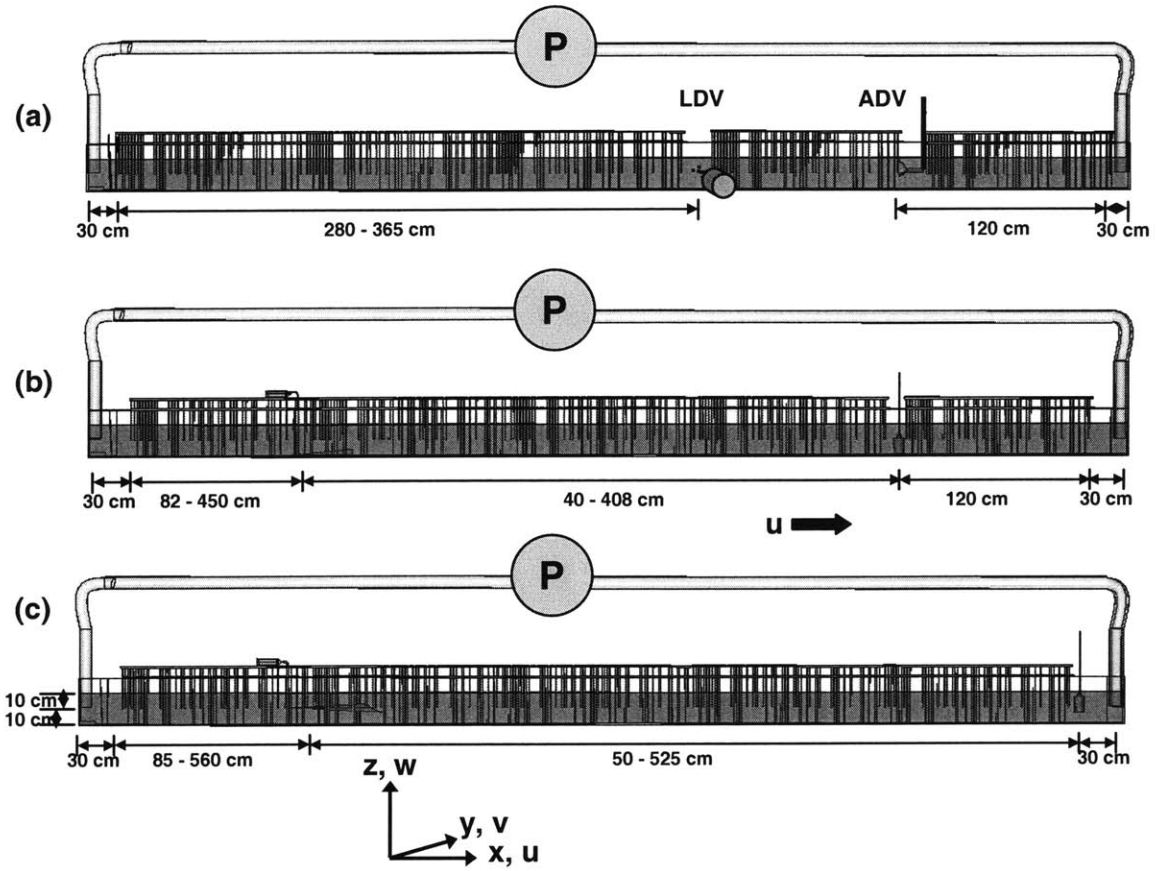

Figure 3-1. Diagram of laboratory setup. The flume is filled with emergent vegetation of two different densities: $ad = 0.024$ in the top 10 cm and $ad = 0.024$ in the bottom 10 cm. The flume is shown in a recirculating mode; however, during some dye studies, the flume was used in a once-through configuration. At the inlet, water entered vertically and was passed through a sponge and several screens to dissipate energy and straighten the flow. At the outlet, water was passed through a screen and exited vertically. (a) Velocity measurements. Either the LDV or the ADV was used at one time. The LDV was positioned near the middle of the flume looking sideways through the plexiglass flume and across the water column; the ADV was positioned 1.2 m from the end looking upstream into the flow. A narrow swath of dowels was cleared for each instrument. The outlet hose was positioned 10 cm from the bed for all velocity measurements (b) Vertical diffusivity measurements. The syringe (attached to a syringe pump, not shown) was used to produce a continuous releases of Rhodamine 6G and WT through a needle near the bed. The fluorometer was positioned 1.2 m from the end of the flume and was moved vertically to profile the evolving dye cloud. (c) Longitudinal dispersion measurements. The syringe was used to produce slug releases at the interface, at 4 cm from the bed, or at 16 cm from the bed. The fluorometer and the outlet hose were both adjusted to match the depth of release.

To represent the vertical variation in stem density that occurs in the field, a denser array (n_{top} = 600 cylinders/m², ad_{top}= 0.024) filled the upper half of the flow area and a less dense array (n_{bot} = 300 cylinders/m², ad_{bot} = 0.012) filled the lower half. These densities fall within the range of observed densities in stands of *S. alterniflora* (Valiela et al., 1978; Leonard and Luther, 1995; Christiansen et al., 2000; Shi et al., 2000). The dowels were suspended from two layers of perforated plastic (3/16" diameter holes with 12 holes per square inch; Ametco Manufacturing Company, Willoughby, OH). The sheets were oriented so that there were no unobstructed longitudinal flow channels, and the dowels were arranged randomly in the holes. The plan for the random arrangement included dowels overlapping with the edge of the flume. These dowels were cut in half and placed along the edges of the flume to avoid creating a jet along the flume edge. In total, the cylindrical array extended longitudinally for 6.1 m.

3.2 Field site

To determine whether the processes observed in the laboratory also act in natural systems with fully emergent vegetation, field experiments on a similar scale were carried out at the Plum Island Estuary in Rowley, MA (42.727°N, 70.8478°W using the WGS84/NAD83 coordinate datum). The study site was a small patch of vegetation, primarily *S. alterniflora*, on a small bar in the middle of the Rowley River (Figure 3-2). Massachusetts tides are diurnal; at the south end of the Plum Island Estuary, there is a mean tide of 2.6 ± 0.5 m. Velocity and dye studies were performed on days when the maximum water depth at the field site ranged from 44 to 81 cm, but no measurements were taken when the vegetation was fully submerged. All velocity measurements, dye releases, and dye measurements occurred at least 2 m and no more than 5 m from the edge of the vegetation. Previous studies have shown that vertical velocity profiles are established within 50 cm of the edge of a vegetated bed (Gambi et al., 1990).

Stem density in the field was measured approximately once per week by casting an 0.11-m^2 frame into the studied area and counting the stems inside it. Four times during the study period, all of the stems inside the 0.11-m² frame were harvested and immediately photographed using a 4.1 megapixel digital camera (DSC-S85 Cyber-shot, Sony, Tokyo, Japan). Four views were taken of each stem in front of a white background: an original orientation, then rotated

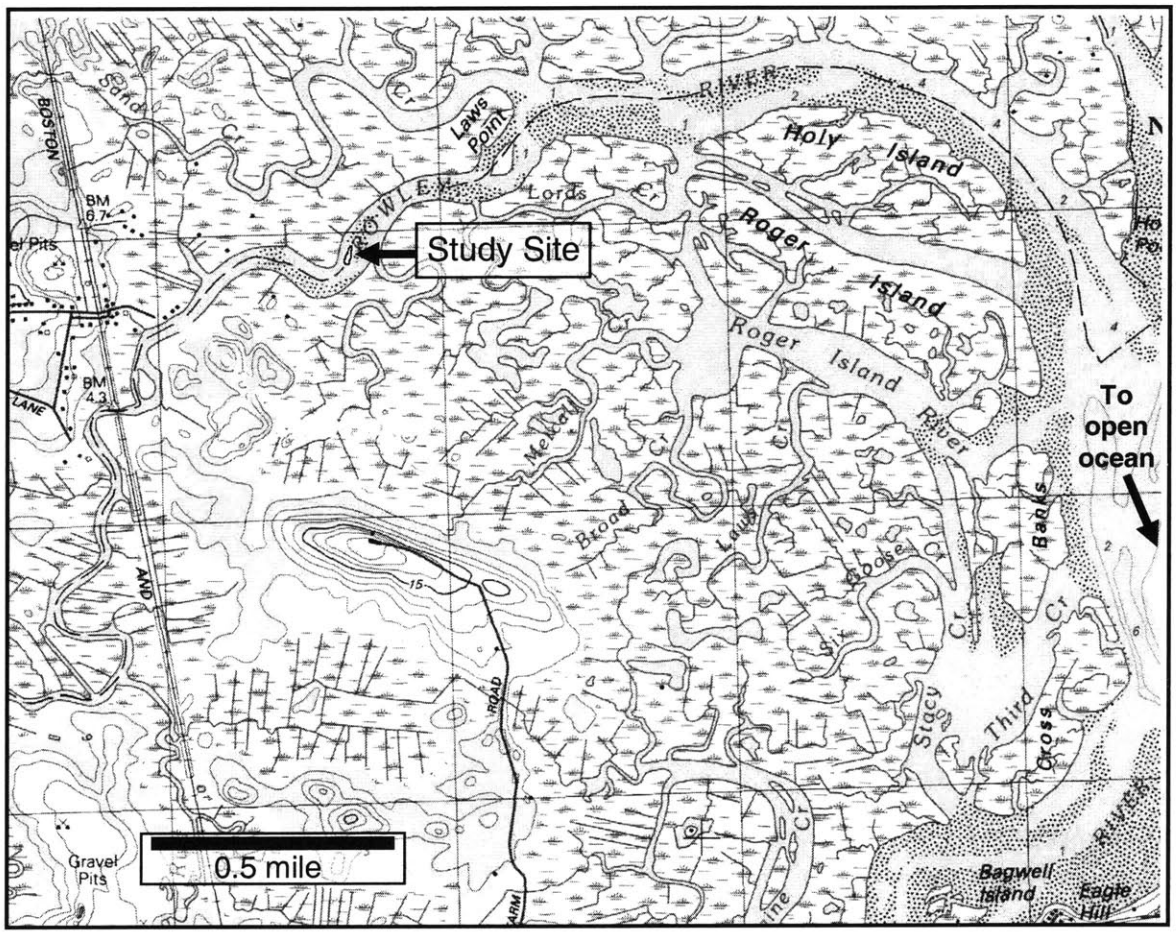

Figure 3-2. Topographic map of the field site. The arrow indicates the location of the field site on a sandbar in the middle of the Rowley River, Plum Island Estuary, Rowley, Massachusetts.

clockwise 45°, 90°, and 135°. Matlab's image processing toolbox was used both to convert the color image to black and white and to count the number of pixels in the stem (Matlab version 6.5.0, release 13.0.1, The MathWorks, Inc.).

Analytical and observational results indicated that the number of pixels per centimeter of stem varied by 15% over the length of a stem due to parallax. Subsequent analysis of the stem corrected for this effect. In addition, there was some variability associated with the choice of which stem view to use in subsequent analysis. For most stems, one of the four images was randomly selected for analysis; analysis of all four views for a subset of 20 stems suggested that the error associated with stem rotation was approximately 20%. Finally, it was necessary to select manually a threshold value to separate the stem from the background during image processing, and a difference of 1% in this value affected the final area by approximately 5%. Calculations of frontal area per unit depth for each stem were then summed over all stems in the sample to estimate total frontal area per unit area bed.

Measurements of stem diameter were performed on stems collected on October 28, 2002. Calipers were used to measure the width of each leaf at 10 cm and 20 cm above the bed on a total of 33 plants collected near the field site.

3.3 Velocity measurements

In the laboratory, water velocity at the lowest flow rate was measured using laser Doppler velocimetry (LDV) with a 2-D probe (Dantec, Mahwah, NJ) with beams oriented to measure longitudinal and vertical velocities. The measurement volume was an ellipse, 0.64 mm by 76 μm. The minimum resolvable flow velocity using this probe is 1 mm/s, including the alignment error, and it is accurate to within 0.2 mm/s. A five-minute velocity record was taken at each point sampled. Preliminary investigation showed that this record length was long enough to allow both the mean longitudinal velocity (u) and the Reynolds stress ($\overline{u'w'}$) to reach within 5% of the values attained after twenty minutes. The laser probe was placed outside the flume, with the beams directed into the water through the flume walls. At the longitudinal location of measurement, a 5-cm-wide swath was cleared of dowels to prevent interference with the laser beams. Since this length-scale is comparable to the stem spacing, the missing dowels were not

expected to affect either the mean flow or turbulence statistics. Measurements were taken between 2.8 m and 3.65 m downstream of the edge of the array.

LDV does not record at a constant data rate. When the flow velocity is higher, more particles pass through the LDV probe's sampling volume, and the LDV probe records more measurements. Data rates using LDV ranged from 10 to 100 Hz, with higher data rates obtained for recently seeded flows (see below), for higher velocities, and when the measurement volume was located farther away from the flume walls and bottom. To remove the velocity bias, statistics and spectra were calculated after interpolating data to 10 Hz.

For the highest flow rate, water velocity was measured using acoustic Doppler velocimetry (ADV) using a three-dimensional (3-D) laboratory probe (SonTek/YSI, Inc.; accuracy ± 0.1 cm/s). The probe was placed 4.9 m downstream of the start of the cylinder array. It was submerged in the water and oriented looking upstream into the dowel canopy. Stems were removed from the measurement volume so as not to interfere with the acoustics. Five-minute-long velocity records were taken at 25 Hz. Because of the width of the sampling head, ADV measurements were not obtained within 3 cm of the bed, the side walls, or the free surface.

During velocity measurements, water in the flume was recirculated using a centrifugal pump (Teel, Dayton Electric Manufacturing Company, Niles, IL). The flow was seeded with 0.18-μm diameter hollow glass spheres (Sphericel by Potters Industries Inc., Valley Forge, PA). To optimize the data collection rate, 12-14 g of seeding was used to seed the 271 L of water in the tank. Over time, the particles in the flow settled out; each section of the canopy was removed and the water in the entire tank was stirred at least once every four hours to resuspend seeding particles.

Local velocities in a cylinder array can vary by more than an order of magnitude, depending on the cylinder arrangement directly upstream of the measurement position (White and Nepf, 2003). To sample this spatial heterogeneity, measurements were repeated at multiple locations in the array; mean velocity, turbulent kinetic energy ($\frac{1}{2}\, u_{rms} + \frac{1}{2} w_{rms}$), Reynolds stress ($\overline{u'w'}$), and turbulent efficiency ($\overline{u'w'}/u_{rms}w_{rms}$) were calculated for each sample point. Vertical profiles were then obtained by averaging together temporal mean values obtained from six

different horizontal positions more than 2 cm away from the sidewall of the flume. For the lowest flow rate, spatially averaged horizontal profiles at 6 and 14 cm above the bottom were obtained by averaging mean values from six different horizontal profiles taken using the LDV probe at different longitudinal positions. For the highest flow rate, spatially averaged horizontal profiles were obtained by vertically averaging three to four measurements taken using the ADV probe at different vertical locations in each of the upper and lower canopies.

In the field, water velocity through the canopy was measured using a two-dimensional (2-D) sideways-looking field ADV probe (FlowTracker, SonTek/YSI, Inc., San Diego, California, range: ± 0.001 m/s to 5 m/s; accuracy: ±1% of measured velocity). The probe was mounted on a gauging staff and used to take repeated 2- to 5-minute-long records (Figure 3-3). Preliminary investigation showed that two to three minutes was long enough for the mean flow readings to stabilize but also short enough for a vertical profile to be completed within a timescale shorter than the tidal variation. The probe was used to take velocity measurements at 1 Hz from 5 cm above the bed to 5 cm below the surface at intervals of 5 cm. A piece of plastic mesh (0.3-mm-diameter holes), cut to the shape of the ADV measurement volume, was mounted to the base of the gauging staff to push down the grass directly below the probe and prevent stems from interfering with measurements. A field 3-D downward-looking ADV probe (SonTek/YSI, Inc.; accuracy ± 0.1 cm/s) was also used to take point measurements in vertical transects at 25 Hz; the length of each measurement ranged from 5 to 20 minutes. The probe was mounted on a tripod and adjusted to a vertical position using a plumb bob and a level. A wire cage was placed around the probe arms to guide plants away from the measurement volume. Dye visualization showed that the mesh had a negligible effect on ambient flow and did not shed vortices or create other instabilities.

Prior to analysis, spikes were removed from each field record. A data point was determined to be a spike if it was both more than 3 standard deviations and more than 3 cm/s from the mean (recommendation of Flowtracker manufacturer for this range of velocities). Spikes could have resulted from sand or other impurities in the flow or from bubbles. In addition, portions of the velocity records affected by boat wakes were deleted.

Figure 3-3. Measuring velocity in the field during ebb tide. The water was approximately 20 cm deep in the vegetation at the time this photograph was taken. Priya is using the Flowtracker; its console is around her neck and the probe head is at the base of the staff she is holding. The 3-D ADV probe is mounted vertically on the tripod on the other side of this stand of vegetation.

In the field, where flow direction was changeable, horizontal velocity was considered to be the absolute value of the vector sum of the x and y velocity records:

$$u = +\sqrt{v_x^2 + v_y^2} \tag{3-1}$$

For each point measurement, the flow direction relative to the probe orientation is:

$$\theta = \arctan(v_y/v_x) \tag{3-2}$$

To correct for small velocity changes over the course of the tide, each profile began and ended with a measurement at the same depth. This depth was high in the water column, where velocities were highest. Other velocity measurements from the profile were then scaled by a factor that accounted for the difference between these repeated measurements. If it is assumed that the velocity changes linearly during each profile, then the beginning velocity, u_{begin}, and end velocity, u_{end}, are related by:

$$u_{end} = u_{begin} + r\,(t_{end} - t_{begin}) \tag{3-3}$$

where r is the rate of velocity change. Solving for r,

$$r = (u_{end} - u_{begin}) / (t_{end} - t_{begin}) = \Delta v/\Delta t \tag{3-4}$$

Similarly, any measurement, u_i, taken at a time, t_i, during the profile, can be scaled to what it would be if it had been taken at the beginning of the measurement period:

$$U_i = u_i - r * (t_i - t_{begin}) \tag{3-5}$$

where U_i represents the corrected velocity.

Individual profiles were evaluated using the following three criteria: they consisted of measurements at three or more measurement different distances from the bed; they had a monotonic velocity increase above 15 cm from the bed; and the mean flow direction, θ, changed by less than 60° over the entire vertical profile. Profiles that met all three of these criteria (see Appendix A) were then aligned to create a composite velocity profile.

Because the water velocity through a salt marsh canopy varies among different tidal amplitudes and over the course of each flooding period (Christiansen et al., 2000; Lynn and Reed, 2002), the depth-averaged velocity, U, ranged from 1.3 to 11.0 cm/s, so the profiles could not be simply averaged at each depth. Instead, the 56 acceptable profiles were normalized by the velocity at 15 cm above the bed (using linear interpolation when no measurement had been taken at this depth). Similarly, Gambi et al. (1990) normalized by the velocity at one depth in their flume study of flow through submerged vegetation and noted that velocity profiles at different depth-averaged velocities collapsed into a single profile. This depth is farther than one stem diameter from the bed, so bottom boundary roughness has a limited effect (Nepf et al., 1997b) and is far enough below the surface in all profiles that Reynolds stresses due to the wind should be negligible. Therefore, it is expected that vegetation drag dominates at this depth. Normalizing by this depth effectively removes variation in velocity magnitude due to differences in surface slope (equation 2-40), thereby allowing comparison of profile shape even when pressure forcing differed.

For both the laboratory and field data, smoothed spectra were plotted using a Parzen window, with the optimal non-dimensional window length determined using the window closing technique to be $L = 64$. Frequencies associated with peaks of spectral energy were compared to predicted vortex-shedding and (for the field data) typical wind wave frequencies.

3.4 Vertical diffusivity measurements

Vertical diffusion was measured by fitting measured concentrations to analytical solutions for vertical concentration profiles downstream of a continuous dye release, as has been previously described by Nepf et al. (1997a). Rhodamine WT was pumped using a syringe pump (Sage by Orion Research Inc., Beverly, MA) in the laboratory and a field sampler (Masterflex Environmental Sampler, Cole-Parmer, Vernon Hills, IL) in the field through a needle placed horizontally in the flow and directed downstream. In the laboratory, the release was positioned at midwidth and, to prevent bottom boundary layer effects, the dye was released 0.5 cm from the flume bottom. In the field, the dye was released 10 cm from the bed (Figure 3-4). The needle was connected to 0.64-cm-diameter tubing, chosen to mimic dowel and vegetation diameter. The inlet velocity of the dye was carefully matched to that of the ambient flow conditions. In the

laboratory, up to three dowels immediately downstream of the release were removed if they interfered with the initial evolution of the plume; in the field, the release was adjusted so that stems immediately downstream of it did not affect the plume (i.e., the dye evolving from the needle; cf. Figure 3-1b).

Dye concentration was measured downstream using a flow-through Rhodamine fluorometer (Seapoint Sensors, Exeter, NH), which was attached to an OS200 CTD (Ocean Sensors, San Diego, CA). The sampling frequency of the fluorometer was ~8 Hz; it could measure as close as 2.5 cm to the bottom or bed. The fluorometer was used to take measurements between 0.5 m and 4 m downstream of the continuous release. In the laboratory, the fluorometer was positioned at midwidth (so at the lateral midpoint of the plume). In the field, the plume tended to wander laterally, so the fluorometer was used to take lateral profiles at various vertical heights above the plume. The maximum concentrations of these profiles were then aligned to produce a vertical profile of dye concentration. The error in the value of D_z calculated by fitting an equation to each vertical profile was calculated by determining what change in D_z yielded a 5% change in the sum of least-squares.

In the laboratory, at the longitudinal location of measurement, a 6.4-cm-wide swath was cleared of dowels to allow the introduction of the fluorometer probe. Since this length-scale is comparable to the stem spacing, the missing dowels were not expected to affect flow or dye transport. Dye visualization showed that it did not markedly perturb the surrounding velocity field.

Water velocity in the laboratory was measured using the LDV or ADV probe (see Section 3.3). Water velocity in the field was measured at the fluorometer by timing how long it took a slug of dye to travel a short distance. The slug release method has been shown to correlate well with measurements of mean velocity (Hosokawa and Horie, 1992). When possible, this estimated velocity was compared with the velocity measured simultaneously by the Flowtracker; the two velocity measurements were typically on the same order of magnitude but were taken in different regions of the canopy and so were not identical.

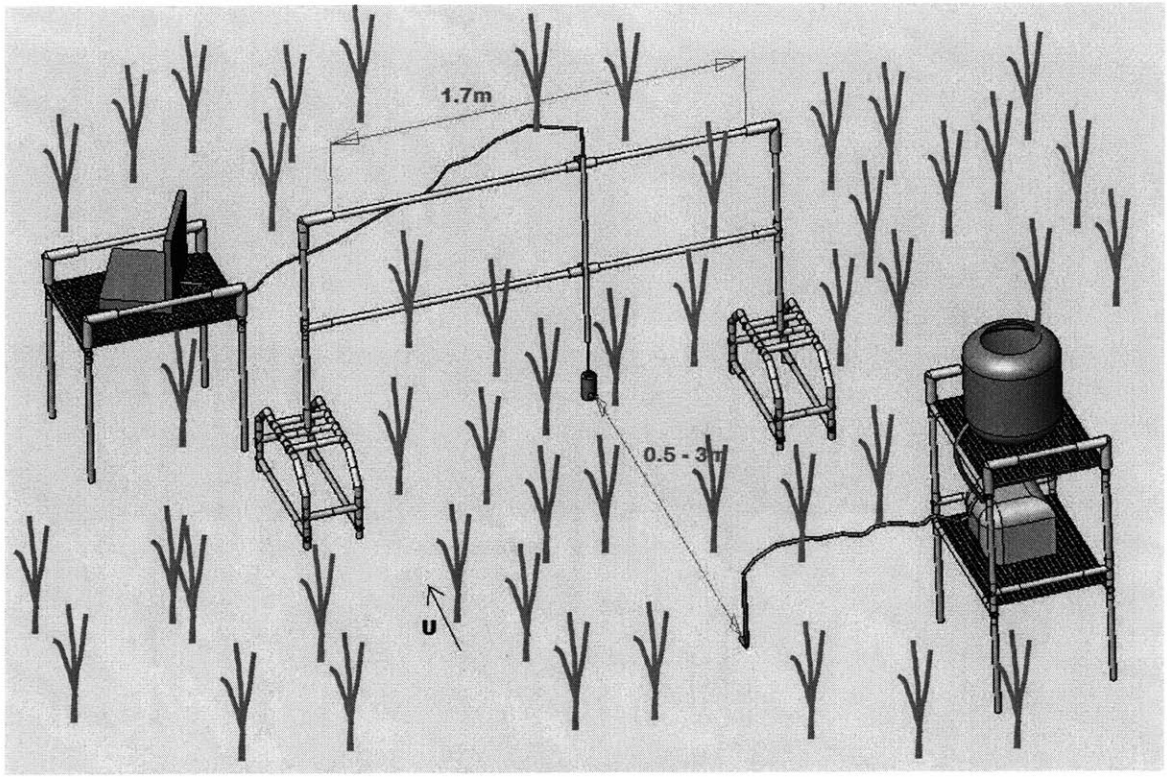

Figure 3-4. Field setup for dye releases. Dye was injected at various distances upstream of the fluorometer, which was located on a traverse for easy lateral adjustment. A field sampler was used to inject dye at a constant rate for continuous releases; a syringe was depressed by hand for slug releases. No equipment protruded into the water column directly upstream of the release and measurement locations.

To allow comparisons among different releases, all measured concentrations were normalized by the release concentration. Normalized readings at the same depth the same distance downstream of the release were averaged together to produce an estimate of the vertical concentration distribution at various locations downstream of the release. Analytical solutions were then fit to these measurements.

A continuous release in a fluid of a constant velocity will evolve such that the downstream lateral profile will be Gaussian (Fischer et al., 1979):

$$C(y,z) = \frac{\dot{m}}{4\pi\sqrt{D_y D_z}} \exp\left(-\frac{(z - z_{release})^2}{4D_z t} - \frac{(y - y_{release})^2}{4D_z t} \right) \tag{3-6}$$

where $\dot{m}$ is the rate of introduction of mass and $y_{release}$ and $z_{release}$ are the y and z coordinates of the release point. Directly downstream of the release, $y - y_{release} = 0$.

In the lower canopy of the laboratory, the bed serves as a no-flux boundary, which is equivalent to doubling the strength of the source. In addition, $t = x/u_{bot}$, and all measurements were taken directly downstream of the point of release The vertical diffusion constant, D_z, is one of the fitting parameters to the shape of the resulting Gaussian curve:

$$C(z) = \frac{2\dot{m}}{4\pi\sqrt{D_{y,bot} D_{z,bot}}} \exp\left(-\frac{(z - z_{release})^2}{4D_{z,bot} t} \right) = C_1 \exp\left(-\frac{u_{bot}(z - z_{release})^2}{4D_{z,bot} x} \right) \tag{3-7}$$

This equation was fit in a least-squares sense to the concentration profiles observed in the field and in the lower canopy in the laboratory, using C_1 and $D_{z,bot}$ as the fitting parameters.

In the laboratory, it was observed that dye built up in the lower canopy just below the boundary between the two stem density layers, so the boundary apparently acted as a partial flux boundary. Fitting an equation not accounting for this effect will overestimate a value for D_z. For comparison, the concentration distribution was also modeled assuming a no-flux boundary at the interface. This situation requires another image source to be placed at $z = h$. Noting that $z_{release} = 0$, the second fitting equation used for the lower canopy in the laboratory is:

$$C(z) = \frac{2\dot{m}}{4\pi t\sqrt{D_{y,bot}D_{z,bot}}}\left\{\exp\left(-\frac{z^2}{4D_{z,bot}t}\right)+\exp\left(-\frac{(z-h)^2}{4D_{z,bot}t}\right)\right\} \tag{3-8}$$

The coefficient outside of the exponential is a constant that depends on D_y, which was not estimated. In addition, $t = x/u_{bot}$. For fitting purposes, this equation can therefore be recast as:

$$C(z) = C_2\left\{\exp\left(-\frac{u_{bot}z^2}{4D_{z,bot}x}\right)+\exp\left(-\frac{u_{bot}(z-h)^2}{4D_{z,bot}x}\right)\right\} \tag{3-9}$$

This curve was fit in a least-squares sense to the laboratory measurements from the lower canopy, using C_2 and $D_{z,bot}$ as the fitting parameters. Because it assumes a perfect no-flux boundary, it is likely to underestimate the true value of D_z.

To derive the fitting equation for the upper canopy in the laboratory, consider a frame of reference moving at the average speed of the upper canopy, $u = u_{top}$. On the centerline of the flume, the concentration is initially zero everywhere. At some time t_*, dye diffusing upward through the bottom canopy reaches the dividing line between the upper and lower canopies, $z = \frac{1}{2}h$. The concentration at the bottom of the upper canopy, C_o, is a function of time, $C_o(t)$. Assuming that it can be approximated as constant, however, and that the centerline of the upper canopy is one-dimensional (the dye diffuses only upward, not outward) then in the moving frame of reference (Fischer et al., 1979):

$$C(z) = C_o\ erfc\left(\frac{z-\frac{1}{2}h}{\sqrt{4D_{z,top}(t-t^*)}}\right) \tag{3-10}$$

where $erfc(z\text{-}h) = 1 - erf(z\text{-}h)$. In a stationary frame of reference, the curve evolves with respect to longitudinal distance, not time. In the upper canopy, $t = (x - x_*)/u_{top}$, where x_* is the x-location where the dye first penetrates into the upper canopy. The profiles reveal that this penetration occurs at about 100 cm downstream of the release. That is, $x_* = 100$ cm, so $t - t_* = (x - 100\text{ cm})/u_{top}$. Substituting this transformation into the equation for concentration,

$$C(z) = C_o \, erfc\left(\frac{(z - \frac{1}{2}h)\sqrt{u_{top}}}{\sqrt{4D_{z,top}(x - 100\ cm)}} \right) \tag{3-11}$$

This curve was fit in a least-squares sense to the laboratory data from the upper canopy, using C_o and $D_{z,top}$ as the fitting parameters.

In the field, all releases occurred at 9 cm above the bed. Vertical concentration profiles were obtained downstream at less than 3 m, after which time the dye had spread 10-15 cm upward. It was therefore assumed that the dye evolved in three dimensions and could be described using a Gaussian curve (equation 3-6). Directly downstream of the release,

$$C(z) = \frac{\dot{m}}{4\pi\sqrt{D_y D_z}} = C_3 \exp\left(-\frac{u\,(z - z_{release})^2}{4D_z x} \right) \tag{3-12}$$

The dye meandered laterally in the field in response to the current direction changing over the course of the flooding period (cf. Christiansen et al., 2000). To ensure that measurements occurred directly downstream of the release, the point of measurements was not fixed. Instead, the fluorometer was used to take repeated transects through the evolving dye cloud and perpendicular to its course. Transects were considered acceptable if the concentration approached zero on both ends. The peak concentration of a given transect was assumed to be directly downstream of the release. The maximum concentrations measured on each of 2 to 16 passes through the cloud were then averaged to find a single concentration at that depth. The curve of concentration over depth was then fit to equation 3-12 in the least-squares sense.

3.5 Longitudinal dispersion, skewness, and patchiness measurements

In both the laboratory and the field, longitudinal dispersion was calculated from individual slug releases of dye (see Figures 3-1 and 3-4). Rhodamine WT or Rhodamine 6G was released from tygon tubing with an outer diameter of 0.64 cm. The end of the tubing was oriented parallel to the direction of flow. In the laboratory, the release velocity was carefully matched to the ambient velocity with the help of a syringe pump (Sage by Orion Research Inc.,

Beverly, MA); in the field, a syringe was depressed slowly by hand. Releases took 0.5 - 2 s each, which was much less than their travel time to the fluorometer (31 to 691 s), so the releases were assumed to be instantaneous slugs.

To prevent dye leaking from the release tube between slugs, after each slug ambient water was slowly sucked back into the tube and the tube was then slowly withdrawn from the water; this perturbation did not markedly affect the released dye cloud. In the laboratory, the recording fluorometer was positioned midwidth and immediately downstream of the dowel array, with the dye released from 50 to 525 cm upstream. The outlet hose was positioned at the same depth as the fluorometer's sampling volume to ensure sampling occurred through the cloud's center.. In the field, the fluorometer was positioned at middepth and downstream of the release point. Only concentration profiles with peak concentrations within the fluorometer's response range (15 to 300 μg/L for Rhodamine WT; 5 to 350 μg/L for Rhodamine 6G) were analyzed.

The following statistical properties of the concentration record, $C(t)$, are useful in subsequent analysis. The zeroth moment, M_o, is the total mass observed by the fluorometer. In one dimension, where $C(t)$ represents the measured concentration over time,

$$M_o \equiv \int_{-\infty}^{\infty} C(t)\, dt \tag{3-13}$$

The first moment, M_1, is the weighted average of the travel time of the observed dye, where the weighting is provided by the concentration at each time. The first moment is defined as:

$$M_1 \equiv \int_{-\infty}^{\infty} t\, C(t)\, dt \tag{3-14}$$

The second moment, M_2, is defined as:

$$M_2 \equiv \int_{-\infty}^{\infty} t^2\, C(t)\, dt \tag{3-15}$$

The third moment, M_3, is defined as:

$$M_3 \equiv \int_{-\infty}^{\infty} t^3\, C(t)\, dt \tag{3-16}$$

The average travel time of the cloud is the time taken by the center of mass to reach the fluorometer:

$$\mu = \frac{M_1}{M_o} \tag{3-17}$$

The variance of the cloud is the second moment with respect to the average travel time normalized by the total mass:

$$\sigma_t^2 \equiv \frac{\int (t-\mu)^2\, C(t)\, dt}{M_o} = \frac{\int t^2\, C(t)\, dt}{M_o} - \frac{2\mu \int t\, C(t)\, dt}{M_o} + \frac{\mu^2 \int C(t)\, dt}{M_o} = \frac{M_2}{M_o} - \mu^2 \tag{3-18}$$

The standard deviation, $\sigma_t = \sqrt{\sigma_t^2}$, is a measure of the length of the cloud in time.

The fluorometer recorded concentration as a function of time. Assuming that the cloud is not changing appreciably as it passes the fluorometer, the fluorometer reading can be translated into a snapshot of the cloud in space by multiplying by its average travel speed, $u_{slug} = x/\mu$. The variance as a function of space is then:

$$\sigma_x^{\,2} \equiv \frac{\int (t-\mu)^2 u_{slug} C(t) dt}{M_o} = u_{slug}\left(\frac{M_2}{M_o} - \mu^2\right) = u_{slug}\sigma_t^{\,2} \tag{3-19}$$

If the diffusive or dispersive process is Fickian, then the resulting concentration distribution will be Gaussian (equation 3-6). In terms of position relative to the release position of the tracer cloud ($x_{release}$, $y_{release}$, $z_{release}$), the solution in three dimensions is:

$$C(x,y,z,t) = \frac{M}{(4\pi t)^{3/2}\sqrt{D_x D_y D_z}} \exp\left[-\frac{(x-x_{release})^2}{4D_x t} - \frac{(y-y_{release})^2}{4D_y t} - \frac{(z-z_{release})^2}{4D_z t}\right] \quad (3\text{-}20)$$

where D_x, D_y, and D_z are the diffusivities in the x, y, and z directions, respectively. In a system advecting in the x direction at speed u, directly downstream of the point of release $y - y_{release} = z - z_{release} = 0$. Directly downstream of the point of release,

$$C(x,t) = \frac{M}{(4\pi t)^{3/2}\sqrt{D_x D_y D_z}} \exp\left[-\frac{(x-ut)^2}{4D_x t}\right] \quad (3\text{-}21)$$

In this situation, the spatial variance, σ_x^2, is directly related to the cloud length.

The cloud skewness, S, is a nondimensional number that characterizes the shape of a distribution (Press et al., 1992). For a concentration distribution as a function of time,

$$S = M_3/\sigma_t^3 \quad (3\text{-}22)$$

A positive skewness ($S > 0$) indicates a distribution biased to short times, with the peak occurring before the center of mass and a long tail stretching out to high time. A negative skewness ($S < 0$) indicates a distribution biased to long times, with the peak occurring after the center of mass.

Before calculating the variance and skewness, all analyzed concentration profiles were normalized by the total area under the curve:

$$C_*(t) = C(t)/M_o \quad (3\text{-}23)$$

Note that the area under the $C_*(t)$ curve is unity and hence is a probability density function (PDF) of the tracer passage time. Therefore, if the dispersion process is identical, curves from different releases will align, even if different masses of tracer are released. In addition, this transformation corrects for the effect of release position. Lateral or vertical diffusion may cause the center of mass of the tracer cloud to wander from directly downstream of the point of release, which would affect the measured value of the uncorrected downstream concentration. However, note that diffusion in each of the three directions is independent of diffusion in any other direction. The above equation for the concentration profile of an instantaneous release (equation 3-20) can therefore be separated to reveal the contributions of diffusion in each of the three directions independently:

$$C(x,y,z,t) = M\left\{\frac{1}{\sqrt{4\pi D_x t}}\exp\left[-\frac{(x-ut)^2}{4D_x t}\right]+\frac{1}{\sqrt{4\pi D_y t}}\exp\left[-\frac{(x-ut)^2}{4D_y t}\right]+\frac{1}{\sqrt{4\pi D_z t}}\exp\left[-\frac{(x-ut)^2}{4D_z t}\right]\right\} \quad (3\text{-}24)$$

White (2002) notes that adopting the frozen cloud hypothesis and normalizing by the total longitudinal mass result in an expression for the downstream concentration that is independent of the lateral and vertical diffusivities:

$$C_*(x) = \frac{C(x)}{\int_{-\infty}^{\infty} C(x)dx} = \frac{\exp\left[-\frac{(x-ut)^2}{4D_x t}\right]}{\int_{-\infty}^{\infty}\exp\left[-\frac{(x-ut)^2}{4D_x t}\right]dx} \quad (3\text{-}25)$$

Therefore, after normalization, tracer clouds from separate realizations will appear identical if they experience the same longitudinal processes, regardless of lateral and vertical motion, if diffusivities are constant temporally and spatially.

Between 5 and 37 releases were performed for several different distances between the release point and the fluorometer in both the laboratory and the field. The coefficient of longitudinal dispersion is defined as the rate of growth in space of these clouds. That value of the longitudinal dispersion coefficient was then calculated assuming a Fickian process, so that

the dispersion constant is proportional to the rate of increase in spatial variance of the tracer cloud (equation 2-25). K_x was calculated from the best linear fit in the least-squares sense to the plot of variance versus time. To give each distance the same weighting, the equation was fit to the mean travel time and mean variance of each distance.

In addition, the ensemble average concentration (curve shape), $\overline{C}(t)$, was calculated for each distance. Calculating the variance for each curve separately has the effect of aligning the curves by the first moment. The ensemble average was then taken after the superposition of the centers of mass. This has the effect of increasing the mean peak concentration and decreasing the variance (cf. Fischer et al., 1979). Because the concentration data are discrete, some interpolation was necessary to enable ensemble averaging. The relative patchiness of each curve, C_{rms}, was then calculated by comparison with the ensemble average:

$$C_{rms} = \sqrt{\frac{1}{N-1}\sum (C - \overline{C})^2} \tag{3-26}$$

where N is the number of concentration measurements in the profile.

Chapter 4

Laboratory Results and Discussion

The next two chapters present and discuss measurements of velocity, vertical diffusivity and longitudinal dispersion performed in a simulated vegetated canopy in a laboratory and in a salt marsh. Data on concentration curve skewness and patchiness are also presented.

4.1 Velocity

4.1.1 Mean flow

Velocity measurements confirmed that for all flow rates water moved faster in the lower, sparser canopy (0-10 cm from the bed, $ad = 0.012$) than in the upper, denser canopy (10-20 cm from the bed, $ad = 0.024$; see Table 4-1). For the lowest flow rate (which produced an average travel velocity of 0.8 cm/s for slugs released at the interface), LDV measurements indicated that mean longitudinal velocities were relatively constant in both the upper and lower canopies (Figure 4-1). The profile shows that the bottom boundary layer is confined to within 1 cm of the bed. For the highest flow rate (which produced an average travel time of 4.1 cm/s for slugs released at the interface), mean longitudinal velocity appears less constant over depth, especially

in the upper canopy. The probe head of the 3-D sideways-looking ADV was too wide to measure the bottom boundary layer directly. Other studies, however, have observed that the thickness of the bottom boundary layer is on the same scale as the stem diameter (Nepf et al.,

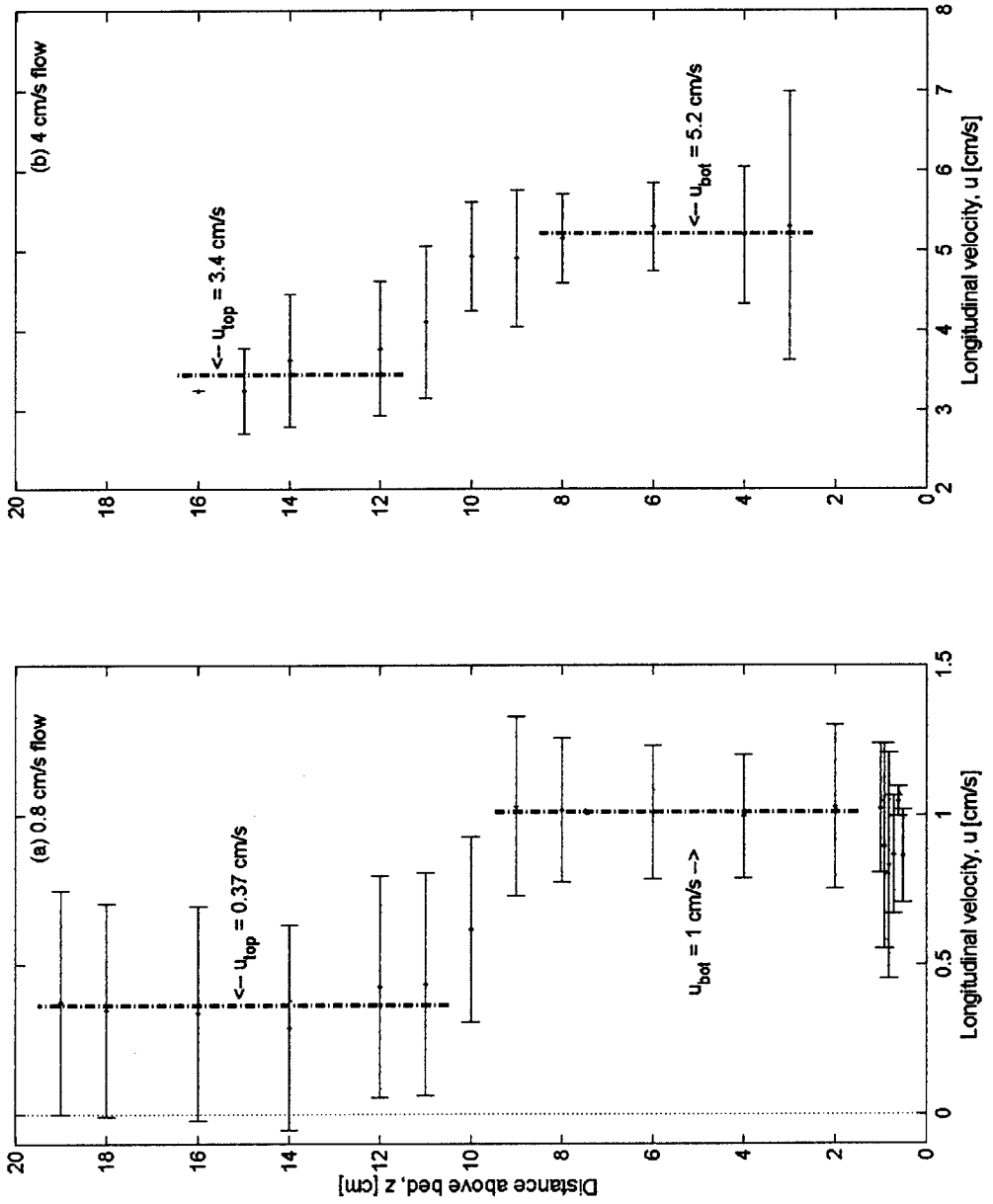

Figure 4-1. Vertical profiles of longitudinal velocity in the laboratory canopy. Data points are means of six measurements taken farther than 2 cm from the flume wall; horizontal bars indicate standard error of the mean across canopy heterogeneity. (a) LDV measurements of velocity in the slowest flow rate (0.8 cm/s as experienced by dye slugs released 10 cm from the bed). (b) 3D ADV measurements of velocity for the highest flow rate (4 cm/s as experienced by dye slugs released 10 cm from the bed). The point with no error bar is the time-averaged velocity at a single location; its error is expected to be comparable to that of the points directly below it.

Table 4-1. Velocity measurements for different flow rates used in the laboratory. All data are mean ± standard error of the mean in cm/s. For LDV and ADV measurements, the standard error represents variability across canopy heterogeneity; for slug travel times, the standard error represents variability among different dye slugs. The interface is located at 10 cm from the bed. LDV measurements were performed at the lowest flow rate in the lower canopy at 6 cm from the bed and in the upper canopy at 14 cm from the bed. 3-D ADV measurements were performed at the highest flow rate in the lower canopy between 3 and 8 cm from the bed and in the upper canopy between 12 and 16 cm from the bed. Slugs were released in the lower canopy at 4 cm from the bed and in the upper canopy at 16 cm from the bed.

Location	Method	Flow rate			
		Lowest	Second lowest	Second highest	Highest
Interface (10 cm)	Point measurements	0.62 ± 0.31	-	-	4.90 ± 0.86
	Slug travel time	0.81 ± 0.03	1.98 ± 0.05	3.08 ± 0.05	4.09 ± 0.08
Lower canopy (0-10 cm)	Point measurements	1.01 ± 0.11	-	-	5.22 ± 0.35
	Slug travel time	1.16 ± 0.02	2.66 ± 0.19	-	5.41 ± 0.07
Upper canopy (10-20 cm)	Point measurements	0.38 ± 0.15	-	-	3.45 ± 0.40
	Slug travel time	0.63 ± 0.02	1.32 ± 0.07	-	2.82 ± 0.03

1997b), so the boundary layer at 4 cm/s is likely to be on the same scale as the 1 cm observed for the lowest flow rate.

Lateral profiles of longitudinal velocity show that each side-wall boundary layer at the lowest flow velocity is less than 2 cm wide and that velocities are roughly constant over the middle 16 cm of the flume (Figure 4-2).

Another way of calculating velocity is from the travel time of the center of mass of a slug release, divided into the distance traveled by the slug ($u = x/t_{avg}$). Inferred velocities for slugs released and measured at 10 cm and 4 cm from the bed agree quite well with the velocities measured at the interface and in the lower canopy, respectively, by the LDV and ADV (Table 4-1). A 3-way ANOVA comparing type of release, canopy of release, and velocity shows indicates that the type of release is not significant ($p > 0.05$), though a 2-way ANOVA in either the top or bottom canopy individually suggests that there is an effect of measurement ($p < 0.05$).

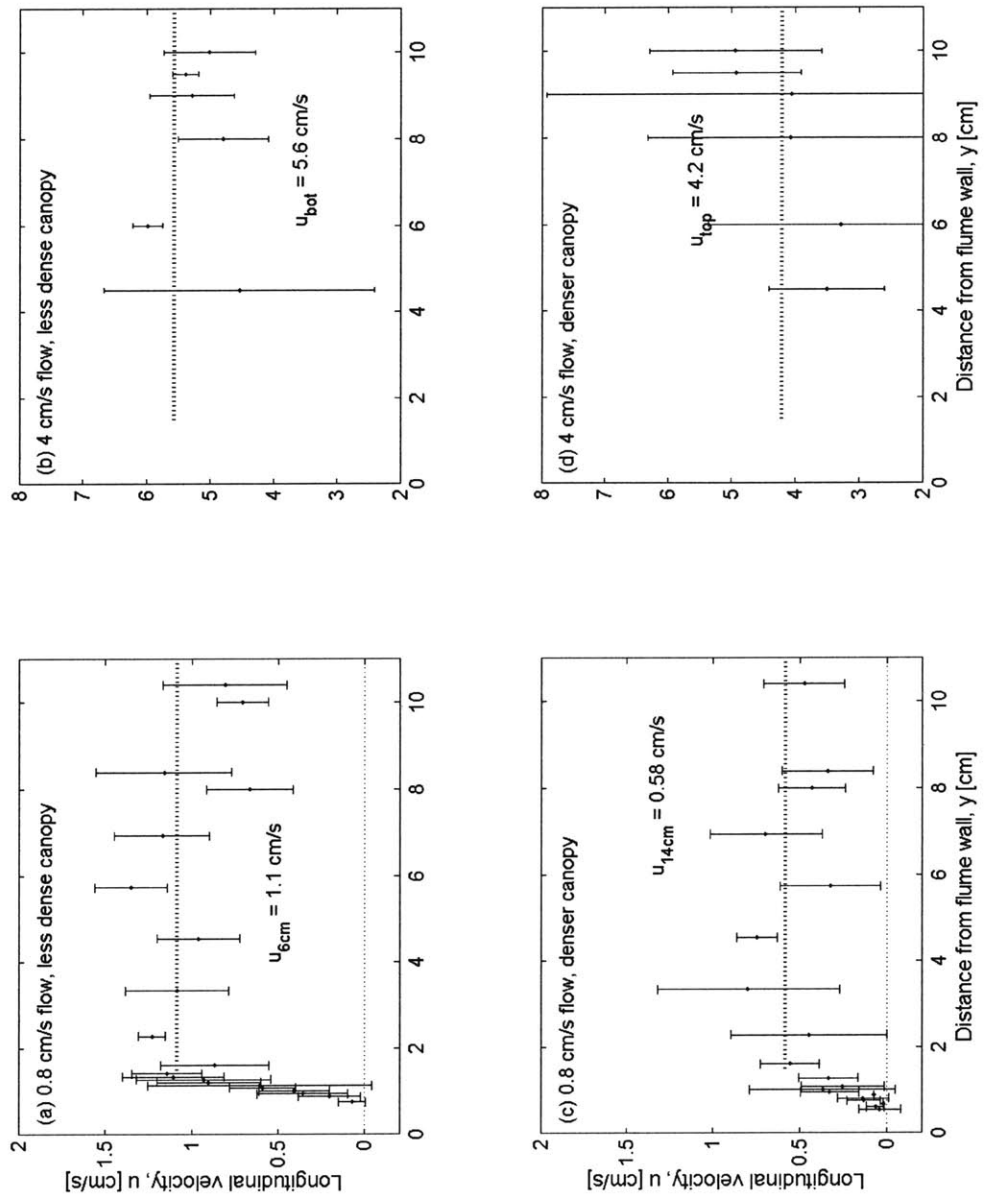

Figure 4-2. Lateral profiles of longitudinal velocity in the laboratory canopy. Data points are means of four to six measurements; horizontal bars indicate standard error of the mean across canopy heterogeneity. (a) LDV measurements of velocity 6 cm from the bed in the slowest flow rate (0.8 cm/s as experienced by dye slugs released 10 cm from the bed). (b) 3D ADV measurements of velocity 3 to 8 cm from the bed for the highest flow rate (4 cm/s as experienced by dye slugs released 10 cm from the bed). (c) LDV measurements of velocity 14 cm from the bed in the slowest flow rate. (d) 3D ADV measurements of velocity 12 to 16 cm from the bed for the highest flow rate.

Table 4-2. Estimated drag for different flow rates in the laboratory, calculated using velocities inferred from the travel time of dye slugs (data repeated from Table 4-1). All data are mean ± standard error of the mean across different slug releases. When calculating Re_d, it was assumed that $\upsilon \sim 0.01$ cm^2/s.

Flow variable	Location	Flow rate			
		Lowest	Second lowest	Second highest	Highest
u [cm/s]	Interface	0.81 ± 0.03	1.98 ± 0.05	3.08 ± 0.05	4.09 ± 0.08
	Lower canopy	1.16 ± 0.02	2.66 ± 0.19	-	5.41 ± 0.07
	Upper canopy	0.63 ± 0.02	1.32 ± 0.07	-	2.82 ± 0.03
Re_d	Interface	51 ± 2	126 ± 4	196 ± 4	260 ± 7
	Lower canopy	74 ± 2	169 ± 12	-	344 ± 7
	Upper canopy	40 ± 1	84 ± 5	-	179 ± 3
C_d	Interface	1.74 ± 0.02	1.41 ± 0.01	-	1.26 ± 0.004
	Lower canopy	1.59 ± 0.01	1.34 ± 0.02	-	1.21 ± 0.003
	Upper canopy	1.88 ± 0.02	1.54 ± 0.02	-	1.33 ± 0.004
a [cm^2/cm^3]	Lower canopy	0.019	0.019	0.019	0.019
	Upper canopy	0.038	0.038	0.038	0.038
u_{top}/u_{bot}		0.54 ± 0.02	0.50 ± 0.04	-	0.52 ± 0.01
$(a_{bot}/a_{top})^{1/2}$		0.71	0.71	-	0.71
$[(C_da)_{bot}/(C_da)_{top}]^{1/2}$		0.65 ± 0.01	0.66 ± 0.01	-	0.68 ± 0.002
$\Delta u / U = (u_{top} - u_{bot})/\frac{1}{2}(u_{top} + u_{bot})$		0.59 ± 0.03	0.67 ± 0.13	-	0.63 ± 0.02
$2\left(\frac{1-\sqrt{(C_da)_{bot}/(C_da)_{top}}}{1+\sqrt{(C_da)_{bot}/(C_da)_{top}}}\right)$		0.42 ± 0.002	0.41 ± 0.004	-	0.39 ± 0.001

(For example, velocities calculated from slug releases at 14 cm from the bed, however, are slightly different from the values recorded by the LDV and ADV in the upper canopy.)

If flow through the canopy in the mid-section of the flume depends solely on the balance of pressure forcing and drag due to vegetation, then the shape of the velocity profile will remain constant even as the depth-averaged velocity changes (equation 2-40). In particular, since there is a sharp demarcation between the two different canopy densities, it would be expected that there is a step change in the velocity profile, with velocity constant over depth at a value U_{bot} in the lower canopy and constant over depth at a different value, $U_{top,}$ in the upper canopy. In fact, the velocity at both the lowest and highest flow rates did appear relatively constant within each of the upper and lower canopies (Figure 4-1). In addition, the interface between the upper and lower canopies is approximately 2 cm wide for both the lowest and the highest flow rates.

Over the studied velocity range, there is a clear relationship between the velocities in the upper and lower canopies and at the interface between them (Figure 4-3). There was a linear relationship between the velocity experienced by the slugs released and measured at the interface and that experienced by the slugs released and measured in the lower canopy ($r^2 = 0.998$) and that experienced by the slugs released and measured in the upper canopy ($r^2 > 0.999$). Based on the drag forcing, it should be true that $U_{top}/U_{bot} = [(C_d a)_{bot}/(C_d a)_{top}]^{1/2}$. Results were slightly lower than theory (Table 4-2).

Even though the mean velocity profile is relatively constant, the canopy contains a large amount of stem-scale heterogeneity. The sampling volumes of both the LDV and ADV are on the order of 1 cm long, so they cannot revolve heterogeneity on a scale smaller than that of a 0.6-cm diameter stem. The remaining heterogeneity is still large, however, which presents difficulties for averaging over it. For example, the average velocity observed for 36 locations in the upper canopy at the lowest flow rate is 0.38 ± 0.15 cm/s (mean weighted by variance ± standard error of the mean over canopy heterogeneity weighted by variance), but the average velocity observed for 54 different locations on a lateral profile 16 cm above the bed is 0.58 ± 0.07 cm/s, even though it appears that velocity is constant over depth and width in the upper

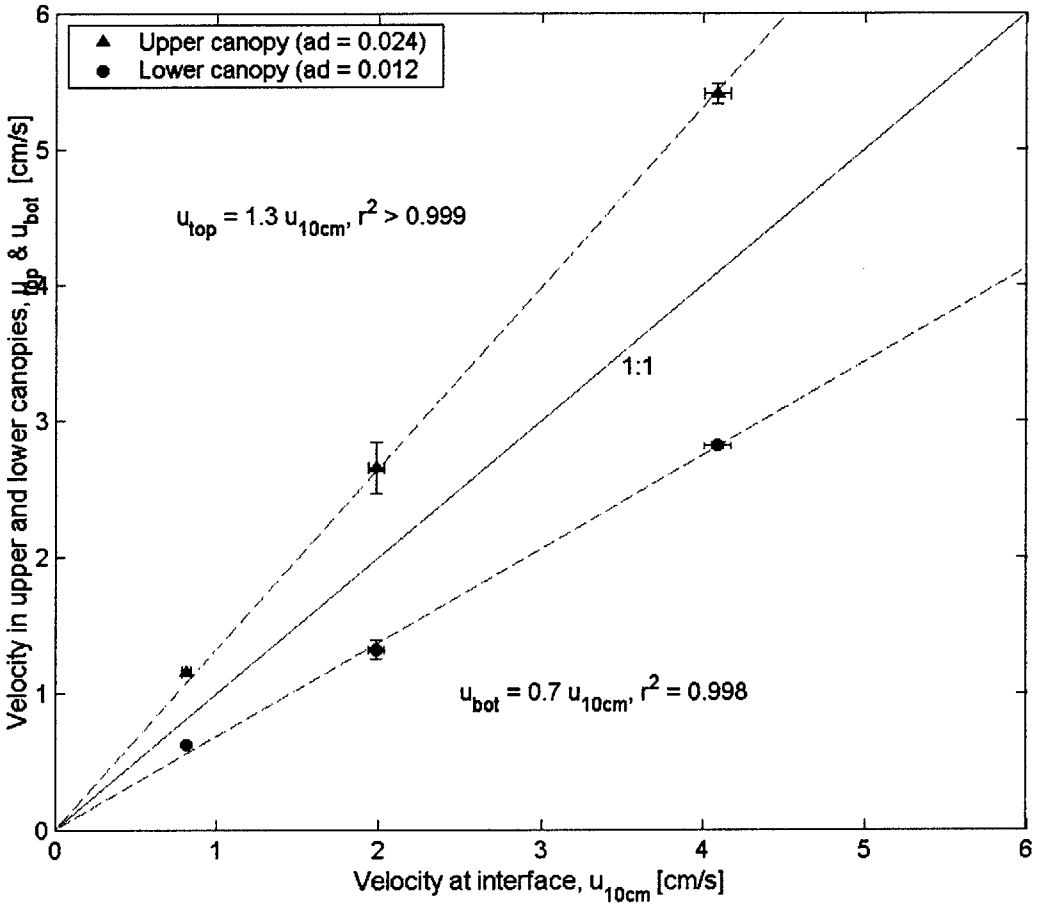

Figure 4-3. Velocities experienced by slug releases moving through the laboratory canopy. Velocities are calculated based on the average travel time of the center of mass. Vertical and horizontal bars indicate standard error of the mean across different slug releases.

canopy at this flow rate. The extremely heterogeneous velocity field makes it difficult to infer a canopy-averaged flow rate from a few point measurements and also contributes to dispersion.

Within uncertainty, mean vertical velocities farther than 2 cm away from the flume walls and bottom at both the lowest and highest flow rates in both the upper and lower canopies were indistinguishable from zero with no trends (data not shown). However, there is net vertical motion within the side boundary layer in the upper canopy at the lowest flow rate (Figure 4-4). (Data were not collected within 2 cm of the flume wall for any other flow rate.) The increased stem drag, acting in concert with the finite-width flume, apparently creates secondary circulation.

4.1.2 Spectra

In general, spectra are similar to those observed in other canopies (Leonard and Luther, 1995; Finelli, 2000): the majority of flow energy is concentrated at lower frequencies, then cascades down to high frequencies.

Spectra at the lowest and highest flow rates both lack clear features indicating instabilities in the flow (Figures 4-5 and 4-6). In particular, they lack a peak near the expected vortex shedding frequency, $f_{shed} = u_{local}S/d$, which equals 0.3 Hz in the lower canopy and 0.1 Hz in the upper canopy for the low flow rate and 1.7 Hz in the lower canopy and 0.8 Hz in the upper canopy for the high flow rate.

4.1.3 Turbulence and Reynolds stresses

Turbulence levels, as measured by $u_{rms}/u_{avg,canopy}$, are higher in the lower canopy for both the lowest and the highest flow rates (Figure 4-7). When normalized by the average flow velocity, the relative amount of turbulence decreases in the higher flow condition (Table 4-3). Similarly, Finelli (2000) observed that the magnitude of turbulence intensity was similar between slow and fast flow conditions, so the relative amount of turbulence decreased.

Zavistoski (1994) normalized her velocity profiles of flow around an array of circular

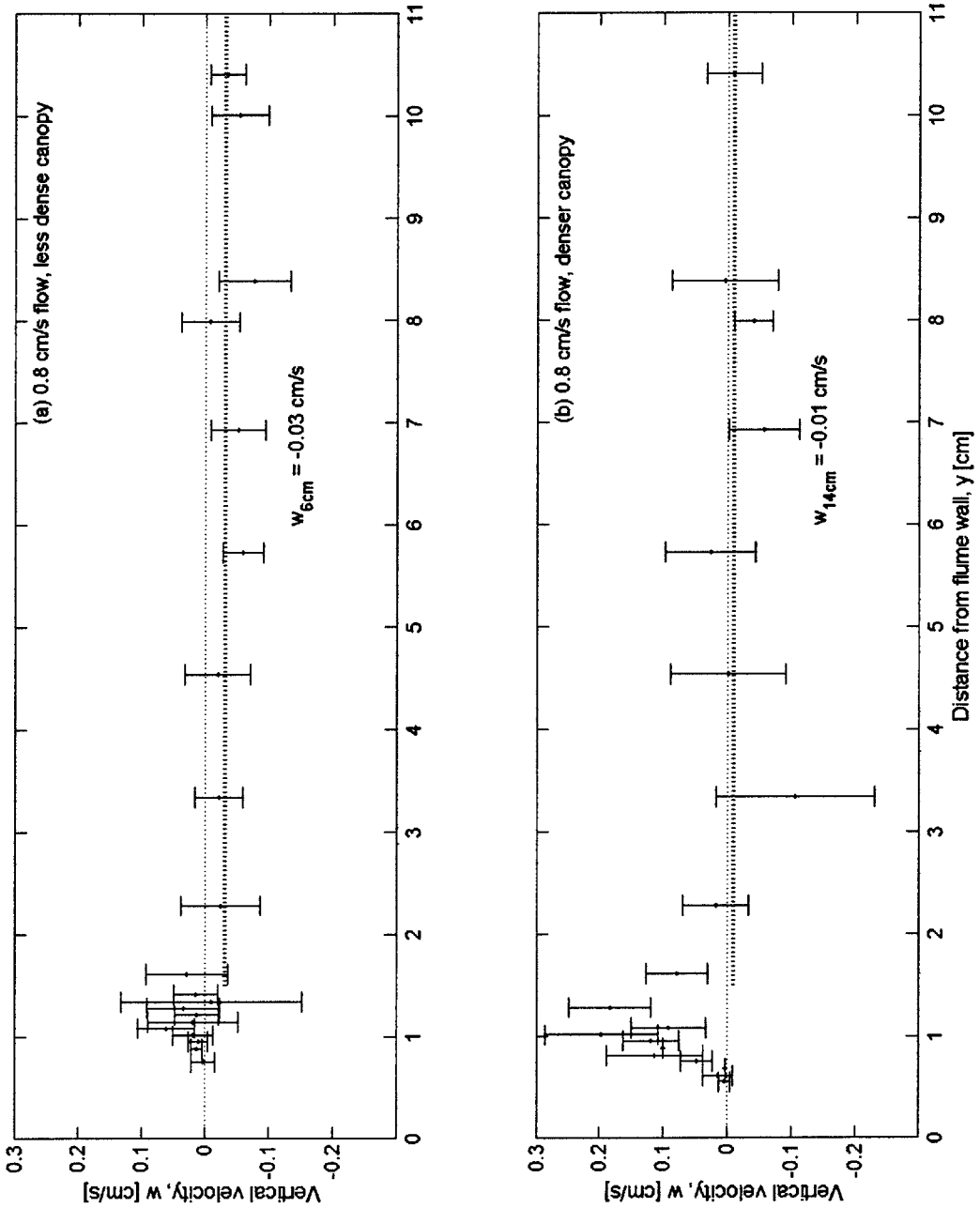

Figure 4-4. Lateral profiles of vertical velocity in the laboratory canopy. Measurements were taken using an LDV at the slowest flow rate (0.8 cm/s as experienced by dye slugs released 10 cm from the bed). Data points are means of four to six measurements; horizontal bars indicate standard error of the mean across canopy heterogeneity. (a) Measurements 6 cm from the bed. (b) Measurements 14 cm from the bed.

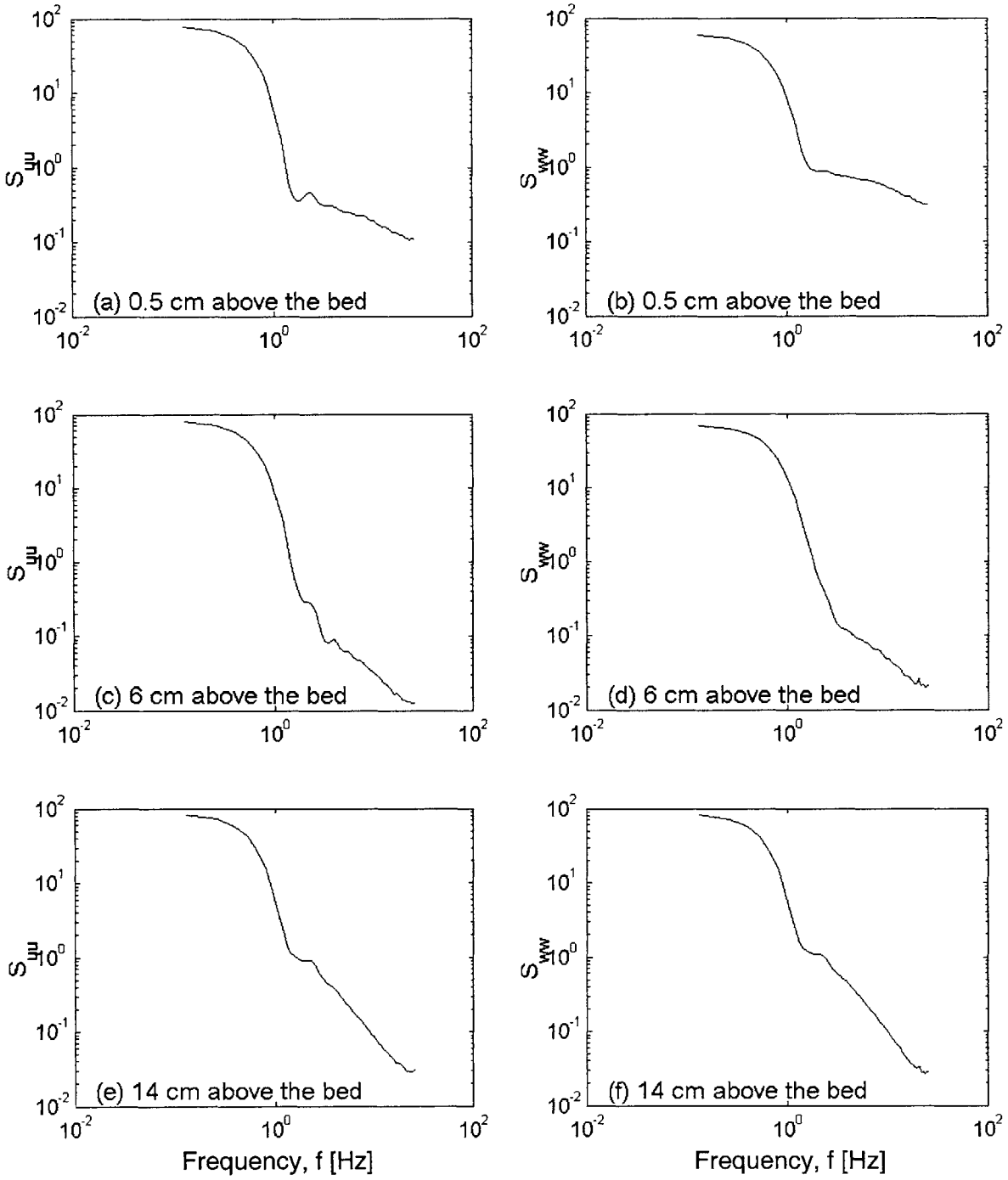

Figure 4-5. Spectra of velocities in the laboratory canopy for the lowest flow rate. Spectra are calculated from 15-minute LDV records using a Parzen window with a nondimensional length $L = 64$. (a), (c), & (e) Spectra of longitudinal velocity, u, at various distances above the bed. (b), (d), & (f) Spectra of vertical velocity, w, from the same velocity records.

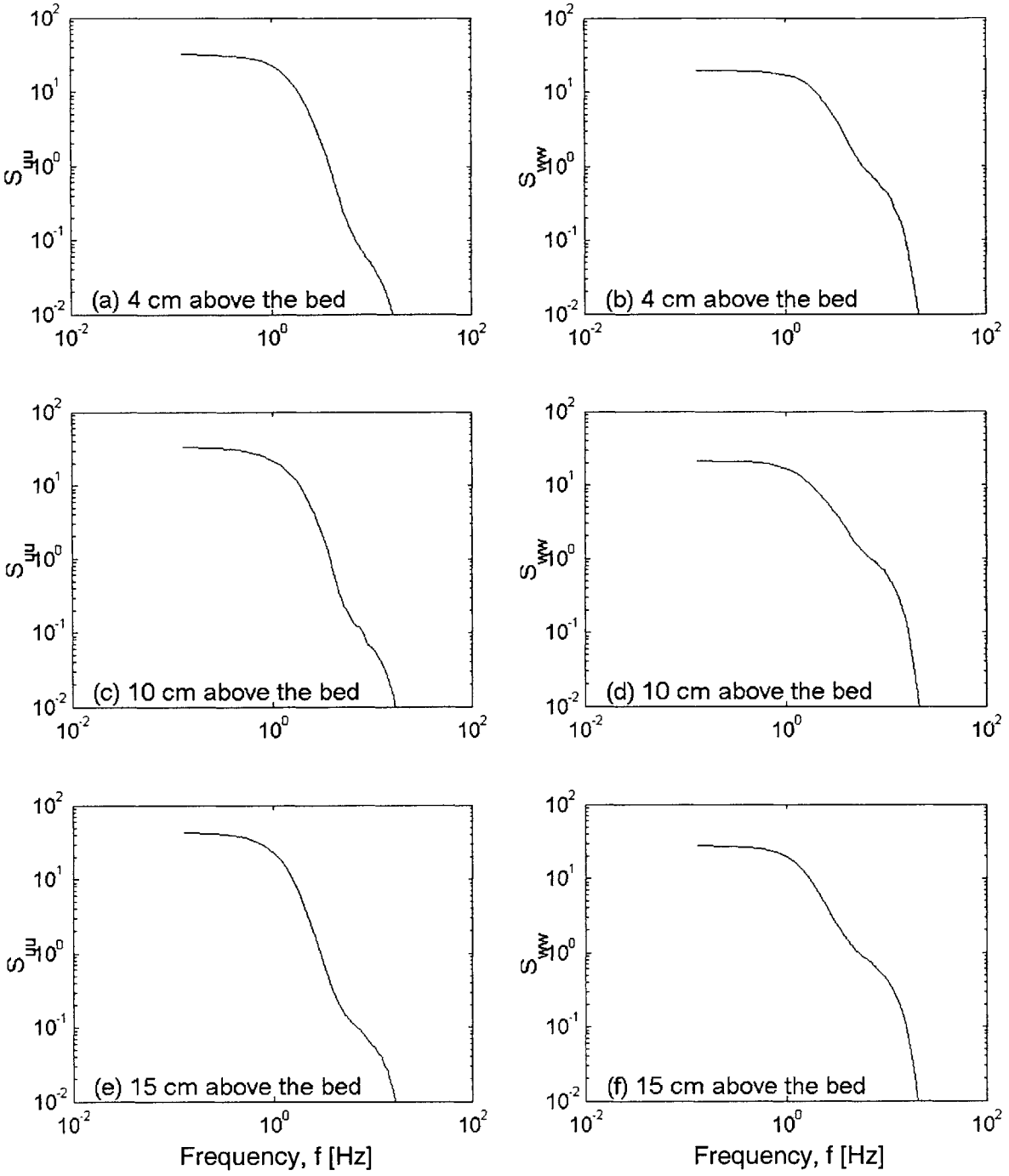

Figure 4-6. Mean spectra of velocities in the laboratory canopy for the highest flow rate. Spectra are averages over 6 spectra calculated from 5-minute ADV records using a Parzen window with a nondimensional length $L = 64$. (a), (c), & (e) Spectra of longitudinal velocity, u, at various distances above the bed. (b), (d), & (f) Spectra of vertical velocity, w, from the same velocity records.

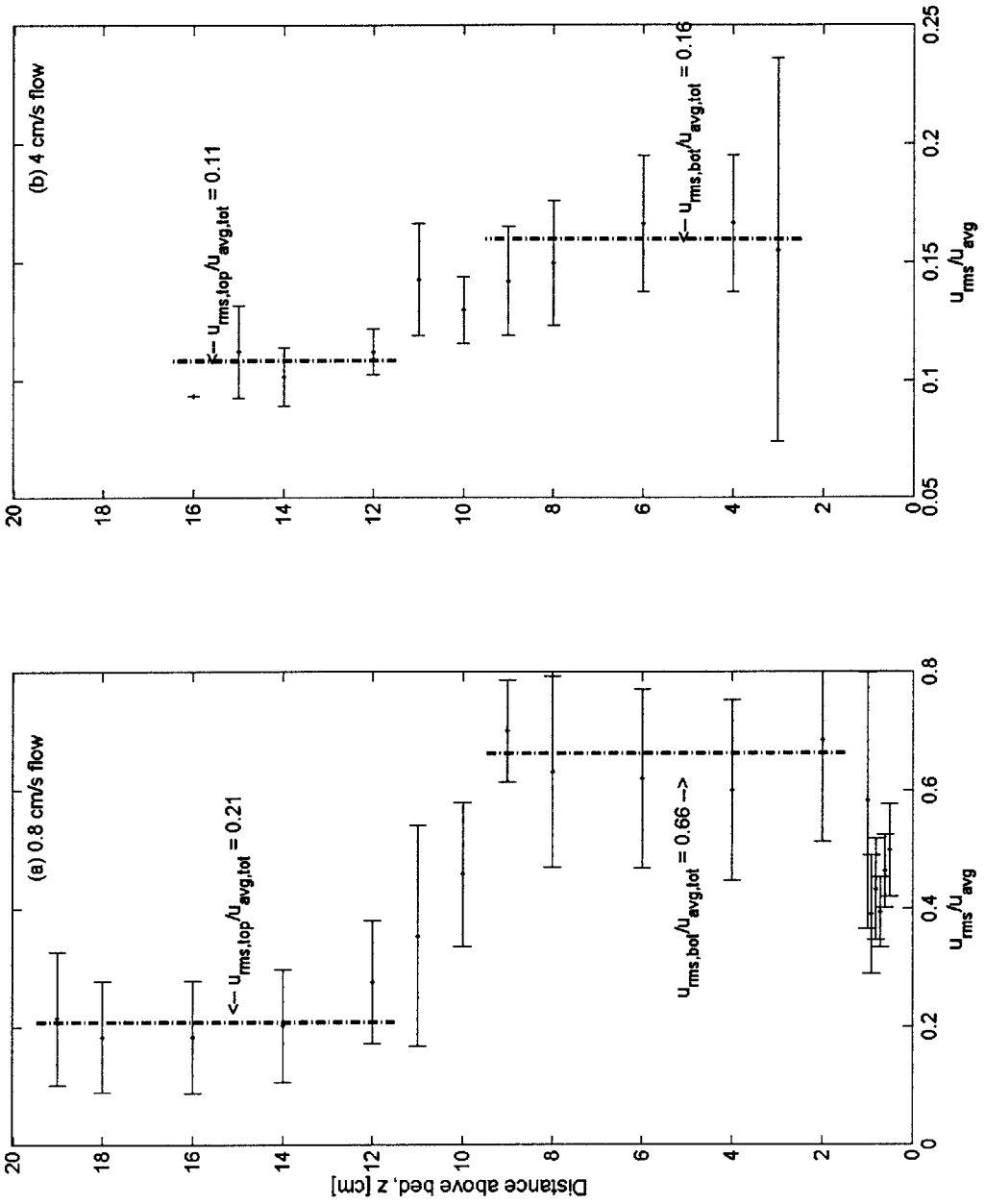

Figure 4-7. Vertical profiles of longitudinal turbulent energy in the laboratory canopy. Measurements are presented as $u_{rms} = \sqrt{u'}$, normalized by the average flow velocity for the entire profile. Data points are means of six measurements taken farther than 2 cm from the flume wall; horizontal bars indicate standard error of the mean across canopy heterogeneity. (a) LDV measurements of energy for the slowest flow rate (0.8 cm/s as experienced by dye slugs released 10 cm from the bed). (b) 3D ADV measurements of energy for the highest flow rate (4 cm/s as experienced by dye slugs released 10 cm from the bed).

Table 4-3. Turbulence statistics for different flow rates used in the laboratory. All data are mean ± standard error of the mean, where the standard error represents variability across canopy heterogeneity. LDV measurements were performed at the lowest flow rate in the lower canopy at 6 cm from the bed and in the upper canopy at 14 cm from the bed. 3-D ADV measurements were performed at the highest flow rate in the lower canopy between 3 and 8 cm from the bed and in the upper canopy between 12 and 16 cm from the bed.

Flow variable	Location	Flow rate	
		Lowest	Highest
u_{rms}/u_{avg}	Lower canopy	0.66 ± 0.06	0.16 ± 0.02
	Upper canopy	0.21 ± 0.04	0.11 ± 0.01
$u_{rms,top}/u_{rms,bot}$	-	0.33 ± 0.07	0.68 ± 0.08
Reynolds stress, $\overline{u'w'}$ [cm^2/s^2]	Lower canopy	-0.02 ± 0.01	-
	Upper canopy	-0.003 ± 0.003	-
Turbulent efficiency, $\overline{u'w'}/\sigma_u\sigma_w$	Lower canopy	-0.24 ± 0.09	-
	Upper canopy	-0.15 ± 0.17	-

cylinders by the velocity at 10 cm from the bed. She reports values of $u_{rms}/u_{10} = 0.18$ for $ad = 0.008$, $u_{rms}/u_{10} = 0.22$ for $ad = 0.018$, and $u_{rms}/u_{10} = 0.39$ for $ad = 0.068$. Values in the present study are on the same order of magnitude, but they show higher turbulence intensity in the less dense canopy. Similarly, Granata et al. (2001) reported that turbulent energy decreased with increasing plant density.

Vertical profiles of Reynolds stress at the lowest flow rate show that Reynolds stresses peak at the interface between the upper and lower canopies, where the greatest amount of shear is present (Figure 4-8). In addition, Reynolds stresses are larger in the lower canopy than the upper canopy, reflecting the faster velocities and additional turbulent energy present in the sparser vegetation.

Similarly, turbulent efficiency at the lowest flow rate peaks at the interface (Figure 4-9). In terrestrial canopies, an absolute value of efficiency greater than 0.5 indicates that coherent vertical vortices have formed at the shear layer (Raupach et al., 1996). Here, the turbulent

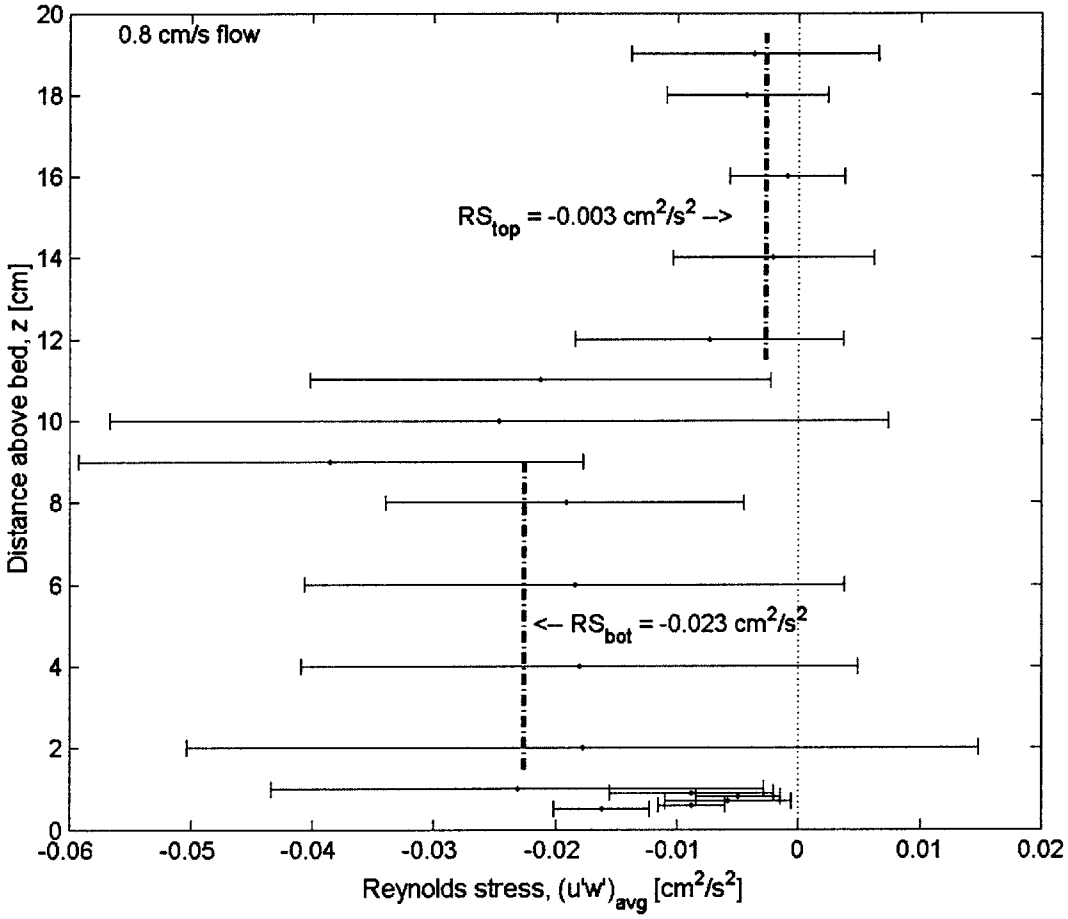

Figure 4-8. Vertical profile of Reynolds stress in the laboratory canopy. Measurements were taken using an LDV at the slowest flow rate (0.8 cm/s as experienced by dye slugs released 10 cm from the bed). Data points are means of six measurements taken farther than 2 cm from the flume wall; horizontal bars indicate standard error of the mean across canopy heterogeneity.

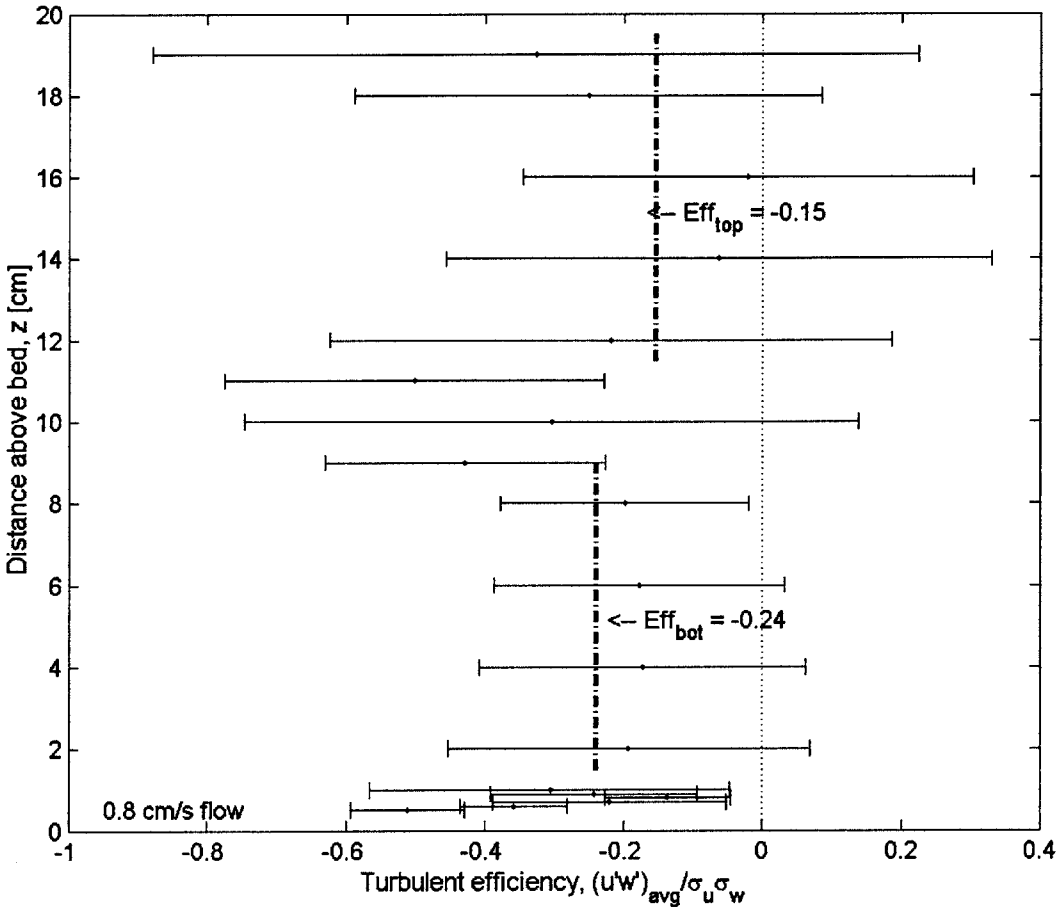

Figure 4-9. Vertical profile of turbulent efficiency in the laboratory canopy. Measurements were taken using an LDV at the slowest flow rate (0.8 cm/s as experienced by dye slugs released 10 cm from the bed). Data points are means of six measurements taken farther than 2 cm from the flume wall; horizontal bars indicate standard error of the mean across canopy heterogeneity.

efficiency is approaching that threshold. Turbulent efficiency is not different between the upper and lower canopies.

4.2 Vertical diffusivity

Vertical diffusivity in the laboratory was calculated from fitting curves to the shape of vertical concentration profiles downstream of a continuous release (Figure 4-10), using the vertical diffusivity as the fitting constant. It is expected that the dye cloud downstream of the continuous release in the lower canopy will have a Gaussian cross-section with an image source at the bed (equation 3-7), so a Gaussian curve was fit to the measurements in the less dense lower canopy downstream of the release (Figures 4-11 and 4-12). An error function is more suitable in the denser upper canopy (equation 3-11), which the dye reaches after it travels over the extent of the lower canopy, so it was used to fit the data between 10 and 16 cm. The measured dye concentrations at greater than 16 cm from the bed (e.g., present at 360 and 408 cm downstream) were not used to calculate vertical diffusivity because they are not predicted by any diffusion model. Instead, it is likely that the vertical jet near the sidewall in the upper canopy (Figure 4-4) is transporting dye up to the surface.

In at least one of the plots [e.g., Figure 4-11(g)], the concentration in the lower canopy near the interface is elevated over the expected Gaussian curve. In addition, during experimentation, dye was observed to accumulate at the interface between the upper and lower halves of the canopy, suggesting that the interface between the two densities behaves as a partial no-flux boundary. It would then be experienced by the lower canopy as partially reflective. Mathematically, a no-flux boundary is equivalent to an image source located an equal distance on the other side of the boundary. Therefore, an additional curve was fit to the data in the lower canopy: a Gaussian profile with an image source at 20 cm from the bed to produce no flux at the interface (equation 3-9). This curve appears to fit the data at least as well as a simple Gaussian profile.

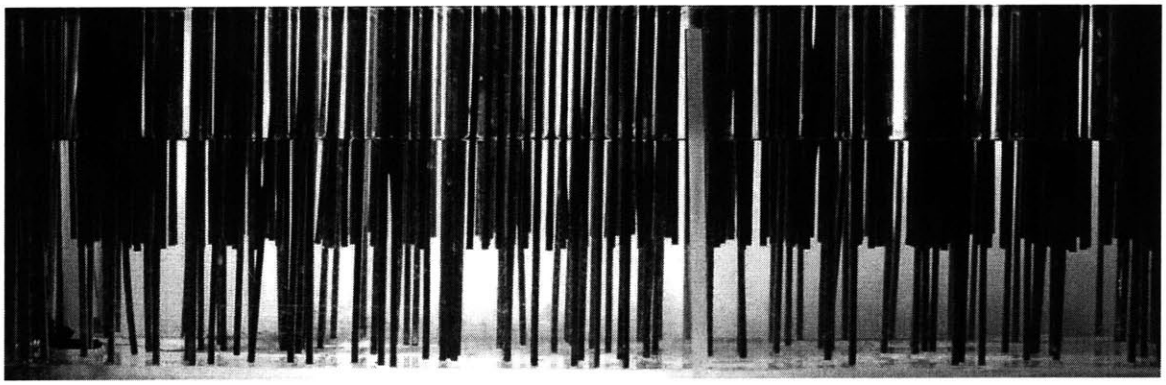

Figure 4-10. Continuous release of Rhodamine WT at the interface in the laboratory flume. The dense ($ad = 0.024$) canopy occupies the top half of the flume and the less dense ($ad = 0.012$) canopy the lower half. Flow is proceeding from left to right with a velocity of 4.1 cm/s at the interface. Individual filaments of dye are visible directly downstream of the injection needle; farther downstream, the cloud is more diffuse and locally well-mixed.

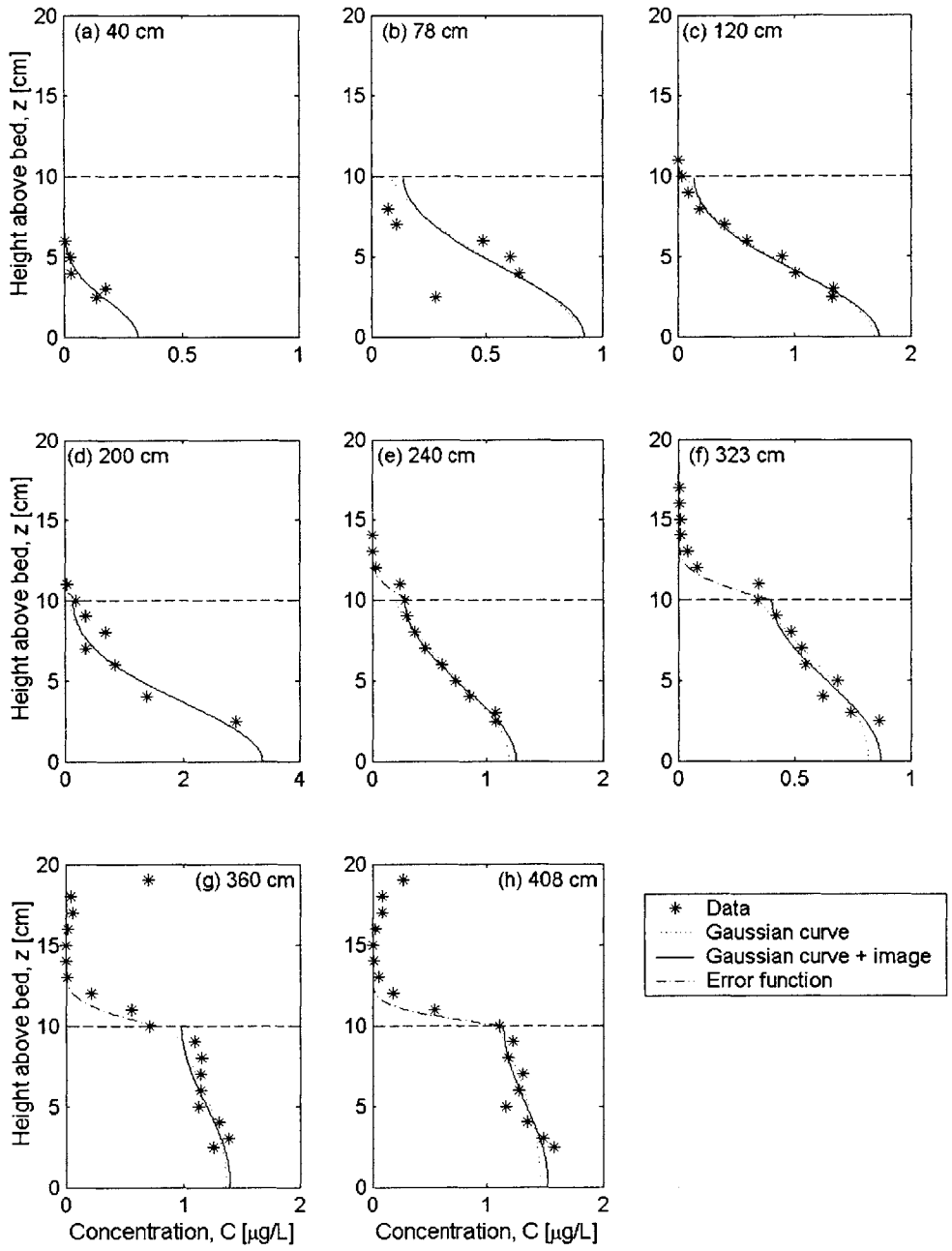

Figure 4-11. Average dye concentrations in the laboratory downstream of a continuous release at the bed with the lowest flow rate. The distance between the release and the measurement location is shown on each subplot. Three best-fit lines are plotted with the data, each using a different fitting curve: data points up to 10 cm from the bed are fit with both a Gaussian curve, assuming a release at the bed, and a Gaussian curve assuming a release at the bed and an image source located at 20 cm from the bed. Data points from 10 cm to 16 cm from the bed are fit with an error function, assuming that the release is located at 10 cm from the bed and 100 cm downstream of its actual position.

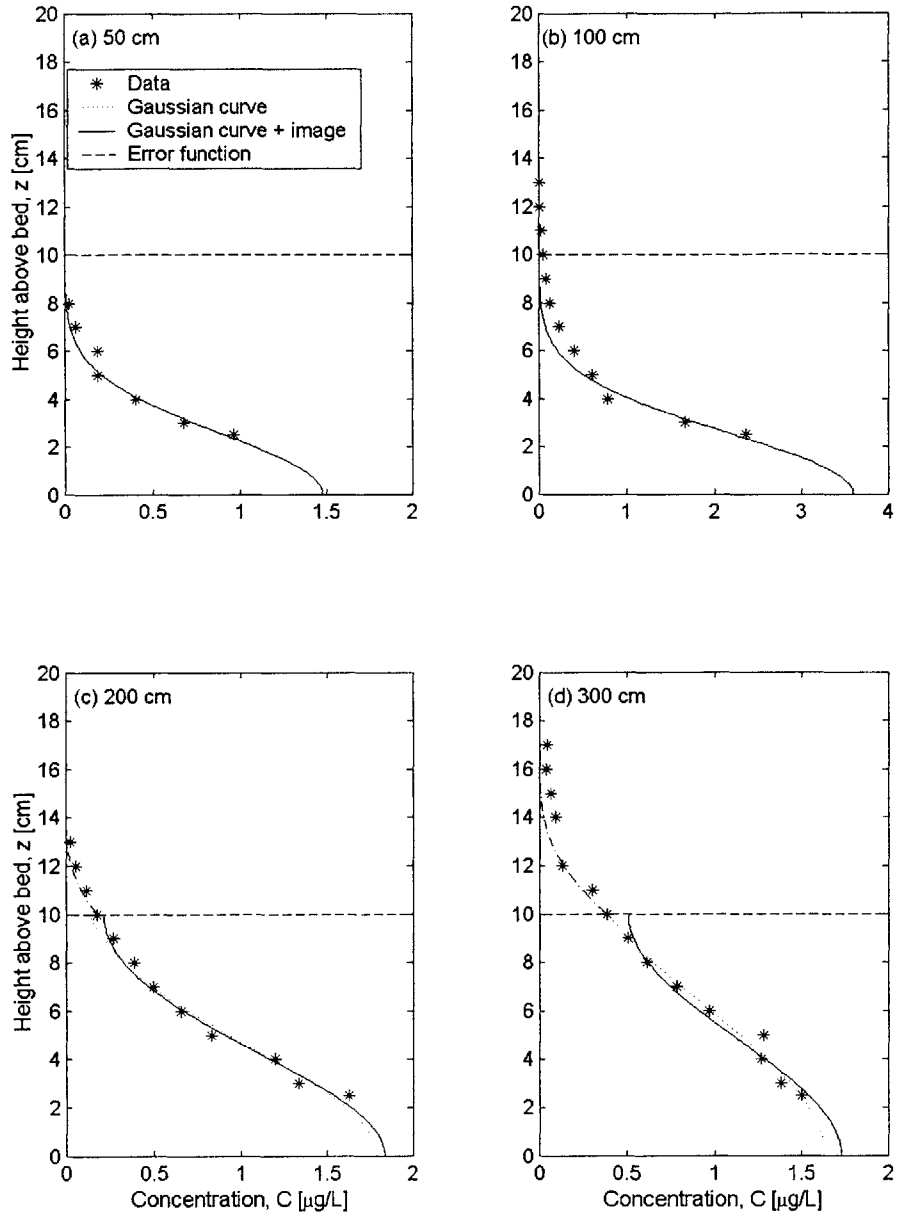

Figure 4-12. Average dye concentrations in the laboratory downstream of a continuous release at the bed with the highest flow rate. The distance between the release and the measurement location is shown on each subplot. Concentration is measured in voltage, which is proportional to dye concentration. Three best-fit lines are plotted with the data, each using a different fitting curve: data points up to 10 cm from the bed are fit with both a Gaussian curve, assuming a release at the bed, and a Gaussian curve assuming a release at the bed and an image source located at 20 cm from the bed. Data points including and above 10 cm from the bed are fit with an error function, assuming that the release is located at 10 cm from the bed and 75 cm downstream of its actual position.

Table 4-4. Vertical diffusion in the laboratory. All data are presented as a spatial mean ± standard error of the mean over various distances downstream of a continuous release.

Vertical diffusivity	Location	Stem density, ad	Flow conditions	
			Lowest flow rate	Highest flow rate
D_z [cm^2/s]	Lower canopy	0.012	0.057 ± 0.025	0.25 ± 0.16
	Upper canopy	0.024	0.002 ± 0.002	0.04 ± 0.08

The vertical diffusivity, D_z, is the fitting constant used to produce the shapes of these curves. Estimates of D_z at various locations downstream of the continuous release at the lowest and highest flow rates are shown in Figures 4-13 and 4-14, respectively. At both flow rates, the vertical diffusivity is much higher in the lower, less dense canopy. This observation further supports the possibility that the interface behaves as a partial no-flux boundary, because dye is transported to the interface more quickly than it can pass through into the upper canopy.

In a spatially unchanging canopy, vertical diffusivity should be constant over space. Within uncertainty, it is constant in the upper canopy at various distances downstream of the release. In the lower canopy, however, especially at the lower flow rate, D_z values calculated using a Gaussian curve without an image source increase rapidly at large distances downstream. The values calculated using an image source, however, remain constant. This difference suggests that the vertical diffusivity constants calculated without an image source are artificially high to account for the elevated dye levels at the interface. Using an image source should therefore give better D_z estimates. Note, however, that the interface is not likely to be a perfect no-flux boundary as was assumed to produce this curve, so these estimates are biased toward lower D_z vales.

Table 4-4 presents spatially-averaged vertical diffusion results. These results are the same order of magnitude as those reported elsewhere for flow through emergent stem arrays. Hosokawa and Horie (1992) reported that a salt solution in 1-3 cm/s flow passing through 4 m of 5-mm-diameter emergent vegetation mimics mixed completely over a water depth of 5-10 cm. These data suggest a vertical diffusivity on the order of 0.02-0.5 cm^2/s. Nepf et al. (1997b)

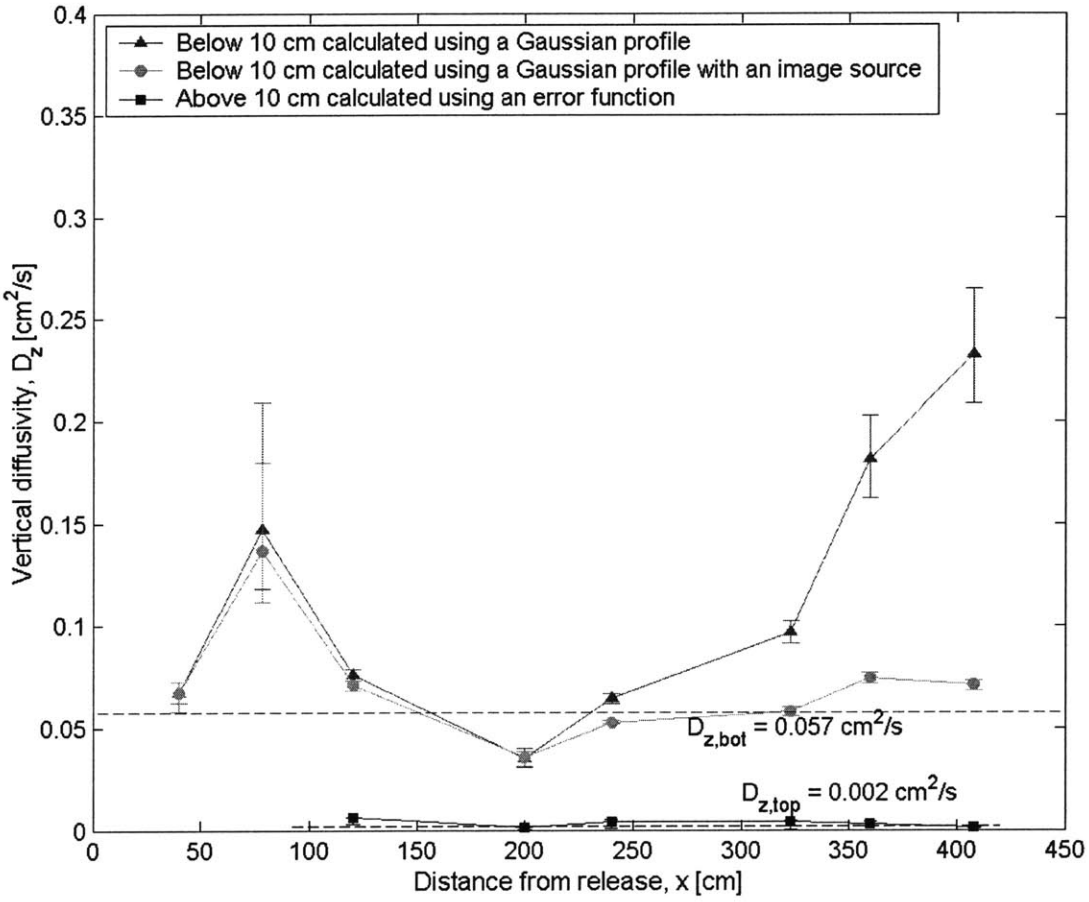

Figure 4-13. Vertical diffusivity in the laboratory as a function of distance in 0.8 cm/s flow. The vertical diffusivity constant is calculated from the curve fits shown in Figure 4-11. Error bars indicate the change in the value of D_z that would produce a 5% change in the sum of squared residuals in the fit. The dotted lines indicate the mean vertical diffusivities over all distances weighted by variance.

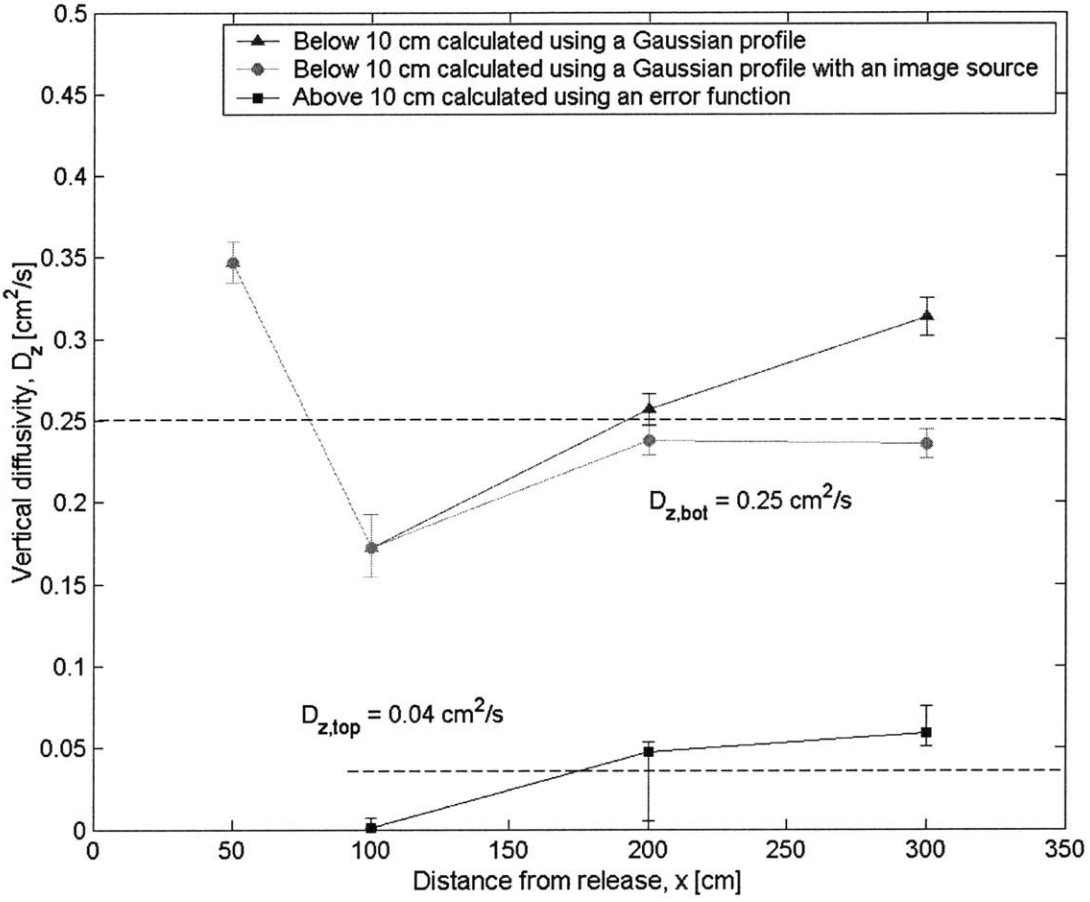

Figure 4-14. Vertical diffusivity in the laboratory as a function of distance in 4.1 cm/s flow. The vertical diffusivity constant is calculated from the curve fits shown in Figure 4-12. Error bars indicate the change in the value of D_z that would produce a 5% change in the sum of squared residuals in the fit. The dotted lines indicate the mean vertical diffusivities over all distances weighted by variance.

determined that in a spatially homogeneous array of emergent circular cylinders in the laboratory, $D_z = 0.09 \pm 0.02$ cm^2/s for $ad = 0.006$ and $D_z = 0.07 \pm 0.02$ cm^2/s for $ad = 0.014$. Results reported by Nepf et al. (1997a) are slightly higher: $D_z = 1.3 \pm 0.1$ cm^2/s for $ad = 0.01$ and $D_z = 1.5 \pm 0.2$ cm^2/s for $ad = 0.015$.

4.3 Longitudinal dispersion

Longitudinal dispersion is proportional to the rate of increase in variance of the curve of concentration versus time for a slug release (equation 2-25 and Figure 4-15). Figure 4-16 shows an example of how concentration and time were nondimensionalized prior to the calculation of variance. Figure 4-17 shows measurements of spatial variance as a function of time since release at the canopy interface. Spatial cloud variance increases over time at all flow rates, indicating that longitudinal dispersion is occurring.

For a Fickian process, K_x is constant, and variance increases linearly with time. At very short timescales, Figure 4-17 indicates that variance initially increases nonlinearly: for all flow rates, the variance at the first time measured falls below the straight-line fit, indicating that K_x is not yet constant. Then, from ~20-250 s (depending on the flow velocity), the dispersion constant approaches a constant value, suggesting that the process dominating longitudinal dispersion has reached its Fickian limit. Nepf et al. (1997a) observed similar values for K_x in a canopy with uniform stem density over height. They reported that $K_x = 2.5 \pm 0.4$ cm^2/s for $ad = 0.01$, $K_x = 2.4 \pm 0.7$ cm^2/s for $ad = 0.015$, and $K_x = 1.2 \pm 0.4$ cm^2/s for $ad = 0.055$ (Nepf et al., 1997a). Interestingly, after this initial constant behavior, the slope of the best-fit line increases abruptly again, indicating a sudden increase in the longitudinal dispersion coefficient. The new, higher slope is also approximately constant, suggesting that another Fickian process has suddenly become important.

All four studied flow velocities exhibit this same abrupt transition to an increased value of K_x (Table 4-5). Furthermore, the transition occurs at the same distance downstream of the release for all velocities (230 ± 30 cm; see Figure 4-18). This effect is also seen when cloud

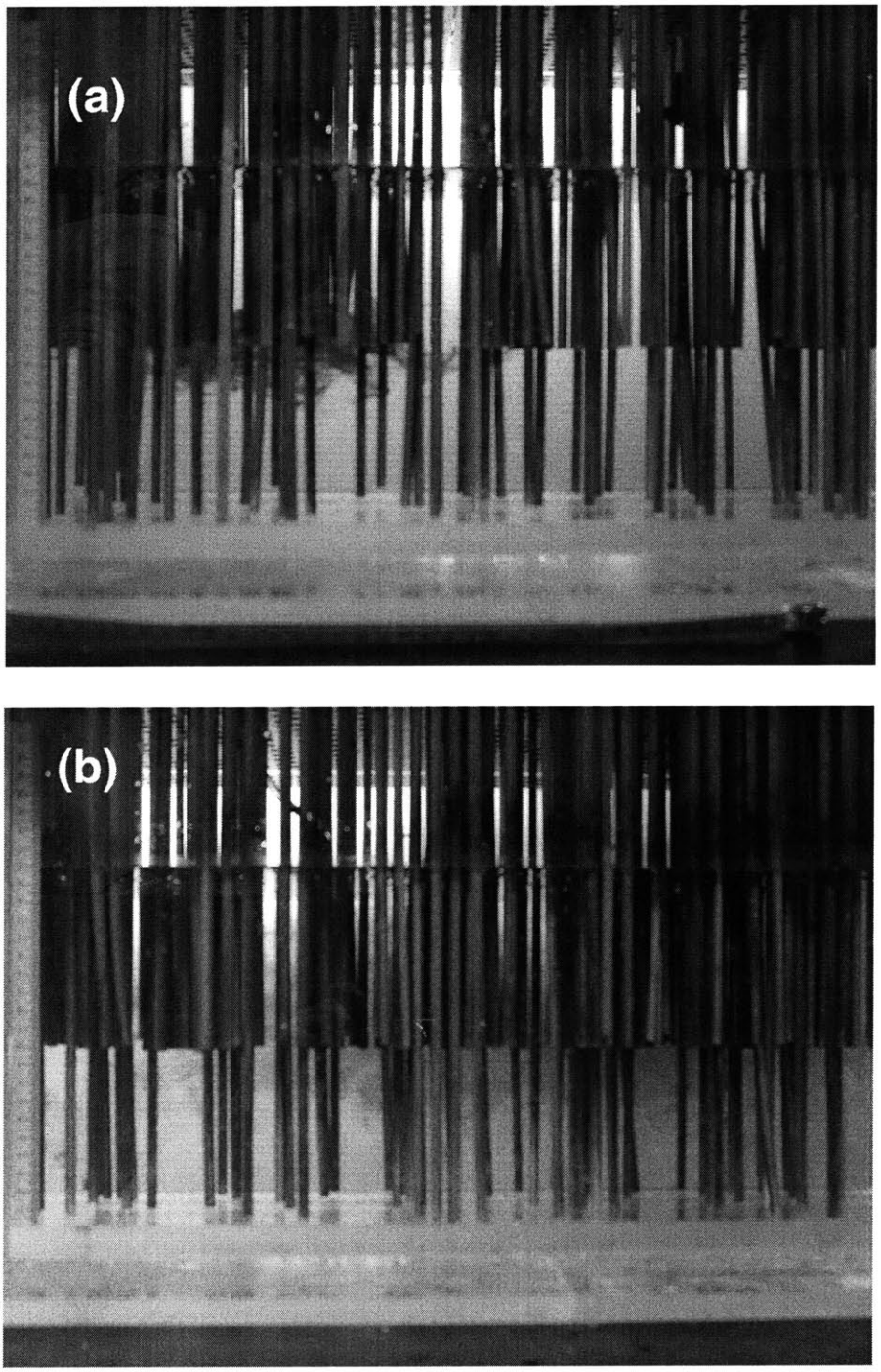

Figure 4-15. Slug releases of Rhodamine WT at the interface in the laboratory flume with dense (ad = 0.024) and less dense (ad = 0.012) canopies. Flow velocity at the interface is 0.8 cm/s. (a) 20 cm downstream of a release at the interface. (b) 55 cm downstream of a different slug also released at the interface. The cloud is starting to tilt as a result of a higher velocity in the lower canopy.

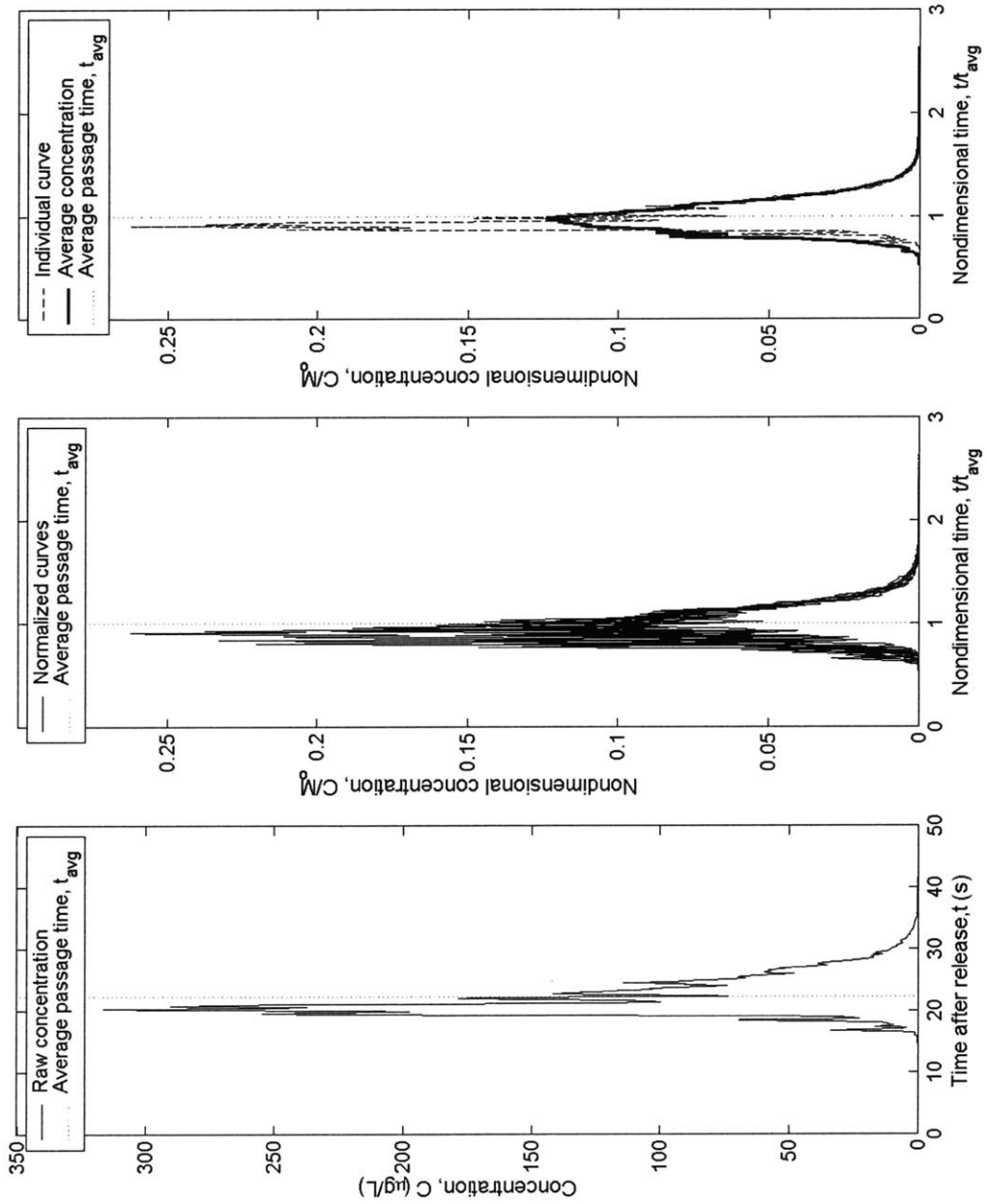

Figure 4-16. Example of calculating normalized concentration for an instantaneous release. (a) The record of concentration as a function of time for a single slug release. The average passage time, $t_{avg} = M_0/M_1$ is also indicated. (b) Each concentration record is normalized by the first moment (M_0) and the average passage time. The resulting records of nondimensional concentration as a function of nondimensional time are superposed, interpolated to the highest sampling temporal frequency, and averaged. (c) The average nondimensional concentration curve is shown as a function of nondimensional time. The deviation of each individual record from this average is then used to calculate C_{rms}.

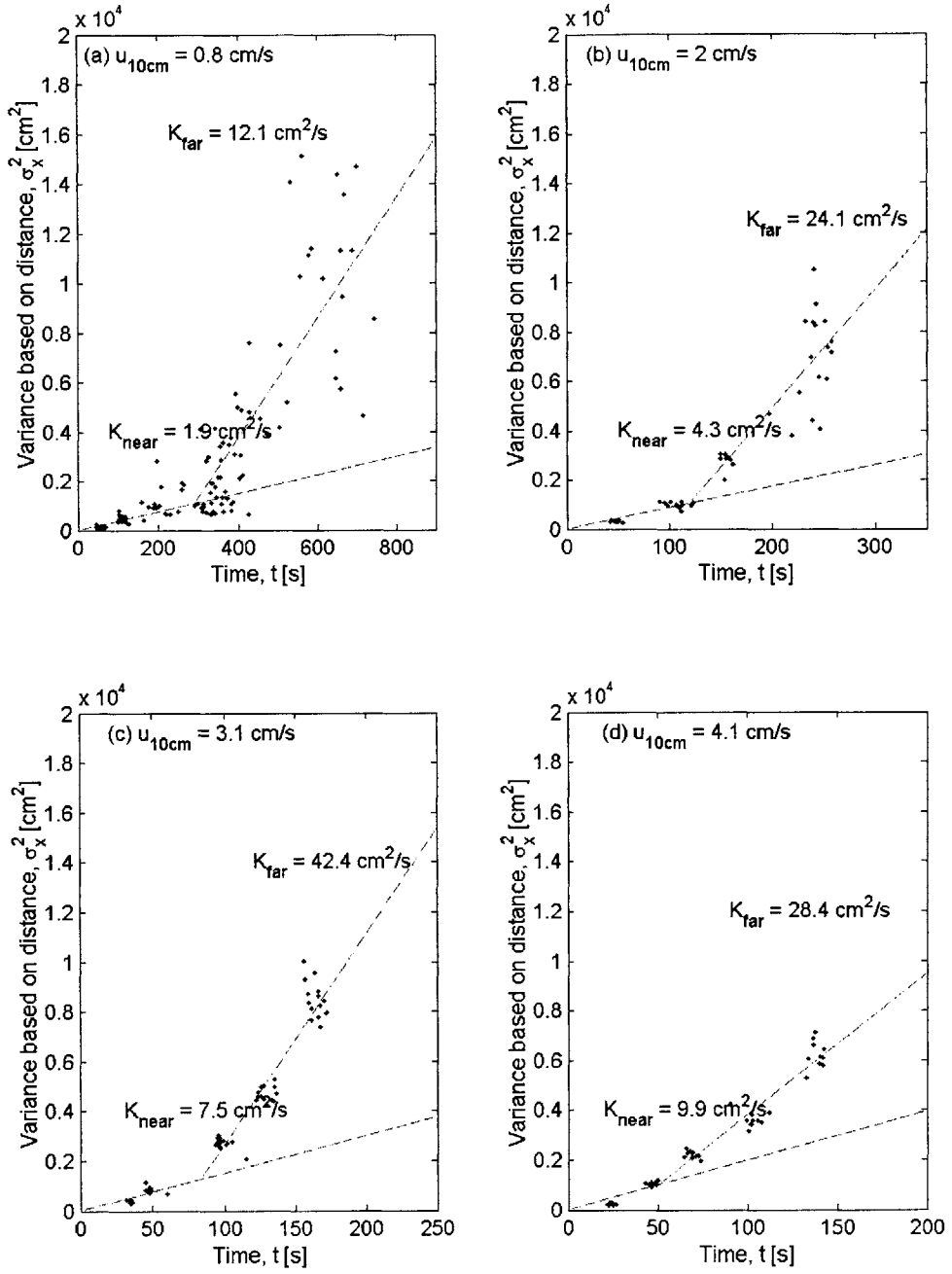

Figure 4-17. Measured cloud variance as a function of time after passing through laboratory vegetation mimics. Each point represents the variance in the record of dye concentration versus time since release for a single dye slug, converted to a spatial variance by multiplication by the average velocity for the slug ($\sigma_x = \sigma_t * x/t_{avg}$). All dye was released and measured at 10 cm from the bed, at the interface between vegetation of two different densities. The mean effective flow velocity for each pump setting is the average velocity experienced by the dye clouds' centers of mass. Straight lines are best-fit in the least squared sense to portions of the data.

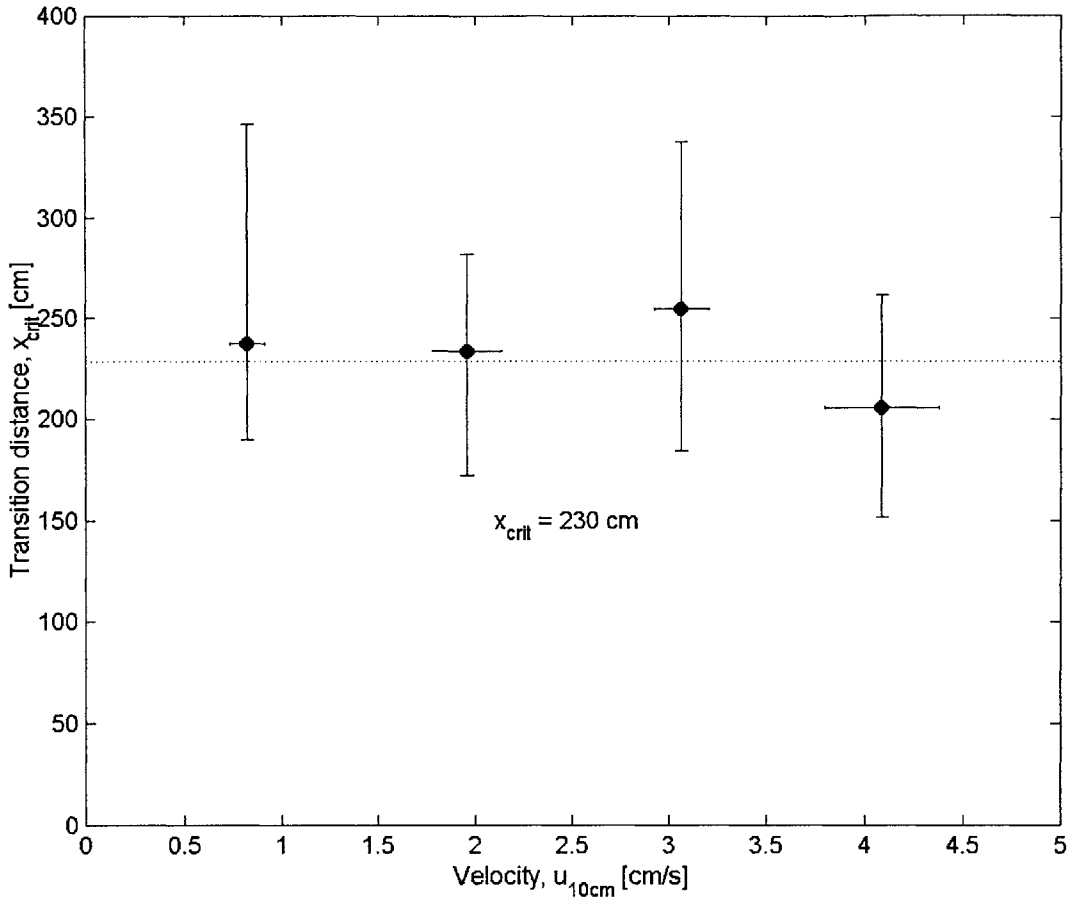

Figure 4-18. Distance downstream of an instantaneous laboratory slug release at which the dispersion coefficient abruptly increases. Horizontal bars indicate the standard error of the mean velocity over all releases at that velocity. Vertical bars indicate the range of distances over which this transition could occur given reasonable fits for the intersection between the upper and the lower slopes in Figure 4-17.

Table 4-5. Longitudinal dispersion in the laboratory. All data are presented as a spatial mean ± standard error of the mean over different slug releases at the interface. Dispersion constants are normalized by the local velocity at the interface as determined by slug releases.

Variable	Distance downstream	Flow rate			
		Lowest	Second lowest	Second highest	Highest
K_x [cm^2/s]	< 250 cm	1.9 ± 0.1	4.3 ± 0.2	7.5 ± 0.6	9.9 ± 0.6
	> 250 cm	12 ± 1.0	24 ± 3	42 ± 2	27 ± 2

variance is plotted against distance (Figure 4-19). Within ~250 cm of the release, the rate of increase in variance is similar for all velocities. After 250 cm, however, variance increases much more rapidly with distance, and there is considerably more variation between and among flow conditions, suggesting that a different dispersive process has become important.

The magnitude of the coefficient of longitudinal dispersion at both short and long times tends to increase with increasing flow velocity (Figure 4-20 and Table 4-5). The trend is significant for K_x measured within 250 cm of the release ($r^2 = 0.997$ for a linear fit) but not for K_x measured at farther distances downstream. Note that, as the velocity decreases toward zero, the dispersion constant will also approach zero, as is predicted by these straight-line fits (see Figure 4-20). As a result of this velocity dependence, the longitudinal dispersion constant normalized by the velocity and stem diameter is approximately constant at different flow rates at both short and long distances downstream.

Slug releases were also performed at 4 cm from the bed (6 cm from the interface into the less dense canopy) and 16 cm from the bed (6 cm from the interface into the denser canopy). For short times, the variance of these curves tracked the results of the releases at 10 cm (Figure 4-21). In addition, although the data are not conclusive, they suggest that the transition to the regime of increased longitudinal dispersion occurred farther downstream, especially for the slugs released in the upper canopy. When variance is plotted against distance (Figure 4-22), the variance of the slugs released at the interface increases rapidly after 250 cm, but the variance of the slugs released farther away from the interface remains lower until at least 450 cm downstream.

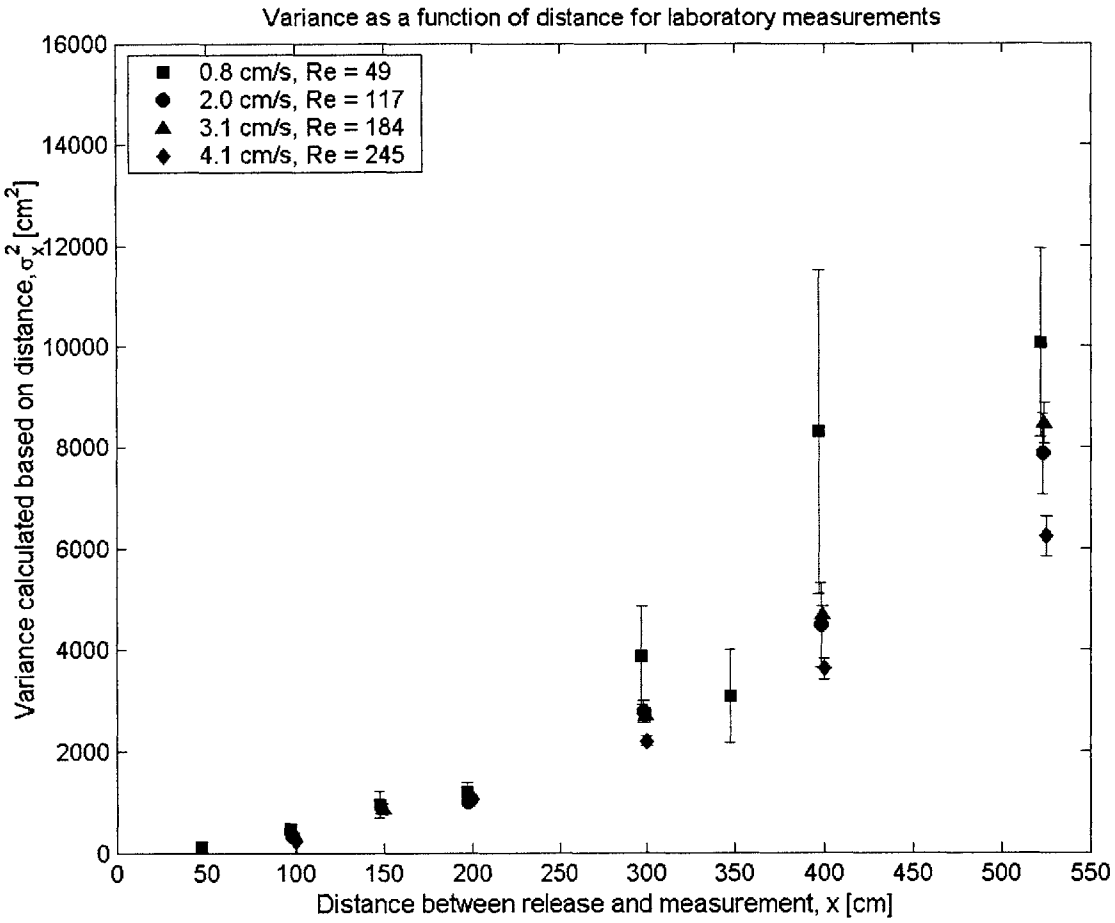

Figure 4-19. Measured cloud variance as a function of distance after passing through laboratory vegetation mimics. Points represent means weighted by variance for each of four flow rates; vertical bars indicate standard error of the mean weighted by variance. Data points at the same distance are offset slightly to distinguish error bars.

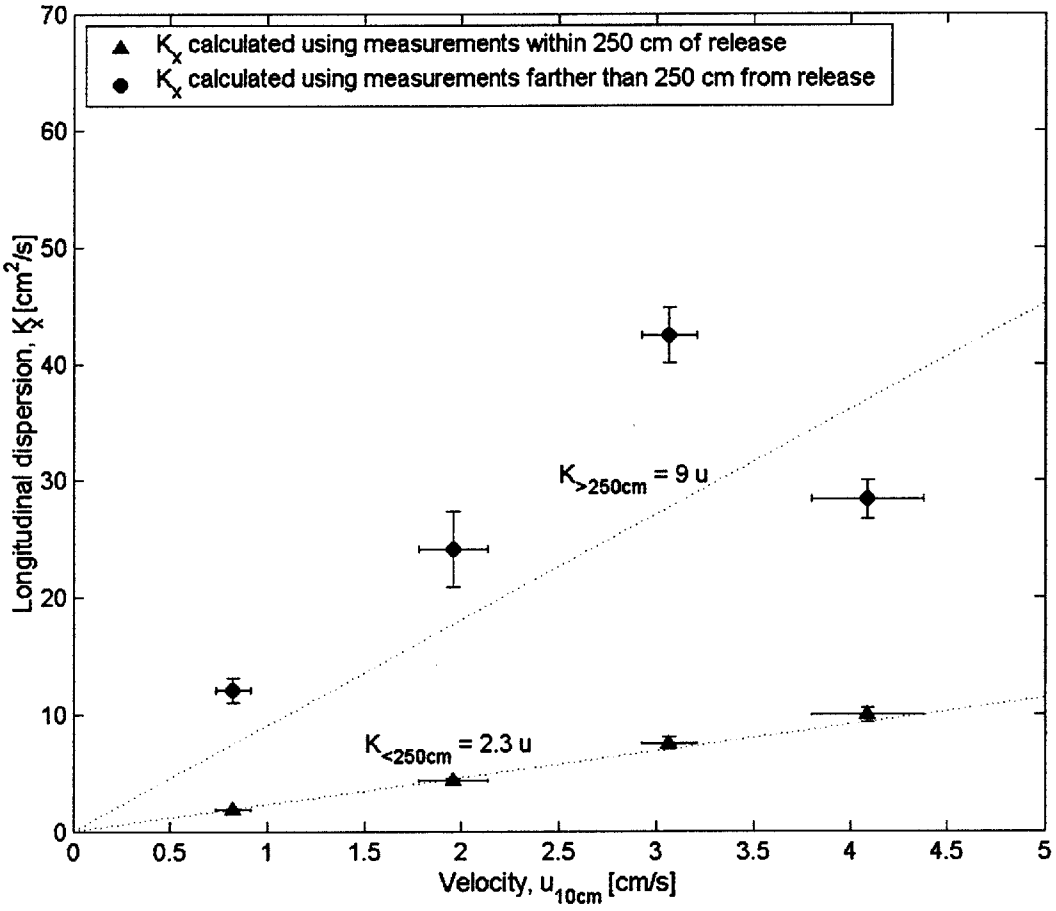

Figure 4-20. Longitudinal dispersion coefficients as a function of water velocity calculated from dye slugs in the laboratory. All slugs were released and measured at the interface between two different vegetation densities. Horizontal bars represent standard error of the mean velocity when calculated from the average travel time of the center of mass of each cloud. Vertical bars represent the value of dispersion constant that produces a 5% increase in the squared residuals. Lines are least-squares fits to all longitudinal dispersion coefficients at each distance, weighted by error.

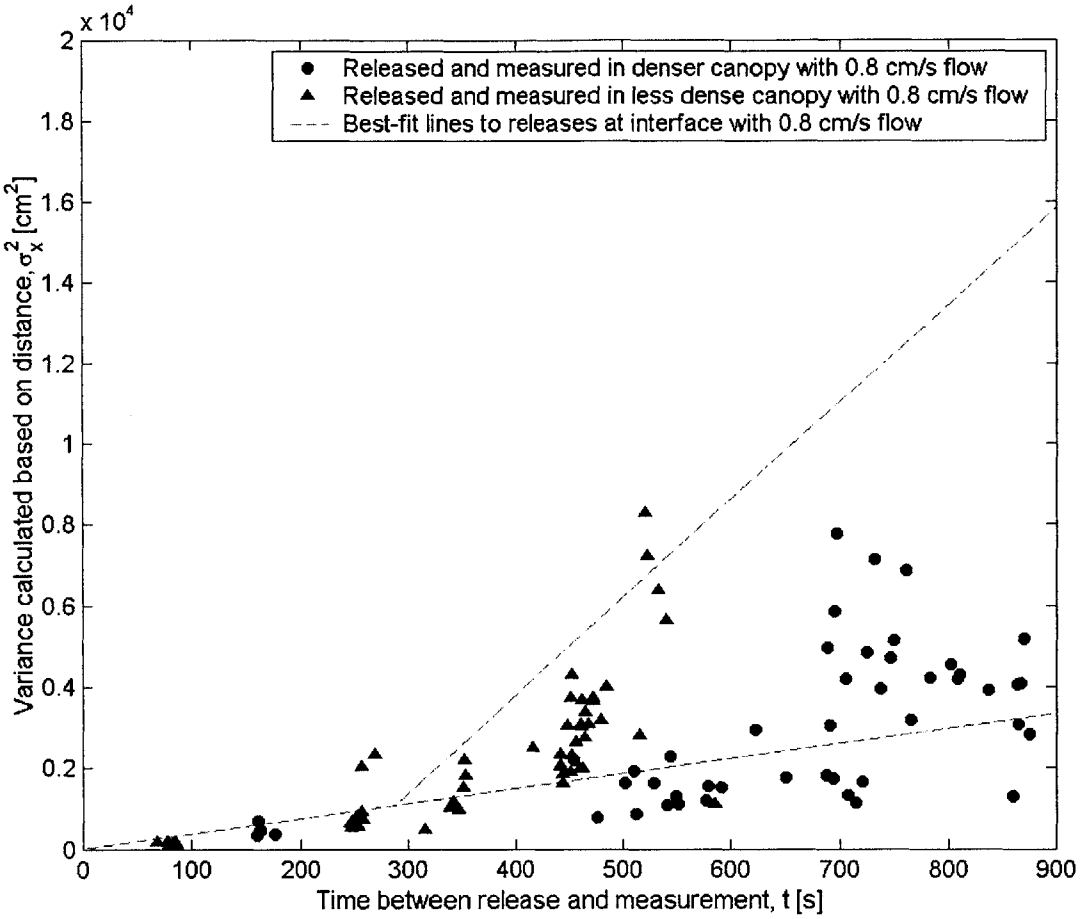

Figure 4-21. Measured cloud variance as a function of time after passing through either the upper or lower canopy of vegetation mimics. Slugs released in the less dense canopy were released and measured at 4 cm from the bed; slugs released in the denser canopy were released and measured at 16 cm from the bed. The flow velocity for all points was the lowest flow rate (~0.8 cm/s). Dotted lines indicate the best-fit lines to slug releases at the interface at this flow velocity (cf. Figure 4-17a).

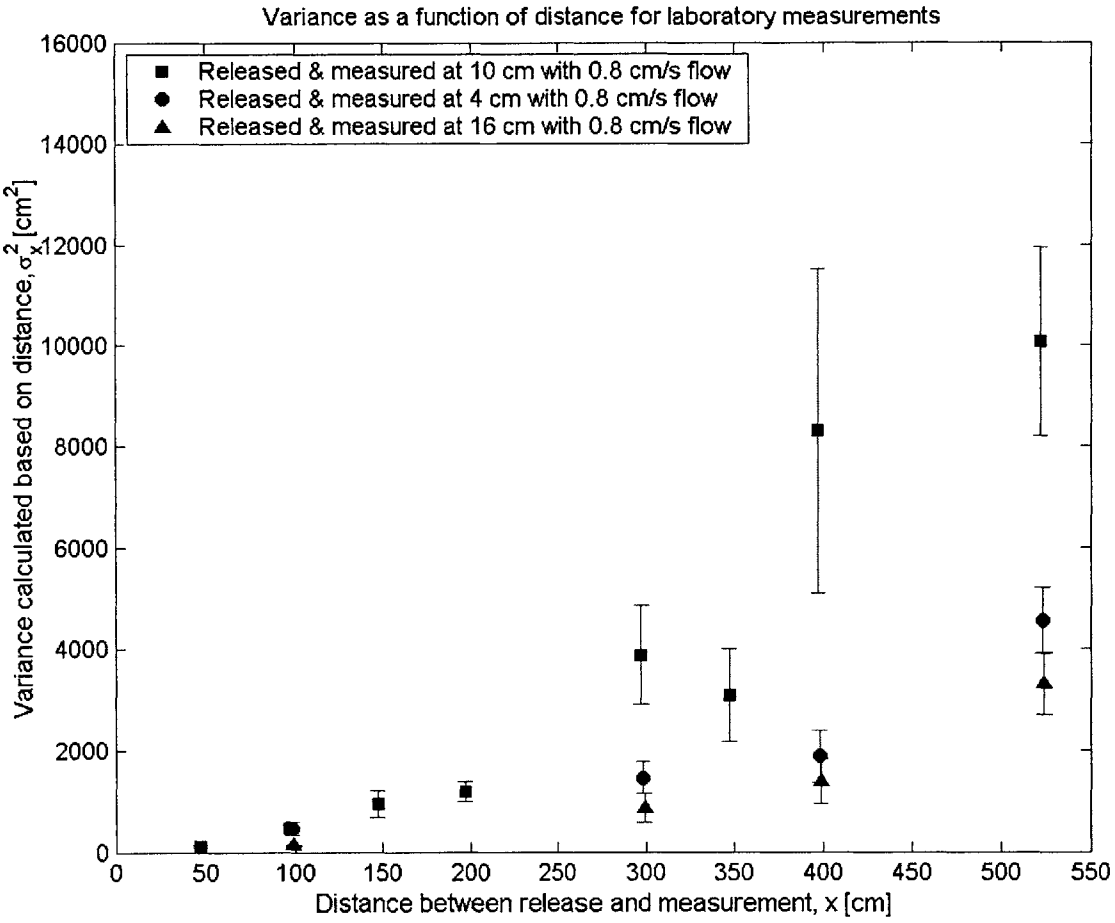

Figure 4-22. Cloud variance as a function of distance for releases at the lowest flow rate. Data are shown for releases at the interface (10 cm from the bed), in the less dense canopy (4 cm from the bed), and in the denser canopy (16 cm from the bed). Vertical bars represent standard error of the mean weighted by variance.

4.4 Skewness

The shape of the concentration distribution of an evolving slug provides important information about the mixing processes affecting the cloud. When Fickian processes dominate, the cloud will have a symmetrical shape, and *S* will equal 0. For each velocity, as the length of vegetation through which the dye passes increases, the concentration profiles become less skewed (Table 4-6; Figure 4-23). The curve peak approaches the center of mass, suggesting that whatever dispersion process is responsible for the observed dispersion is approaching the Fickian limit. Similarly, White (2002) found that clouds became more symmetrical between 1.5 and 3.5 m downstream of a release in an emergent canopy. It is even likely that there are two observable

Table 4-6. Skewness and patchiness of clouds at different distances downstream of slug releases at the interface in the laboratory. Data are presented as mean ± standard error of the mean across slug releases.

Variable	Flow velocity, u	Distance downstream							
		50 cm	100 cm	150 cm	200 cm	300 cm	350 cm	400 cm	525 cm
Skewness, S	0.8 cm/s	1.4 ± 0.3	1.0 ± 0.2	0.8 ± 0.5	-0.03 ± 0.2	1.0 ± 0.3	1.5 ± 0.2	0.6 ± 0.6	0.5 ± 0.2
	2.0 cm/s	-	0.7 ± 0.1	-	0.4 ± 0.1	0.5 ± 0.1	-	0.5 ± 0.3	0.9 ± 0.1
	3.1 cm/s	-	1.1 ± 0.4	1.0 ± 0.2	-	0.4 ± 0.1	-	0.5 ± 0.1	0.7 ± 0.1
	4.1 cm/s	-	0.7 ± 0.1	-	0.6 ± 0.1	0.2 ± 0.1	-	0.2 ± 0.1	0.09 ± 0.06
Patchiness, C_{rms}/C_{avg}	0.8 cm/s	2.0 ± 0.4	0.8 ± 0.1	1.0 ± 0.2	1.0 ± 0.1	0.8 ± 0.2	1.2 ± 0.3	1.1 ± 3	0.5 ± 0.1
	2.0 cm/s		0.7 ± 0.1	-	0.4 ± 0.1	0.4 ± 0.1	-	0.4 ± 0.1	0.4 ± 04
	3.1 cm/s		0.4 ± 0.1	0.4 ± 0.1	-	0.4 ± 0.1	-	0.3 ± 0.02	0.3 ± 0.03
	4.1 cm/s		0.6 ± 0.2	-	0.4 ± 0.03	0.2 ± 0.03	-	0.2 ± 0.1	0.2 ± 02

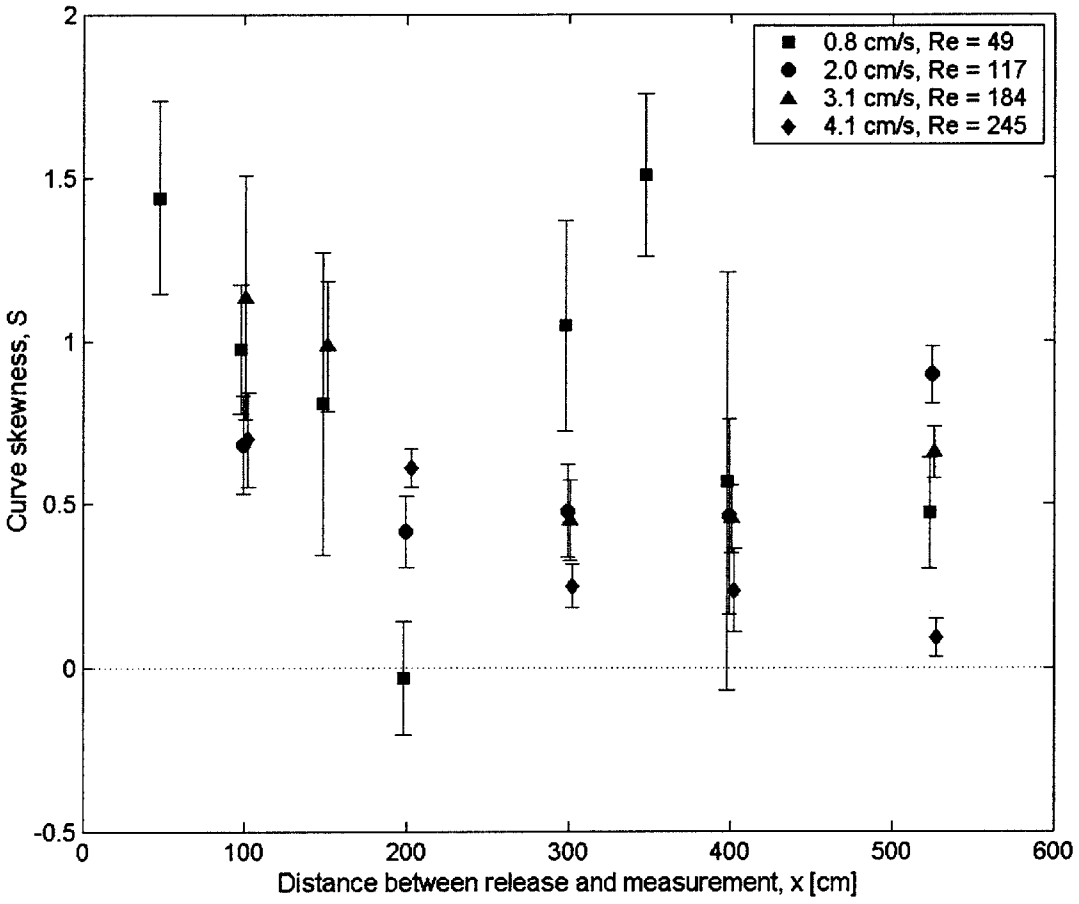

Figure 4-23. Skewness as function of distance for slug releases in the laboratory. All slugs were released and measured at the interface between two different vegetation densities. Vertical bars represent the standard error of the mean for skewness, weighted by variance.

dispersion processes in the present study. Skewness decreases for all velocities up to 250 cm, then tends to increase again for measurements downstream of 300 cm. This provides further support for the presence of one process that dominates at distances < 250 cm and is then replaced by another process at longer distances.

4.5 Patchiness

Because different slugs take different paths through the random canopy, the concentration trace measured for each release is patchy (cf. Figure 4-16, which shows a representative example). When curves from multiple individual slugs are superposed and averaged, the concentration curve becomes much smoother (Appendix B). Even for the longest distances, however, neither the averaged nor the individual curves approach the smoothness noted by White and Nepf (2003), suggesting that the small-scale mixing they observed for $Re_d > 200$ has not become important.

One measure of curve patchiness is the standard deviation of the concentration deviation of each curve from the ensemble average, normalized by the ensemble-averaged concentration, C_{rms}/C_{avg} (equation 3-26). This measure of relative patchiness tends to decrease with distance, as the cloud passes through more dowels, for all velocities (Figure 4-24). This effect has been observed elsewhere for open channel flow with no obstructions (Webster et al., 2003) and in an open channel downstream of cylindrical vegetation mimics (Finelli, 2000). Webster et al. (2003) also observed that $C_{rms}/C_{avg} \approx 2$ in an open channel flow. Finelli (2000) reported that, for both open channel and vegetated conditions, slugs released into faster flows, and that vegetation increases patchiness relative to an unvegetated case. Patchiness also decreases with increasing Reynolds number (e.g., 525 cm downstream of the release, C_{rms}/C_{avg} monotonically increases with Re_d). In addition, the curves at 1 cm/s appear much patchier than the clouds at higher velocities, perhaps because of the presence of vortices at higher velocities and not at the lowest flow rate. Similarly, measurements in emergent canopies with constant density over depth have suggested that, for a given stem density, patchiness tends to decline with increasing velocity (Nepf et al., 1997b).

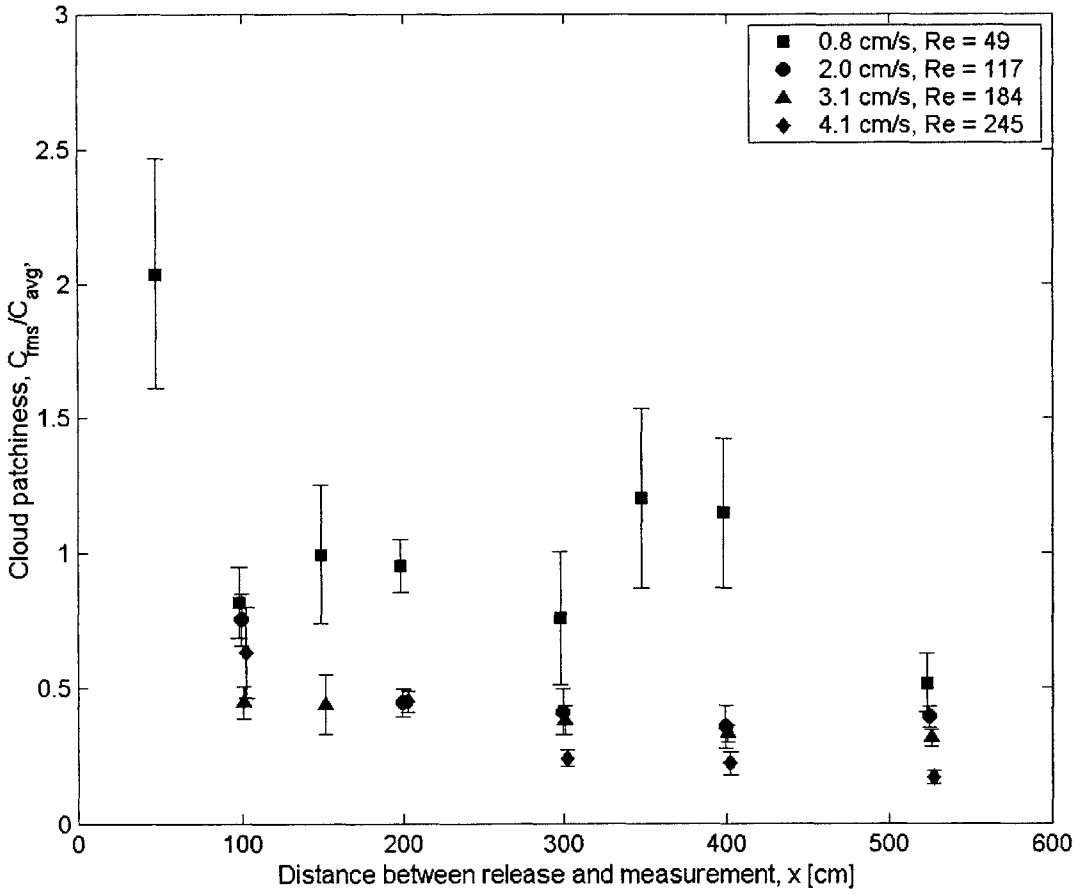

Figure 4-24. Cloud patchiness as a function of distance in the laboratory. All slugs were released and measured at the interface. Vertical bars represent standard error of the mean weighted by variance.

Chapter 5

Field Results and Discussion

5.1 Frontal area

Field measurements were performed in a mature *S. alterniflora* canopy at midseason. Over the course of the measurement period, all the stems from a total of four different plots in the stand used for dispersion measurements were harvested, counted, and photographed. Digital images were then converted to measurements of frontal area (see example in Figure 5-1).

There were two major sources of variability among photographs of different stems. First, projected stem frontal area differs depending on stem orientation. It is possible that stems grow to minimize projected area in the direction of ambient flow. At the field site, however, flow direction is variable, so stems were assumed to be oriented randomly, so the differences in frontal area contributed to variability. The second largest source of error comes from digital image processing.

Because the measurements were performed in the middle of the growing season, total stem frontal area density remained constant over time (Figure 5-2). Figure 5-3 shows vertical profiles of frontal area density for each sampled day along with the total number of stems for each day. For comparison, the frontal area used in the laboratory is also shown. Even though the stem density varies between days by a factor of two, both the shape and the magnitude of the frontal area density curve are relatively constant between profiles. This profile is apparently constant in this region of the marsh during this portion of the growing season.

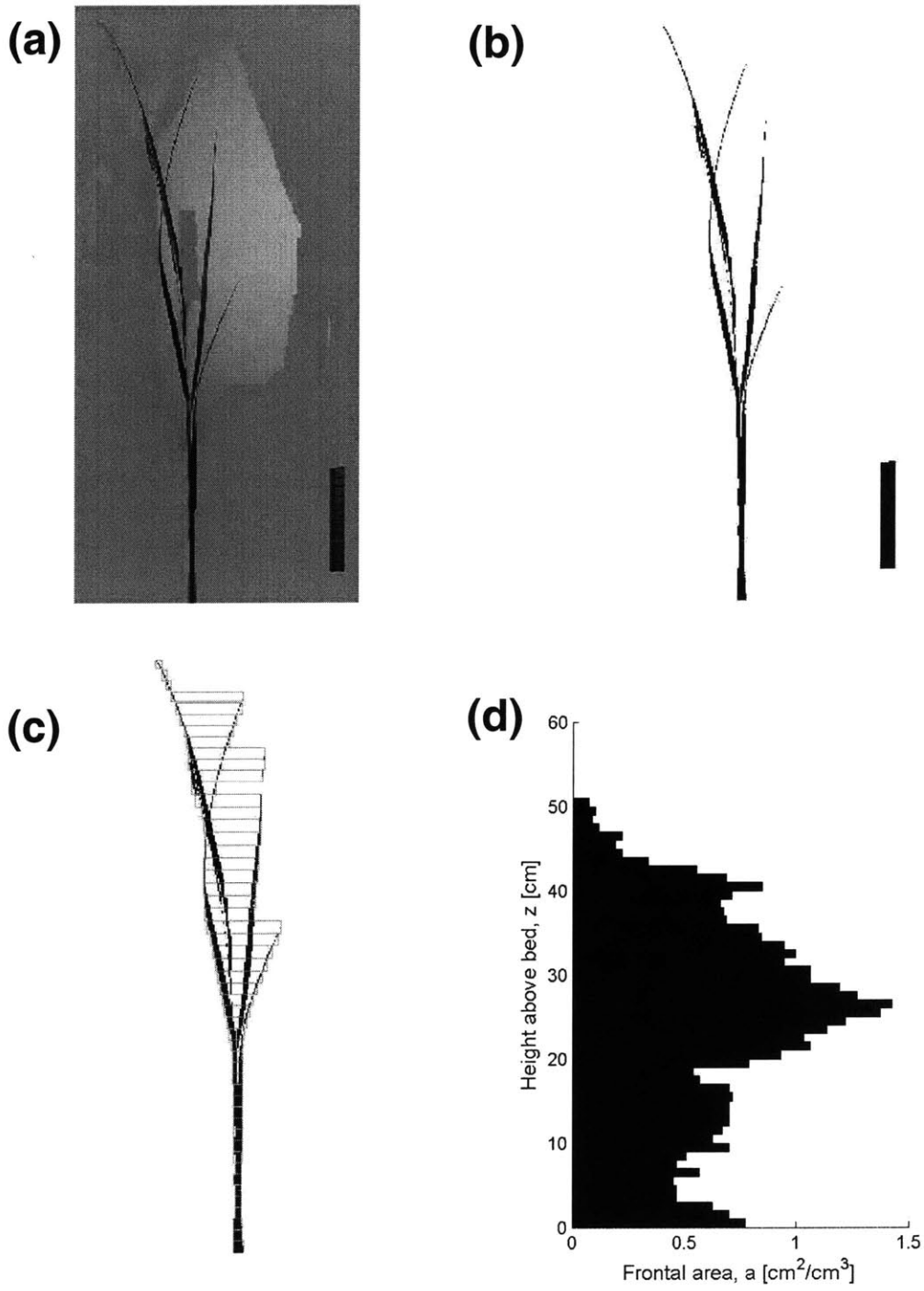

Figure 5-1. Example of the calculation of frontal area for a single stem. (a) Each stem was photographed in front of a white background. This is one of four views of this stem, each taken from a different camera angle. The ruler provides scale. (b) The color image was converted to black and white. (c) The stem was divided into 1-cm-high sections. The number of pixels in each section was determined after correction for parallax. (d) The number of pixels in each section was counted and converted to a measure of frontal area for this stem. The frontal areas for all stems from each plot were summed to provide a measure of total frontal area per unit flow volume.

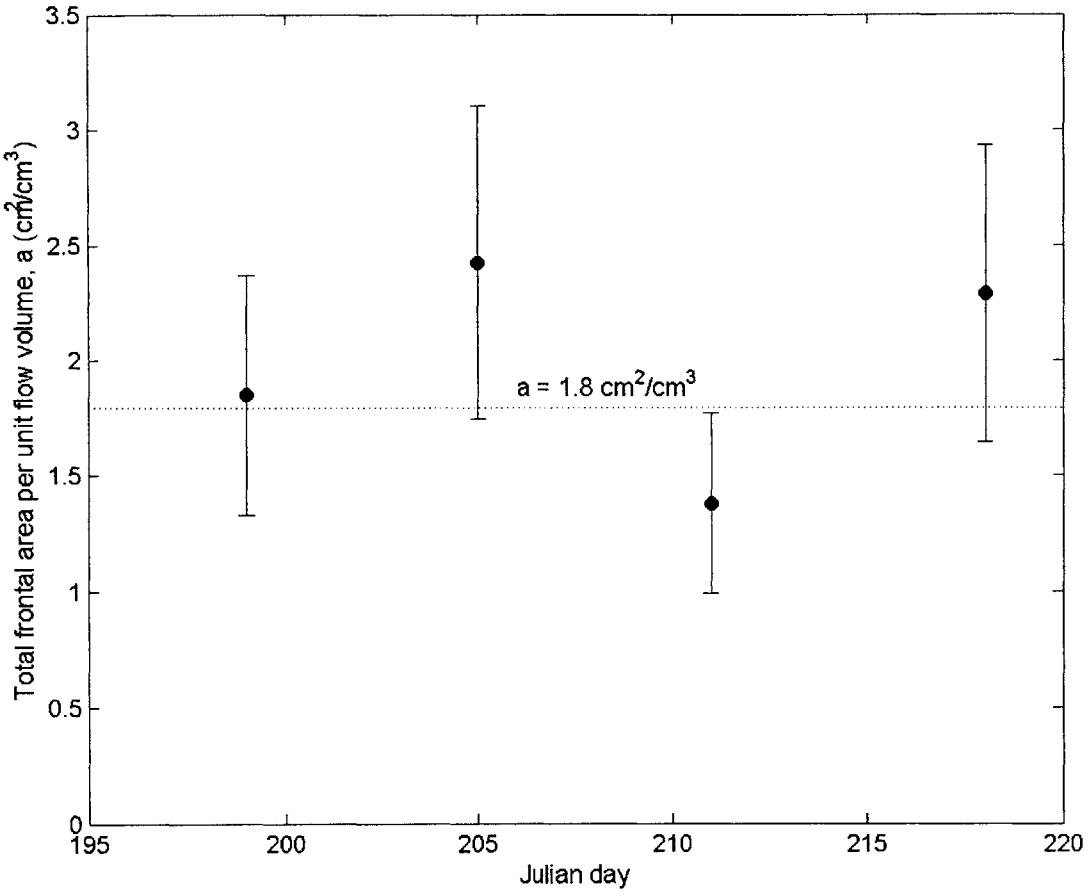

Figure 5-2. Stem frontal area per unit bed surface area, summed over depth, for each of the four sampling dates (July 18, July 24, July 30, and August 6) during the field measurement season. Each value shows the total frontal area calculated from digital photographs of all stems within an 0.11 m^2 area of the bed. Error bars indicate the sum of variability in stem orientation (~20%) and error due to digital image processing (~5% from selection of the appropriate threshold level).

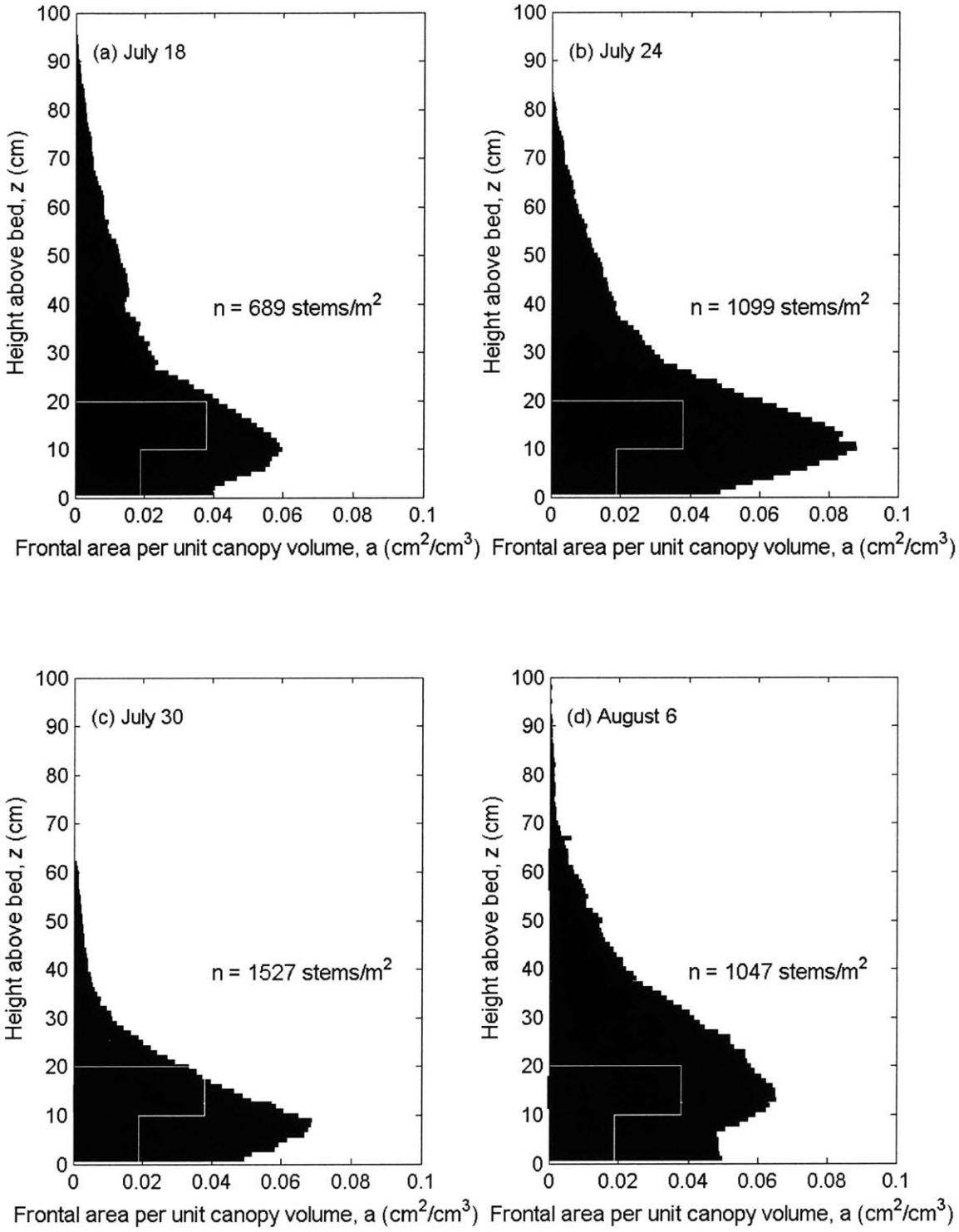

Figure 5-3. Vertical profiles of stem frontal area per unit canopy volume for the field site. Each profile was taken on a different day. Numbers indicate the stem density at each location. The white outline indicates the corresponding frontal area values for the laboratory measurements.

Figure 5-4 shows the mean stem frontal area density from these four measurements. Note that the frontal area density is a strong function of height, peaking at 11 cm from the bed and then slowly diminishing to nearly zero at 100 cm above the bed. Leonard and Luther (1995) reported a similar stem frontal area profile in a *S. alterniflora* marsh, with the peak density at 10-15 cm from the bed.

Each *S. alterniflora* stem produced several leaves (cf. Figure 5-1), each of which decreased in diameter along their length. As a result, the total frontal area density decreased with distance from the bed. Stem diameter was found to be 0.17 ± 0.08 cm (mean ± standard error of the mean across different leaves) at 10 cm from the bed and 0.12 ± 0.06 cm at 20 cm from the bed. Similarly, Valiela et al. (1978) reported that *S. alterniflora* stems in the field have a median stem diameter of just less than 0.2 cm. Although the error associated with this stem diameter is large, it is clear that diameter is a strong function of height. Nonetheless, for subsequent calculations d will be assumed to equal to 0.15 ± 0.07 cm throughout the field canopy.

5.2 Velocity

5.2.1 Mean flow

Flow speeds through the natural marsh canopy through both flood and ebb tides were 0.7 to 13 cm/s at 15 cm above the bed. Similarly, Leonard and Luther (1995) measured velocities < 15 cm/s through a creekside stand of *S. alterniflora*, with speeds declining to < 5 cm/s at interior marsh sites. All field velocity profiles consisting of measurements at three or more distances from the bed, with a monotonic velocity increase above 15 cm from the bed, are shown in Appendix A. Assuming an average stem diameter of 0.4 cm, these velocities indicate $Re_d = 13$-520. The actual range of Reynolds numbers present in the canopy is likely even larger, since both flow speed and stem diameter change over depth.

The composite velocity profile for the field measurements (Figure 5-5; Table 5-1) reveals that, as expected, the horizontal velocity through the natural canopy changes over depth. Similar

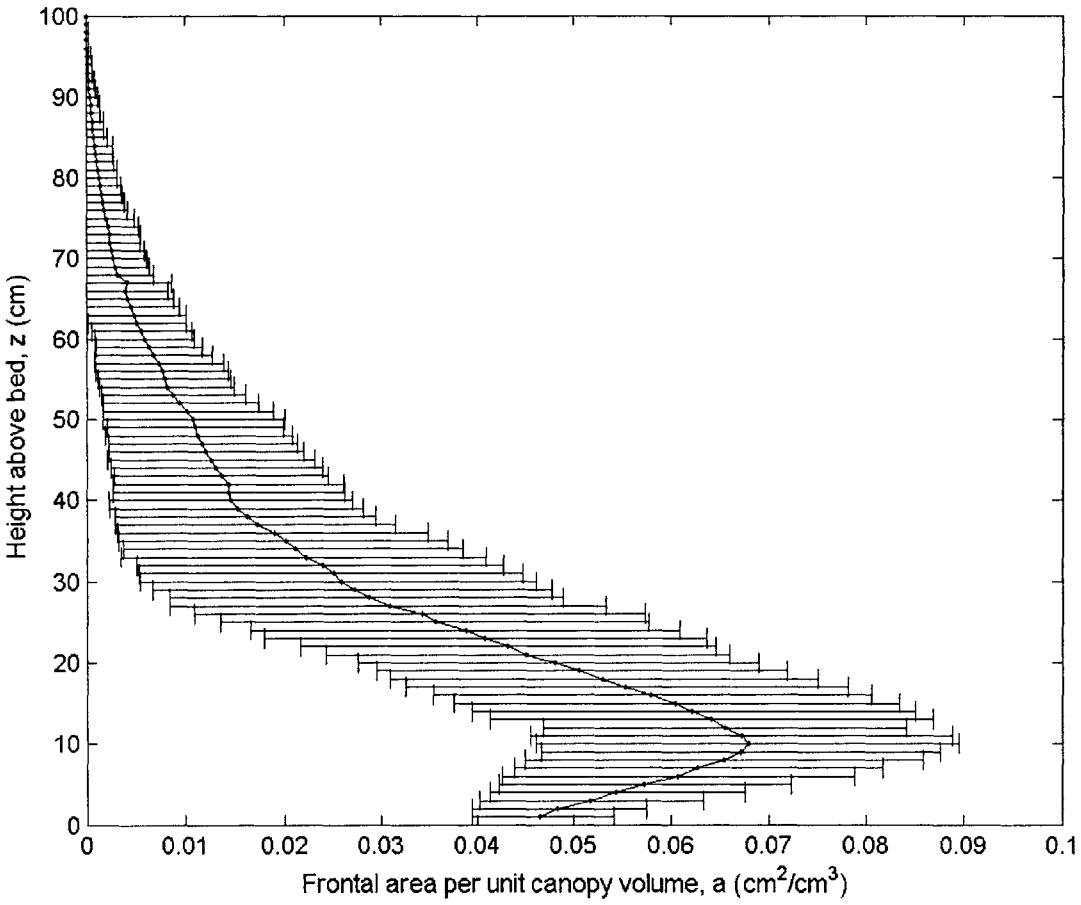

Figure 5-4. Average stem frontal area density for the field sampling site. The value at each distance from the bed is the mean of results from four 0.11-m^2 plots, each harvested on a different day during the sampling period. Horizontal bars indicate standard error of the mean due to variability among the four different plots.

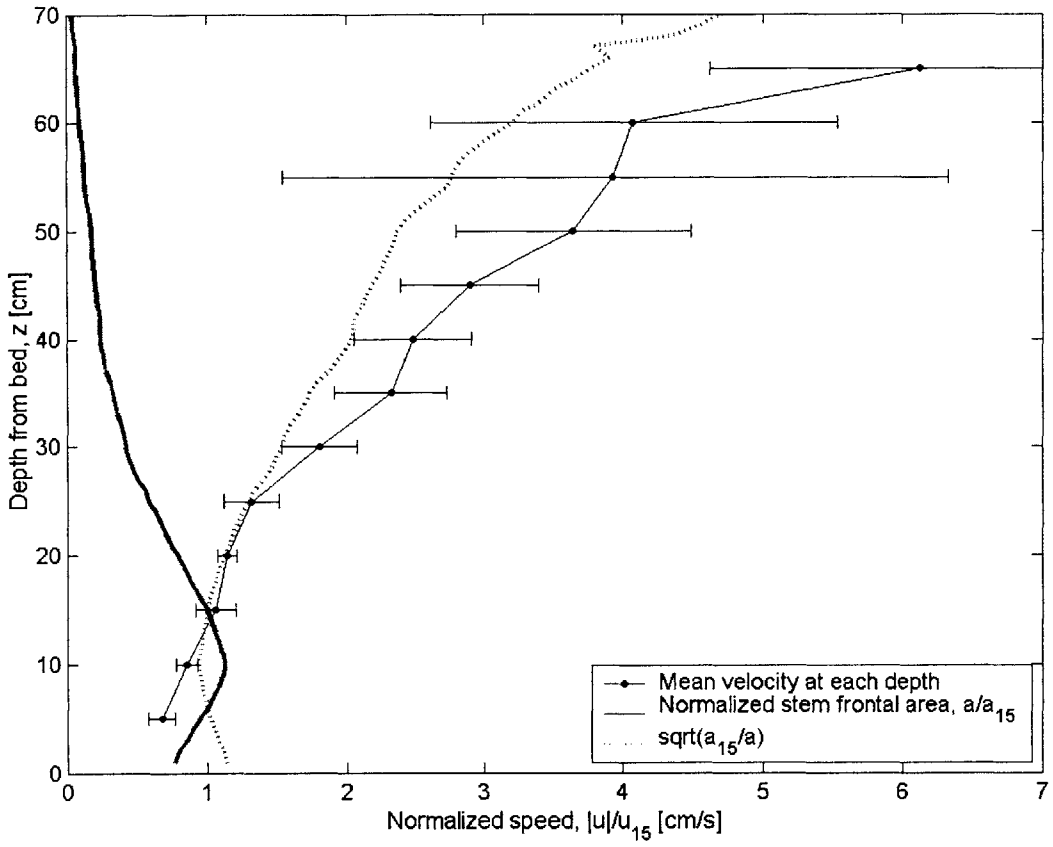

Figure 5-5. Vertical profile of velocity in the field. Each point is the mean of between 2 and 45 3-minute measurements. Because measurements were taken at different times in the tidal cycle and on different days, all points are normalized by the measured velocity at 15 cm from the bed. Horizontal bars indicate standard error of the mean among the different measurements. The curves of normalized stem frontal area a/a_{15} and $\sqrt{a_{15}/a}$ are shown for comparison.

Table 5-1. Velocity, frontal area, and estimated drag as a function of depth in the field. Velocity measurements are normalized by the velocity 15 cm above the bed. Reynolds numbers are calculated assuming $d = 0.15 \pm 0.07$ cm and $\upsilon = 0.01$ cm^2/s. All data are mean ± standard error of the mean reflecting spatial variability in velocity and frontal area.

z [cm]	u/u_{15}	Re_d	C_d	a [cm^{-1}]	$(a_{15}/a)^{1/2}$	$[(C_da)_{15}/C_da]^{1/2}$
5	0.7 ± 0.1	10 ± 5	3.2 ± 0.7	0.06 ± 0.02	1.0 ± 0.03	0.9 ± 0.2
10	0.9 ± 0.1	13 ± 6	2.9 ± 0.6	0.07 ± 0.02	0.9 ± 0.04	0.9 ± 0.1
15	1.0 ± 0.1	16 ± 8	2.6 ± 0.5	0.06 ± 0.02	1.0 ± 0.05	1.0 ± 0.2
20	1.1 ± 0.1	17 ± 8	2.5 ± 0.5	0.05 ± 0.02	1.1 ± 0.1	1.1 ± 0.2
25	1.3 ± 0.2	20 ± 10	2.4 ± 0.5	0.04 ± 0.02	1.3 ± 0.1	1.4 ± 0.3
30	1.6 ± 0.2	25 ± 15	2.1 ± 0.4	0.03 ± 0.02	1.5 ± 0.1	1.7 ± 0.4
35	2.3 ± 0.4	35 ± 15	2.0 ± 0.3	0.02 ± 0.02	1.7 ± 0.2	2.0 ± 0.5
40	2.1 ± 0.4	35 ± 20	1.9 ± 0.3	0.015 ± 0.012	2.0 ± 0.2	2.4 ± 0.7
45	2.9 ± 0.5	40 ± 20	1.8 ± 0.3	0.013 ± 0.011	2.2 ± 0.2	2.6 ± 0.8
50	3.6 ± 0.8	55 ± 30	1.7 ± 0.2	0.011 ± 0.009	2.4 ± 0.2	2.9 ± 0.9
55	3.9 ± 2.4	60 ± 45	1.7 ± 0.2	0.008 ± 0.007	2.8 ± 0.3	3.5 ± 1.6
60	4.1 ± 1.5	60 ± 35	1.7 ± 0.3	0.006 ± 0.005	3.2 ± 0.3	4.0 ± 1.7
65	6.1 ± 1.5	90 ± 50	1.5 ± 0.2	0.004 ± 0.005	3.8 ± 0.5	5.0 ± 2.0

results have been observed previously in laboratory (Shi et al., 1995) and field studies (Ackerman and Okubo, 1993; Leonard and Luther, 1995) of natural vegetation. At 10 cm from the bed, where the frontal area density is highest, the velocity is approximately 3 times lower than it is at 50 cm, where the frontal area density is very low. Leonard and Luther (1995) also reported that the largest reduction in longitudinal velocity occurs at the vertical level of highest stem density. Although the mean velocity profile does not reveal a near-bed jet, reflecting the reduction in stem frontal area at the bed (cf. Figures 5-1 and 5-4), several individual profiles exhibit increased velocity at 5 cm from the bed (Appendix A).

When vegetative drag and pressure forcing are balanced in the canopy, it is expected that the normalized velocity $u(z)/u_{15} = \sqrt{(C_d a)_{15}/C_d a(z)}$ (equation 2-40). As Table 5-1 shows, at

40 cm from the bed and below, this equality is nearly true, suggesting that the flow in this region is in fact drag-dominated. Above 40 cm, the normalized velocity profile deviates from the shape of $\sqrt{(C_d a)_{15} / C_d a(z)}$, suggesting that wind shear and other surface processes have become important. As distance away from the bed increases, stem density decreases toward zero, the longitudinal velocity increases, and the variability in the longitudinal velocity increases dramatically as wind shear stress begins to affect the flow (Figure 5-5).

Previous studies have noted a difference in near-surface velocities through a bed of aquatic vegetation. Ackerman and Okubo (1993) found that velocities in a bed of *Z. marina* were highest above 80 cm from the bed, when the relative leaf area declined to less than a third of its maximum value. Similarly, Leonard and Luther (1995) reported that velocities above the canopy height of the marsh grass *Distichlis spicata* become more heterogeneous and increase. Jenter and Duff (1999) attributed higher velocities in the top 15 cm of the water column in a bed of *Cladium jamaicense* (sawgrass) to wind-induced shear.

When the water level is higher than 40 cm, so the bulk of the vegetation is submerged, the effect of the vegetation begins to approach that of a roughness level below a free stream flow (Ghisalberti and Nepf, 2002; Shi and Hughes, 2002). The velocity profile is expected to be logarithmic above a submerged canopy, with flow speeds reduced inside the canopy by 10-50% of the free-stream velocity (Gambi et al. 1990). Even when the canopy is over-topped, however, flow through the vegetation will still be drag-dominated and can be described similarly to an emergent canopy (Nepf and Vivoni, 2000).

5.2.2 Spectra

At the Reynolds number present in the flow (Table 5-1), it is possible that some stems are shedding vortices. Spectra of both horizontal and vertical motion at various distances above the bed show a peak between 0.85 and 1.76 Hz (Figure 5-6). Because the stem diameter, stem shape, and flow velocity all change over depth, it is difficult to predict the frequency of vortex shedding if it is present. As an example, for a water velocity of 2 cm/s, the Strouhal number, *St*, is approximately 0.15 whether the stems are modeled as round cylinders 0.4 cm in diameter or

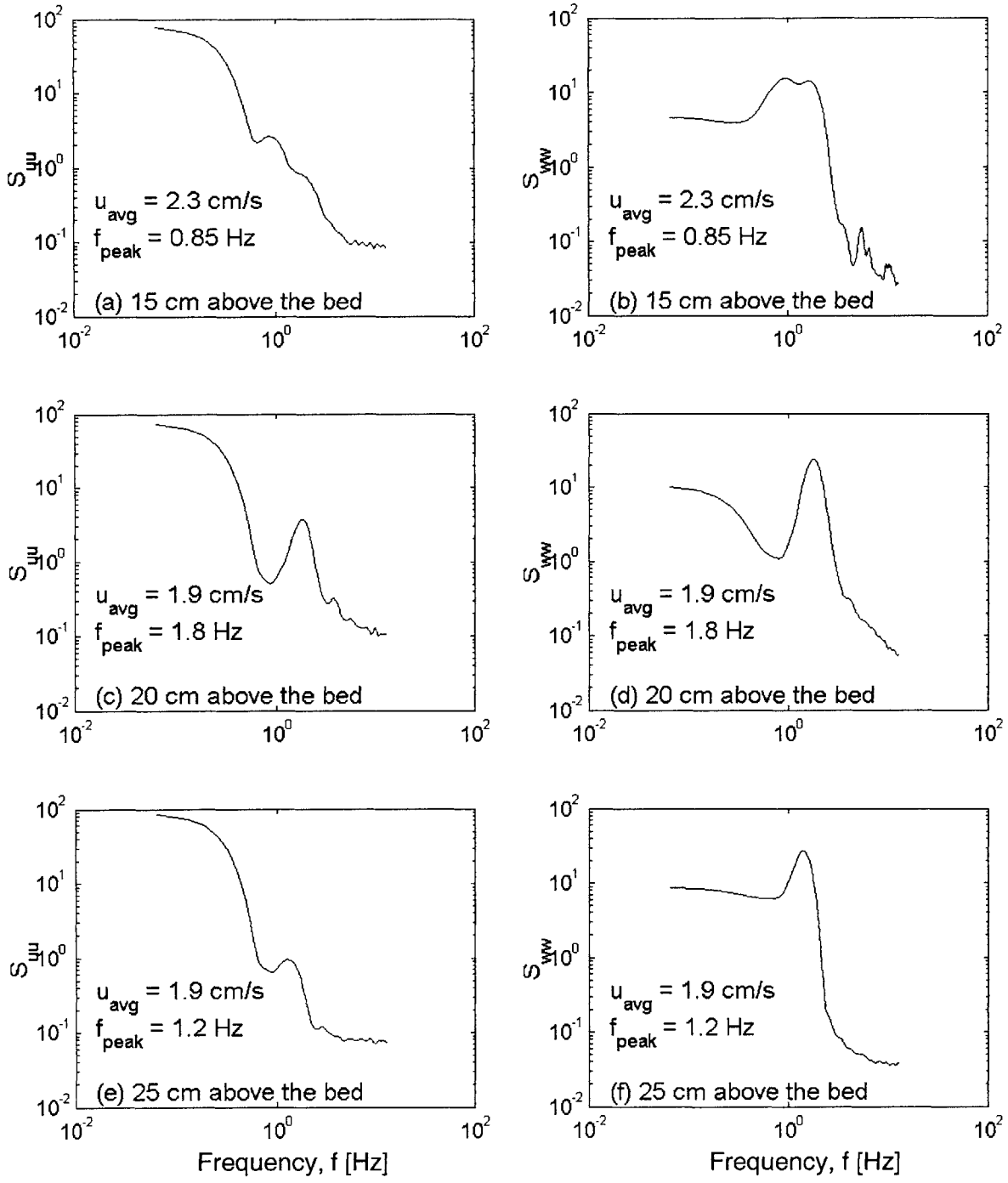

Figure 5-6. Spectra of velocity in the field. A downward-looking 3D ADV probe was used on three different days to take 7- to -20-minute long records at various heights above the bed. For each measurement depth, the spectra of vertical and horizontal motion are both shown. Each subplot also shows the mean horizontal flow speed and the frequency of the peak near 1 Hz.

flat plates 0.6 cm wide. Vortex shedding is then expected to occur at $f_{shed} = StU/d = 0.75$ Hz. The observed spectral peak frequency is therefore similar to the expected frequency for vortex shedding.

It is more likely, however, that the peak is associated with surfaces waves, which typically have a frequency near 1 Hz on the East Coast of the United States. The peak does not affect the intercept of the energy cascade at higher frequencies and so does not contribute any energy to the spectra. This spectral signal is characteristic of a wind wave but not vortex formation, which would be contributing spectral energy. In addition, the peak frequency is present at approximately the same frequency in both horizontal and vertical velocity records and has a higher spectral density in the vertical record, but vortex shedding is primarily a 2-D horizontal phenomenon. The observable peak in the spectra is therefore attributable to wind waves.

S. alterniflora canopies dampen wave energy (Knutson et al., 1982), so velocity records from locations father into the canopy should contain a reduced wave signal. Spectra presented by Leonard and Luther (1995) for flow 10 cm above the bottom of an interior location in a *S. alterniflora* marsh reveal a similar fall-off in energy between 0.1 and 1 Hz but lack any peaks in the 1 Hz range. Associated velocities were < 5 cm/s. If it is assumed that $d \approx 0.15$ cm, this velocity is associated with $Re_d < 75$, so it is not surprising that vortex shedding was not observed even when the wind wave influence was absent.

5.2.3 Turbulence

Turbulent intensity increases toward the surface because of the higher velocity and surface shear stresses there (Figure 5-7). When averaged by the local velocity, turbulence intensity also increases slightly. In other *S. alterniflora* canopies, turbulence intensity has also been observed to increase with distance away from the bed (Leonard and Luther, 1995).

Because of the confounding surface wave influence, Reynolds stresses and turbulent efficiency were not analyzed for field data.

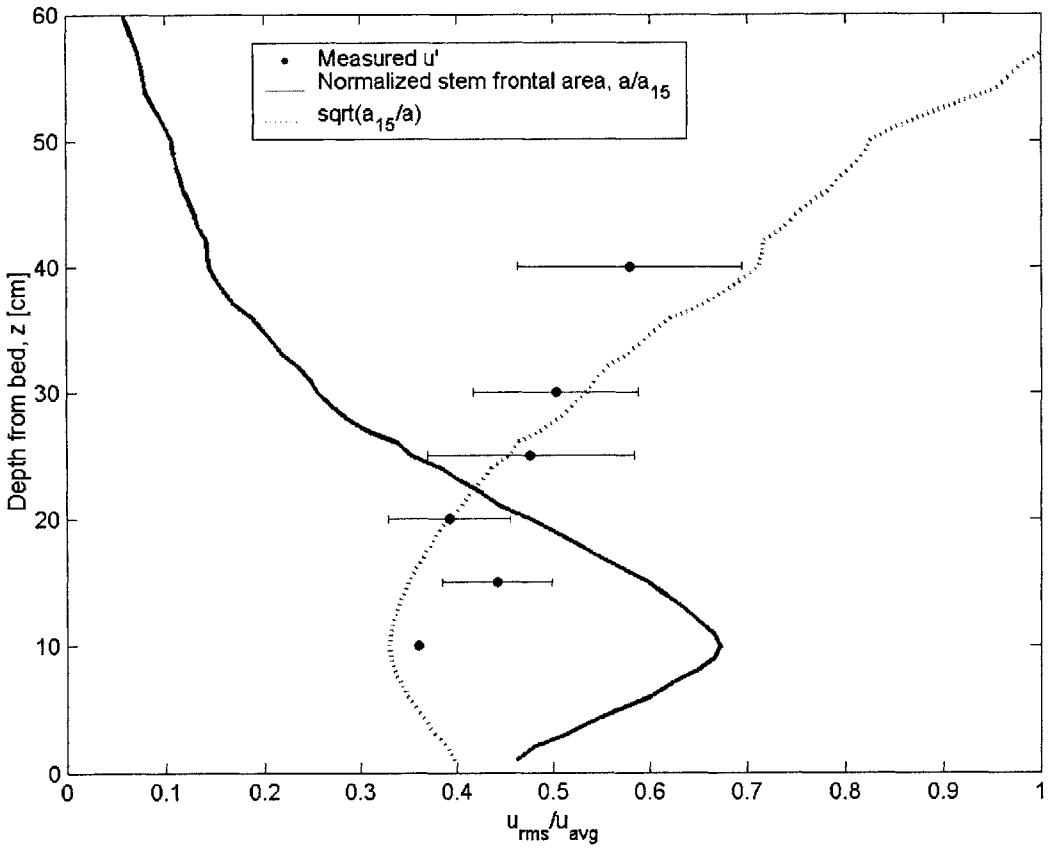

Figure 5-7. Vertical profiles of longitudinal turbulent energy in the field. Measurements are presented as $u_{rms} = \sqrt{u'}$, normalized by the average flow velocity for the entire profile. Data points are means of measurements taken using a 3D downward-looking ADV; horizontal bars indicate standard error of the mean across canopy heterogeneity. The point with no error bar is the time-averaged velocity at a single location; its error is expected to be comparable to that of the points directly above it. For comparison, the shapes of the curves of normalized stem frontal area a/a_{15} and $\sqrt{a_{15}/a}$ are shown.

Table 5-2. Turbulence statistics for different flow rates used in the field. All data are mean ± standard error of the mean, where the standard error represents variability across canopy heterogeneity, except for the single measurement at 10 cm from the bed.

z [cm]	u_{rms} [cm/s]	$(u/u_{15})_{rms}$
10	0.9	0.36
15	0.9 ± 0.1	0.44 ± 0.06
20	0.8 ± 0.2	0.39 ± 0.06
25	1.0 ± 0.2	0.48 ± 0.11
30	1.0 ± 0.2	0.50 ± 0.09
40	1.1 ± 0.3	0.58 ± 0.16

5.3 Vertical diffusivity

Vertical diffusivity in the field was estimated from fitting Gaussian curves to vertical concentration profiles downstream of a continuous dye release. Figure 5-8 illustrates how lateral transects through the evolving cloud were aligned by peak concentration; the peak concentration of each curve was averaged to provide a mean concentration at each depth and each longitudinal position downstream of the fluorometer. Releases were performed between 9 andj 12 cm from the bed, and downstream depths were measured relative to the release depth. It was assumed that the bed is a perfectly absorbing boundary, rather than a no-flux boundary, so that dye that diffuses downward does not affect the shape of the curve above the release depth. All of the resulting vertical concentration profiles appear to follow a Gaussian profile relatively well (equation 3-12; Figure 5-9), suggesting that diffusive processes are indeed responsible for vertical dye transport.

Figure 5-10 shows the values of D_z calculated for various distances between the release and measurement locations. These seven vertical profiles resulted from clouds taking seven different flow paths through the marsh, so the observed spread in D_z estimates also reflects spatial variability present in the marsh.

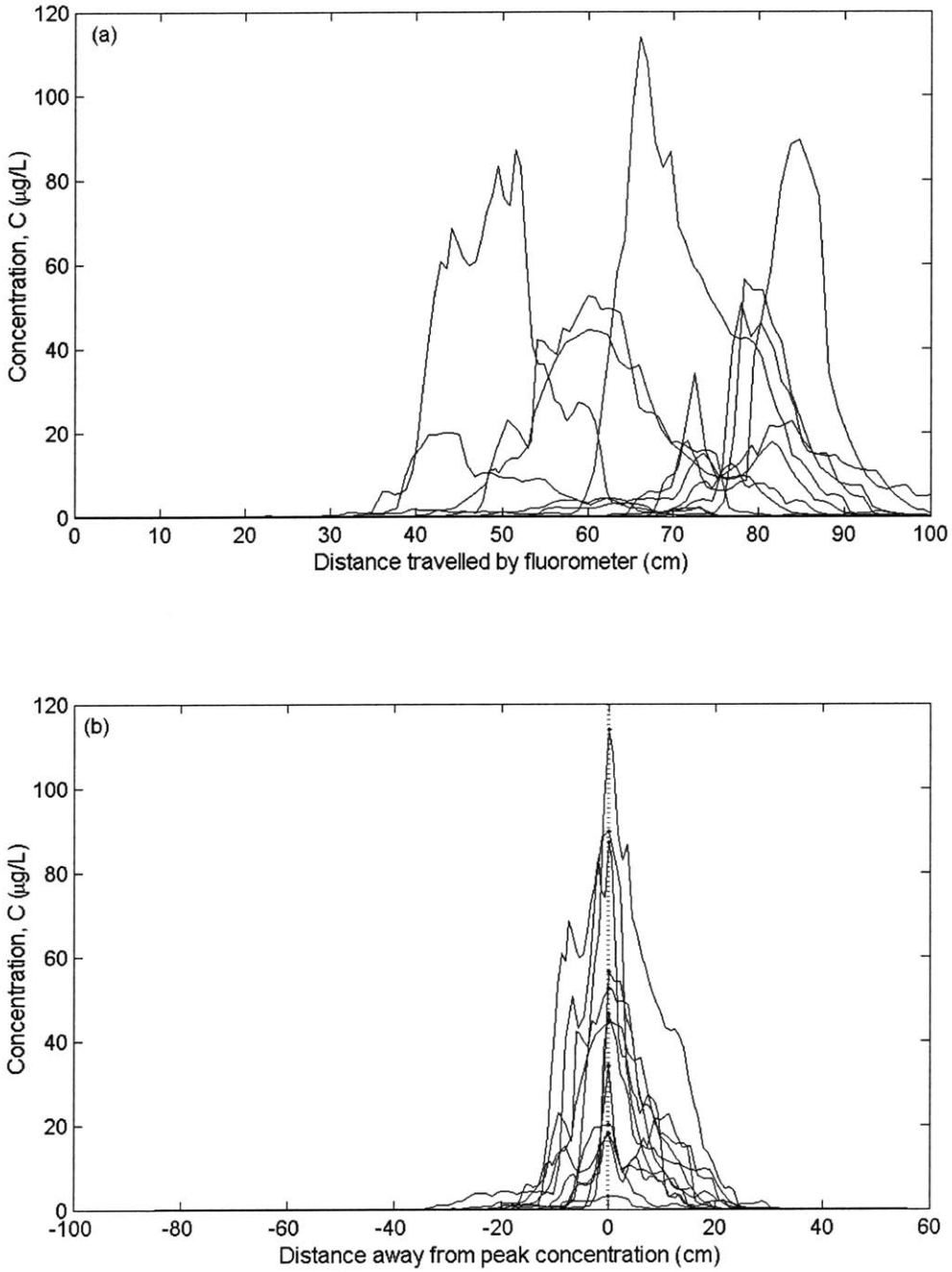

Figure 5-8. Example of calculation of concentration downstream of a continuous dye release in the field. (a) Eleven transects through a dye cloud 100 cm downstream of its release. Because of sway in the ambient current, the position of the peak concentration changes by approximately 22° during sampling at this position. (b) The transects aligned by peak concentration. These peak concentrations are then averaged to produce a single value for concentration at this position.

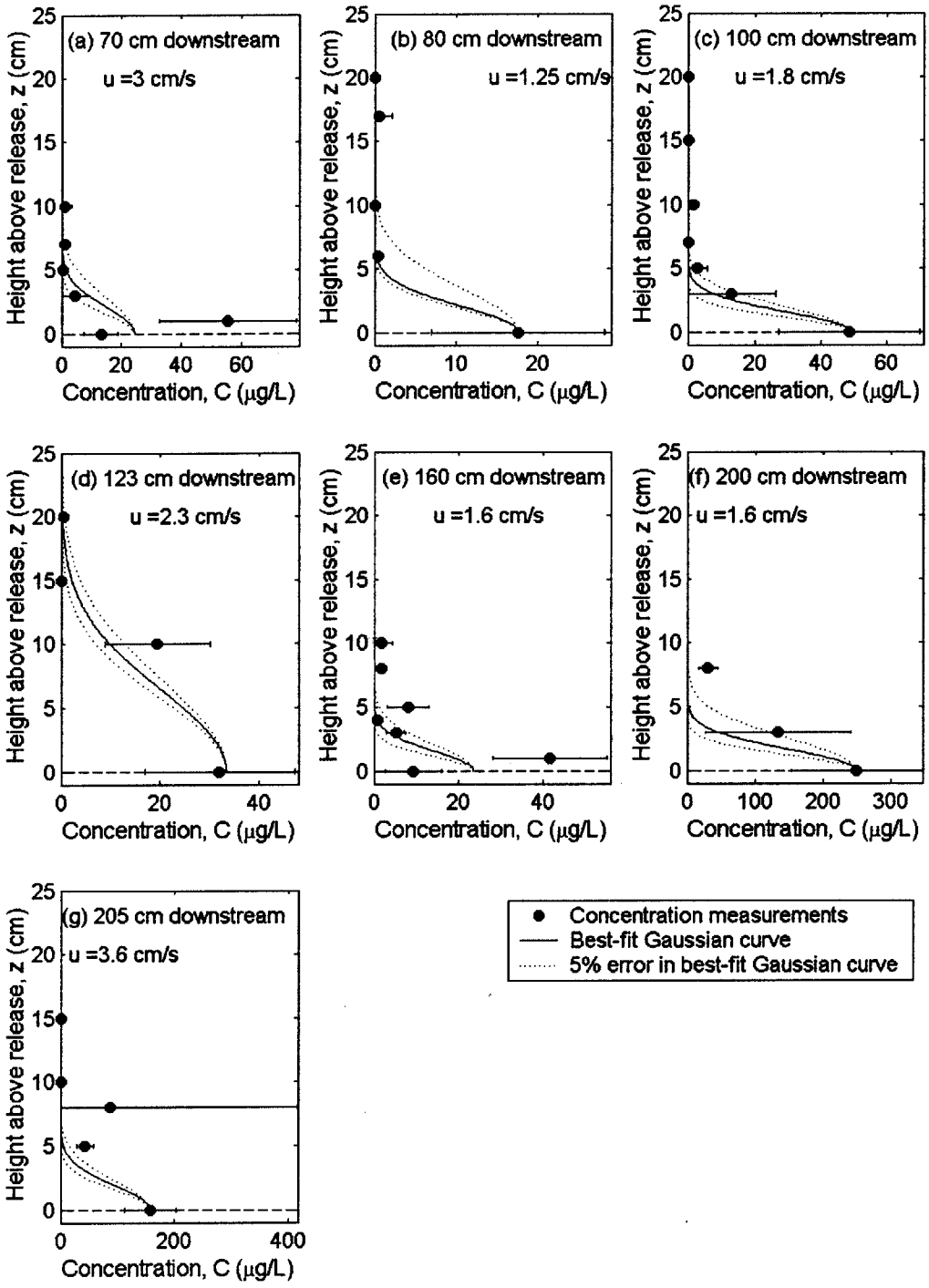

Figure 5-9. Vertical profiles of dye concentration downstream of a continuous dye release in the field. Each point is the mean of the peak concentration on several passes through the dye cloud; error bars represent the standard error of the mean at each distance from the bed. Each profile was measured at a different distance downstream of the point of release. The solid line on each profile is the least-squares best-fit Gaussian curve to these points, weighted by uncertainty. The dotted lines represent the curves that result when the squared residuals are changed by 5%.

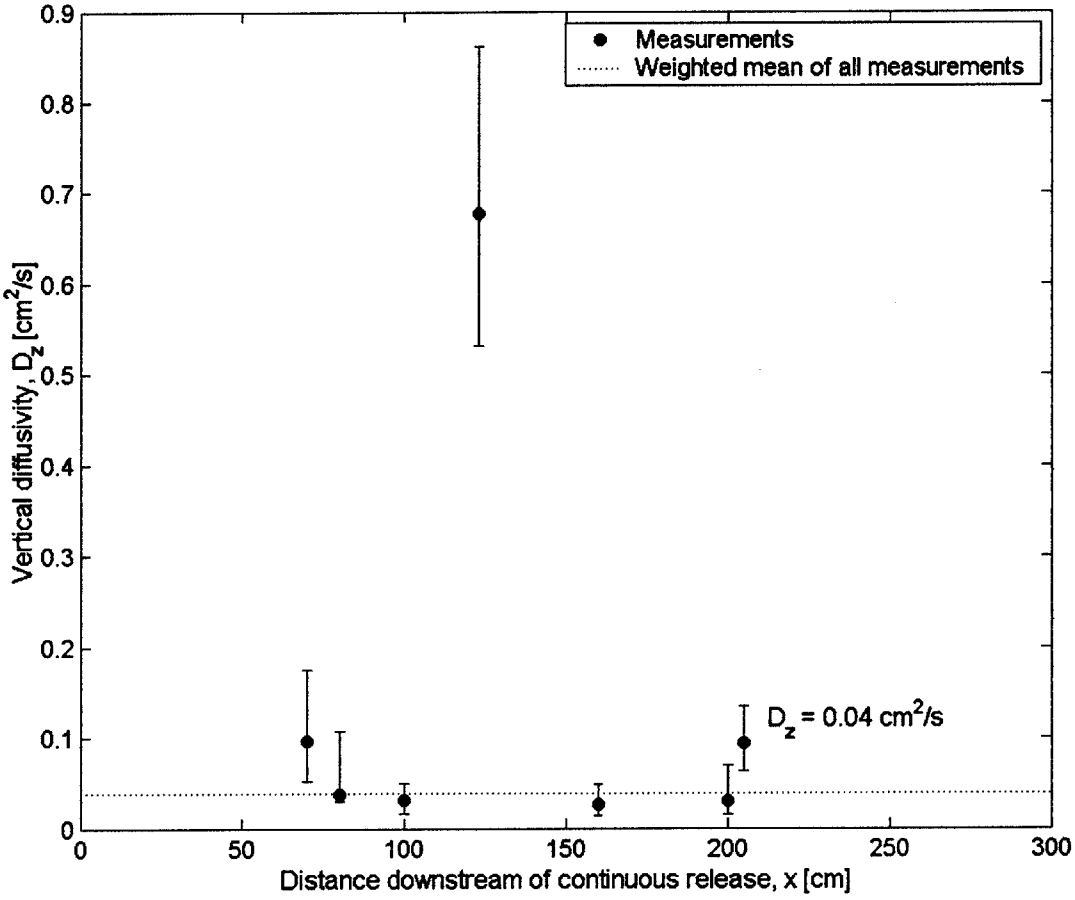

Figure 5-10. Vertical diffusivity constants in the field measured at different locations downstream of a continuous dye release. Values of D_z are derived from the fit of a Gaussian curve to the vertical profiles of concentration: $V = V_o \exp(-uz^2/4D_z x)$. Error bars indicate the value of D_z that produces a 5% change in the least-squares residuals for this fit. The dotted line indicates the mean of all measurements weighted by variance.

Table 5-3. Vertical diffusion in the field. Diffusion constants are estimated from fitting a Gaussian curve to the shape of a continuous dye release in the field. The listed error is the average change in the value of D_z that produces a 5% change in the least-squares residuals for the fit. Velocity measurements indicate the local velocity as determined by slug releases.

Vertical diffusivity	Water velocity					
	1.25 cm/s	1.6 cm/s	1.8 cm/s	2.3 cm/s	3.0 cm/s	3.6 cm/s
D_z [cm^2/s]	0.04 ± 0.04	0.03 ± 0.02	0.03 ± 0.02	0.7 ± 0.2	0.10 ± 0.06	0.09 ± 0.04

The distance between the release and measurement locations does not significantly affect estimated vertical diffusion when the dye is between 10 and 20 cm from the bed. However, vertical diffusion may not be constant over depth. As the dye cloud travels farther and diffuses higher vertically, it will experience a higher flow speed due to the reduced vegetation density, which will likely increase the vertical diffusion coefficient. For example, a slightly higher dye concentration was used to generate the profile 123 cm downstream of release, and dye was detected much higher up in the canopy [over 30 cm from the bed; Figure 5-9(g)]. Perhaps because the dye was experiencing the elevated velocities and lower drag present at these greater distances from the bed, the calculated value of D_z for this profile was much higher than for other profiles.

The mean coefficient of vertical diffusivity in the field is 0.04 ± 0.01 cm^2/s (mean ± standard error of the mean). This value is within the range observed by Nepf et al. (1997b) in a laboratory flume study of emergent vegetation and is slightly higher than the value of 0.003 cm^2/s obtained by Saiers et al. (2003) when measuring particle transport in the Everglades.

Note that, even if D_z below the release depth is as high as 0.1 cm^2/s, the dye will require O(15 m) to travel the 10 cm down to the bed and then diffuse back up to the release depth. Since these measurements were all performed within 2.2 m of the release, the flux condition at the bed does not influence results.

Both turbulent and mechanical diffusion models predict a linear relationship between vertical diffusivity and ambient flow speed, which within error agrees with measurements (Figure 5-11; Table 5-3). No significant relationship was observed when all data were considered because of the large error bars on the measurement taken when the flow velocity was 2.3 cm/s. When Chauvenet's criterion is used to exclude this measurement as an outlier (Taylor, 1997), there is evidence that vertical diffusivity and flow speed are positively correlated, D_z [cm^2/s] = 0.02 u [cm/s] ($r^2 = 0.88$).

5.4 Longitudinal dispersion

Longitudinal dispersion constants were estimated from instantaneous releases in the field. Longitudinal dispersion is directly proportionate to the rate of increase in spatial variance with time (equation 2-25). When all data are plotted together, there is a large amount of scatter in the measured cloud variance as a function of time (Figure 5-12).

On a salt marsh platform, the ambient flow speed and depth change over time as the tide floods and recedes. It was therefore impossible to duplicate flow conditions among releases. Slugs of dye were released from 5 to 44 cm above the bed and while the local flow was moving at a horizontal velocity of 0.2 to 7.7 cm/s. It is likely that the observed scatter in the cloud widths resulted from differences in the conditions under which the measurements were taken. In particular, differences in flow velocity will affect the observed travel time between release and measurement, and differences in release depth will affect the density of the vegetation through which the dye passes.

To tease apart the effect of velocity and vegetation density on measured variance, the data were binned into sixteen different groupings (Figure 5-13). The measured curve of vegetation density over depth (Figure 5-4) was used to estimate the vegetation density experienced by dye released at different depths. Four different frontal density levels (<0.03 cm^2/cm^3, 0.03-0.045 cm^2/cm^3, 0.045-0.06 cm^2/cm^3, and >0.06 cm^2/cm^3) and four different velocity levels (< 1.5 cm/s, 1.5 cm/s-2.5 cm/s, 2.5 cm/s-3.5 cm/s, and 3.5-4.5 cm/s) were used to categorize the measurements. These velocity bins roughly correspond to the speeds used in the

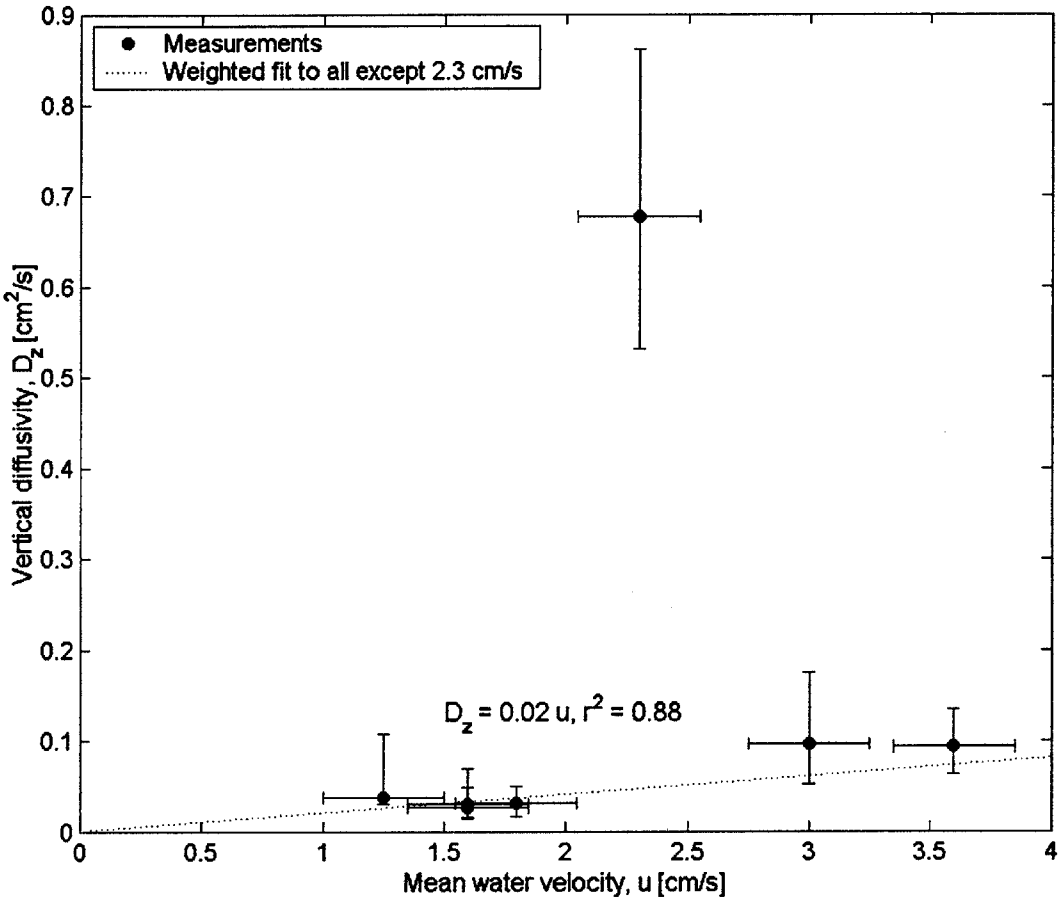

Figure 5-11. Vertical diffusivity as a function of flow velocity. Vertical diffusivity coefficients are estimated from curves fit to vertical dye concentration profiles. Vertical bars indicate the value of D_z that produces a 5% change in the least-squares residuals for this fit. Horizontal bars indicate an error in velocity measurement of 0.25 cm/s. The dotted line is the best-fit straight line through zero weighted by fitting error.

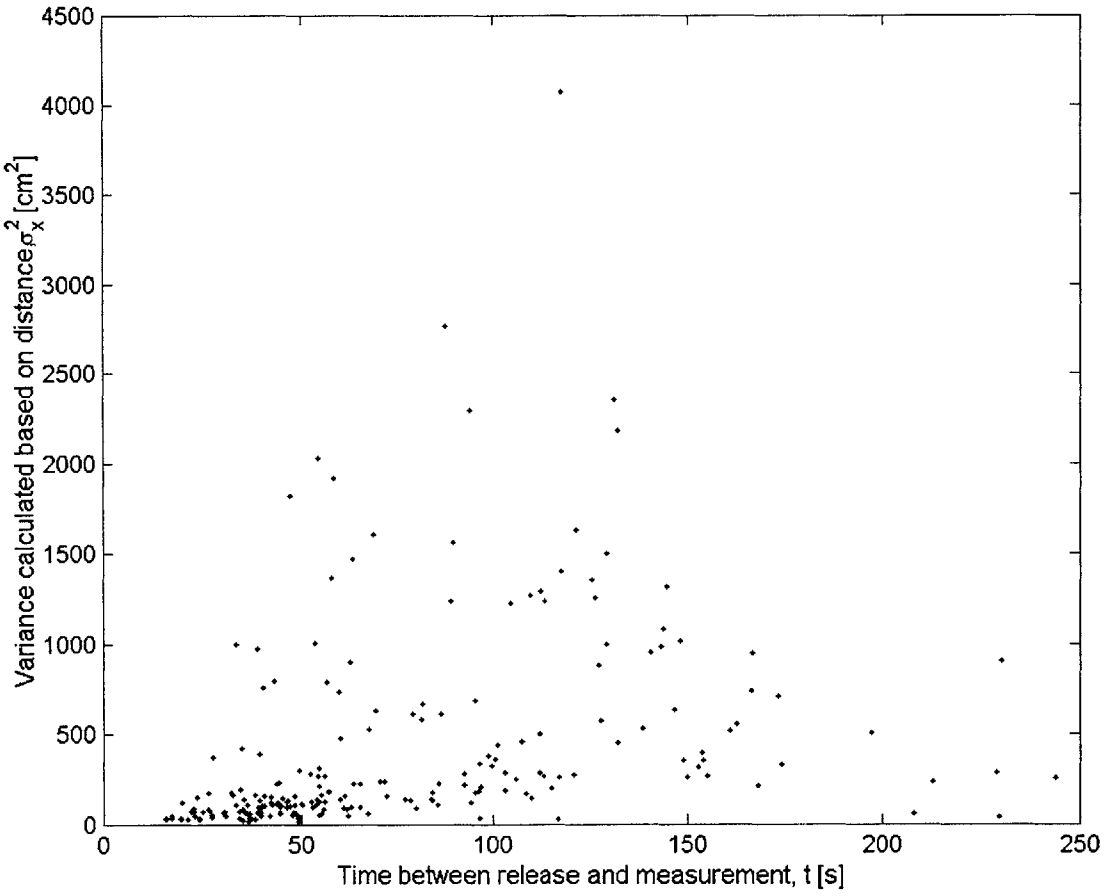

Figure 5-12. Measured cloud variance as a function of time in a natural *S. alterniflora* canopy. Each point represents the variance in the record of dye concentration versus time since release for a single dye slug, converted to a spatial variance by multiplication by the average velocity for the slug ($\sigma_x = \sigma_t * x/t_{avg}$).

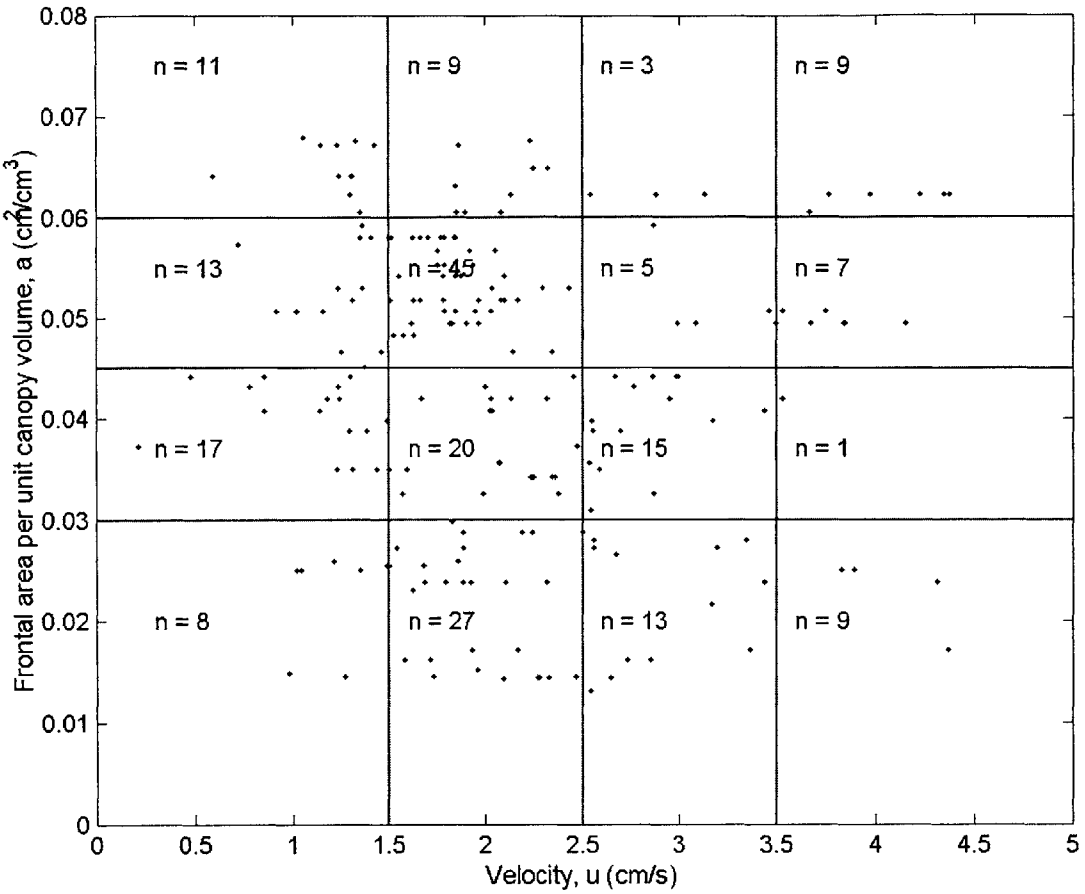

Figure 5-13. Average dye velocity and stem frontal area at release depth for each dye slug in the field. The measurements are shown binned into four different frontal area levels (<0.03 cm^2/cm^3, 0.03-0.045 cm^2/cm^3, 0.045-0.06 cm^2/cm^3, and >0.06 cm^2/cm^3) and four different velocity levels (< 1.5 cm/s, 1.5 cm/s-2.5 cm/s, 2.5 cm/s-3.5 cm/s, and 3.5-4.5 cm/s). The numbers indicate the number of measurements in each bin.

Table 5-4. Longitudinal dispersion in the field. Dispersion constants are calculated from field slug releases for different velocity and frontal area density bins. Error indicates standard error of the mean.

Longitudinal dispersion	Frontal area density	Flow velocity				
		< 1.5 cm/s	1.5 – 2.5 cm/s	2.5 – 3.5 cm/s	> 3.5 cm/s	All velocities
K_x [cm^2/s]	< 0.03 cm^2/cm^3	2.3 ± 0.8	4.9 ± 1.0	8.8 ± 2.7	14.3 ± 2.5	4.1 ± 0.9
	> 0.03 cm^2/cm^3	0.9 ± 0.3	2.3 ± 0.3	14.7 ± 2.7	9.3 ± 1.8	1.3 ± 0.2
	All densities	1.0 ± 0.2	3.4 ± 0.4	11.2 ± 1.7	13.0 ± 1.8	

laboratory study. Because only five slugs were released when the velocity was > 4.5 cm/s, they were not included in calculations and are not shown in Figure 5-13; including them would change estimated dispersion constants by less than 5%.

Longitudinal dispersion constants were estimated from the rate of growth of spatial variance as a function of time since release (Table 5-4). The slope of this fit ($\propto K_x$; cf. equation 2-25) increases over time as the cloud increases in size and encounters more heterogeneity, so multiple measurements at a variety of times must be taken to estimate K_x. Not enough measurements were obtained to estimate K_x reliably for each velocity and frontal area level. When just the frontal area groupings are considered (Figure 5-14), there appears to be a large difference between the measurements obtained for frontal area < 0.03 cm^2/cm^3 (K_x = 4.1 cm^2/s) and the other three groupings (weighted average of K_x = 1.3 cm^2/s; see Figure 5-15). Frontal area is less than 0.03 cm^2/cm^3 in the highest portions of the canopy (> 30 cm from the bed), where wind stress is largest and where velocity changes most rapidly over depth (see Figure 5-5). It is therefore possible that slugs released high in the canopy experience different dispersive processes, in particular elevated shear dispersion.

The different velocity groupings have a larger effect on the observed longitudinal dispersion (Figure 5-16). Because there appears to be a difference when in frontal area is greater than and less than 0.03 cm^2/cm^3, dispersion constants were calculated separately for slugs released at depths with frontal area greater than and less than 0.03 cm^2/cm^3. For all groupings,

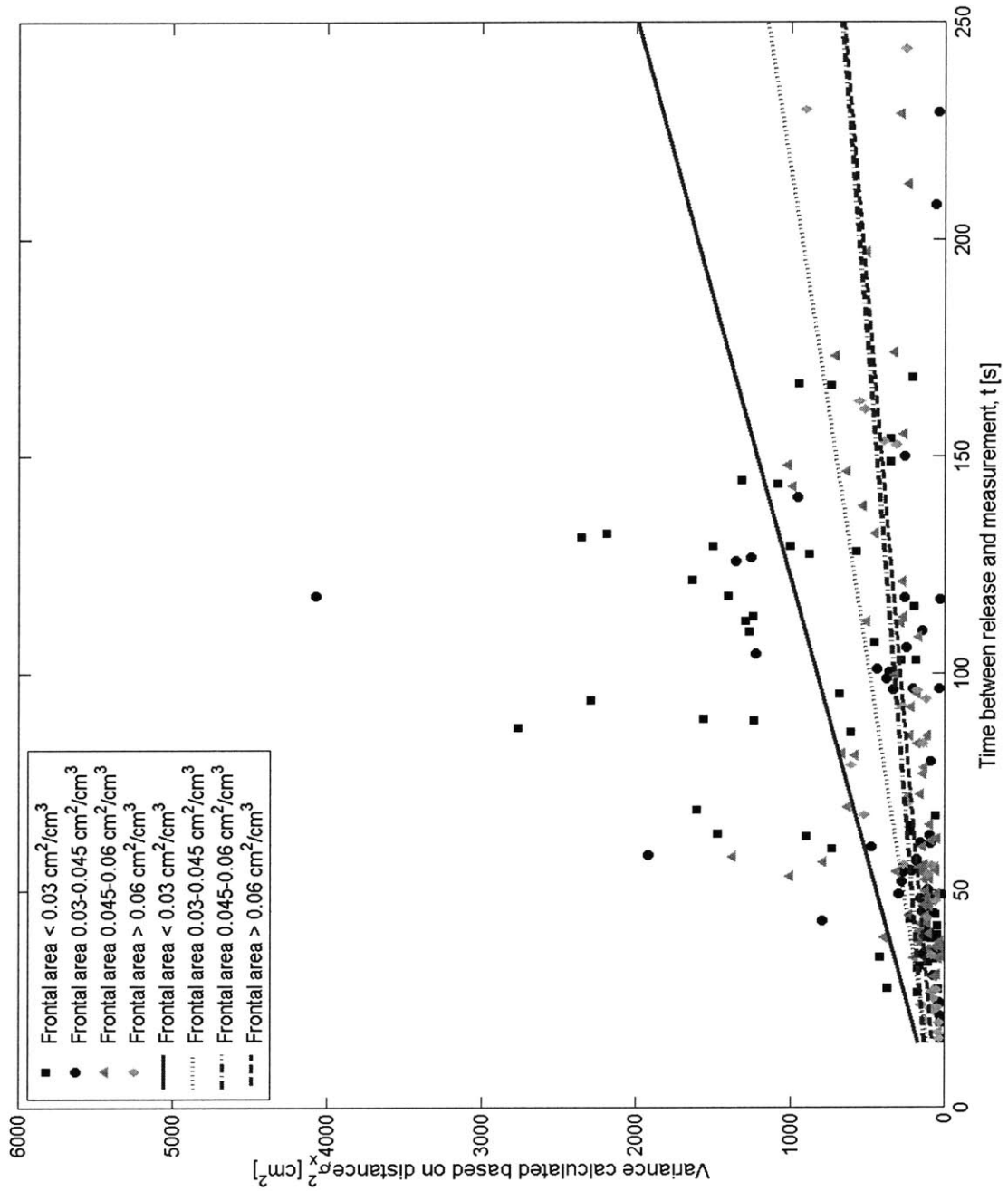

Figure 5-14. Field measurements of cloud variance binned by estimated frontal area. Each point represents the spatial variance of a dye cloud for a single dye slug release. The lines are best-fit straight lines to the different frontal area bins. Assuming a Fickian model, the dispersion constant is directly proportionate to the slope of the linear fit between spatial variance and time ($K_x = ½\ d\sigma_x/dt$).

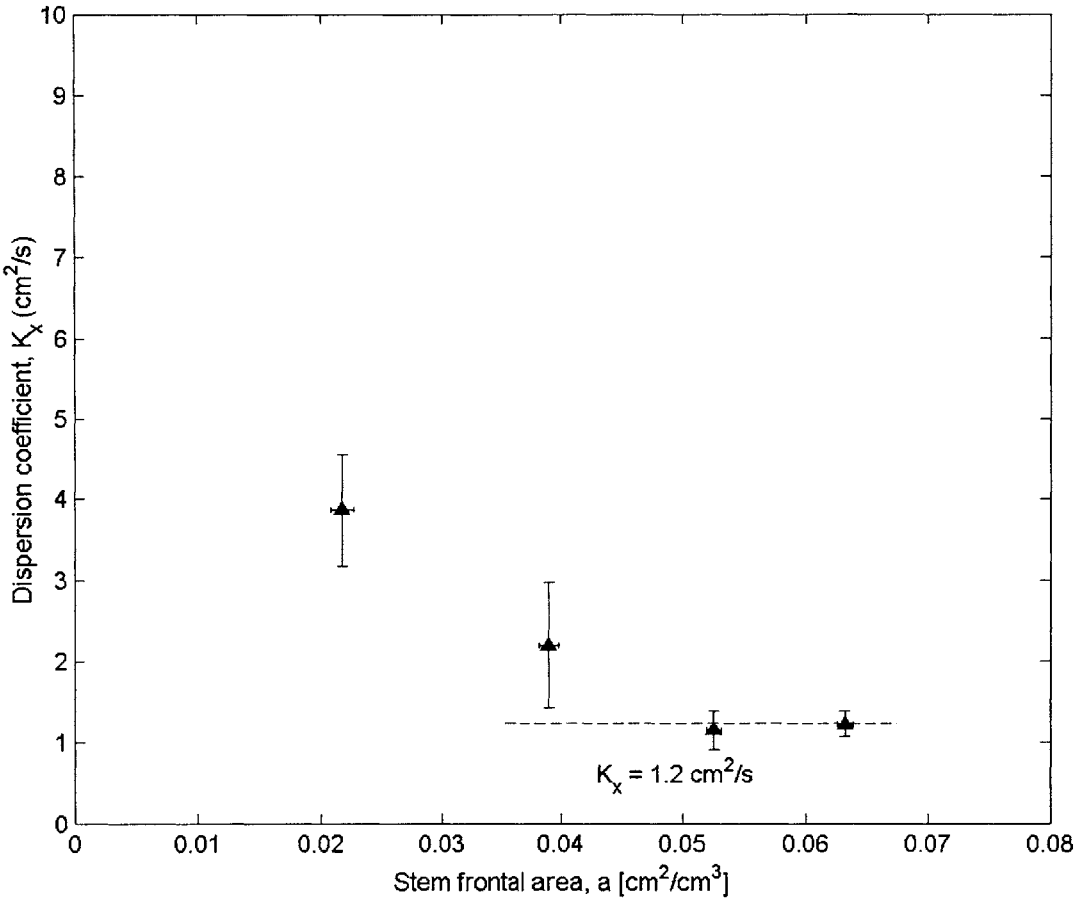

Figure 5-15. Dispersion constants for field measurements as a function of stem frontal area. Dispersion coefficients are calculated from the slope of the plot of spatial variance versus time since release ($K_x = ½\ d\sigma_x/dt$). Vertical bars indicate error in the dispersion constant fit. Horizontal bars indicate standard error of the mean frontal area density for each bin. In addition, the average K_x weighted by variance is shown for the three larger frontal area groupings.

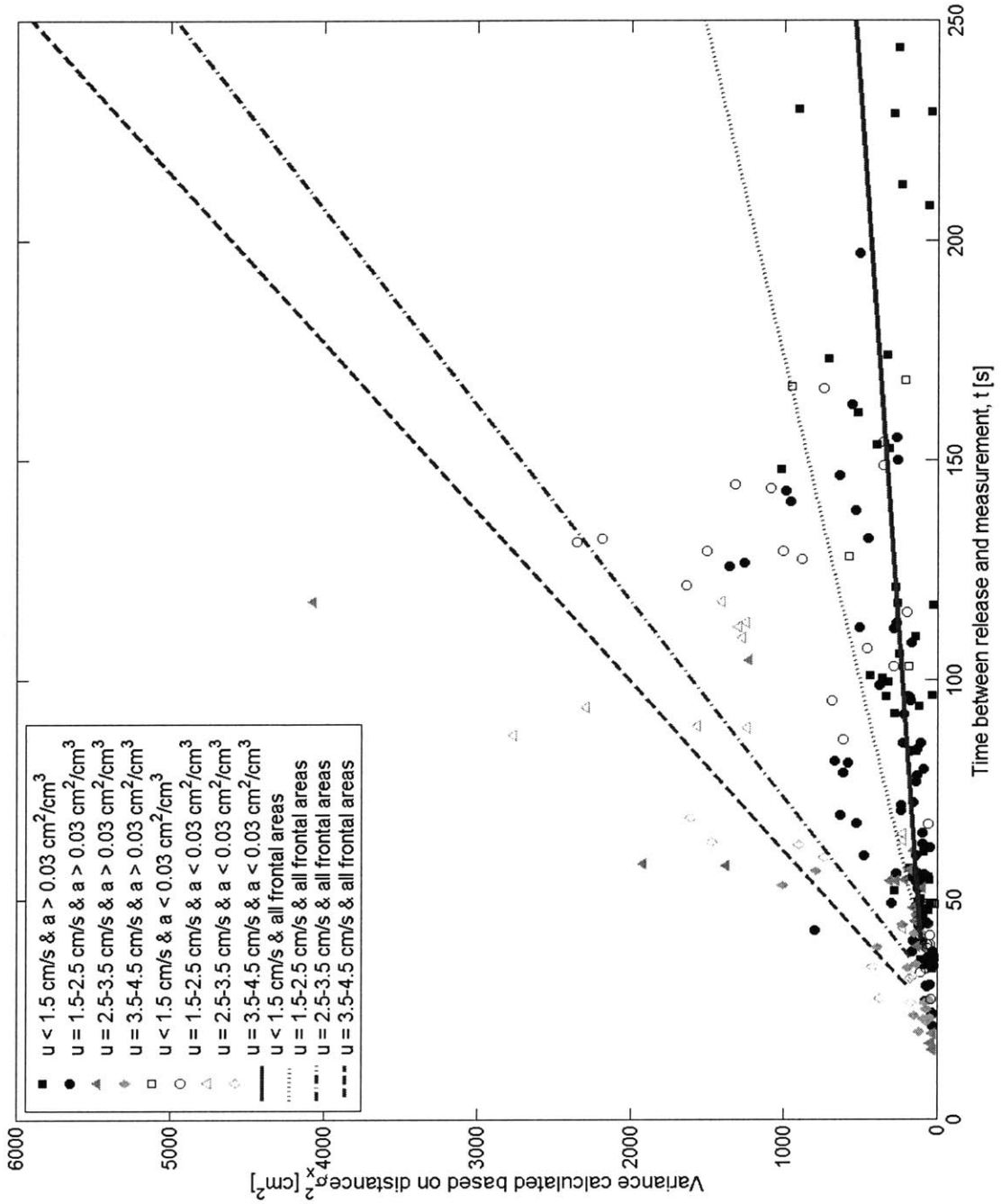

Figure 5-16. Field measurements of cloud variance binned by velocity. Each point represents the spatial variance of a dye cloud for a single dye slug release. The lines are best-fit straight lines to all the measurements (both <0.03 cm^2/cm^3 and >0.03 cm^2/cm^3) in the different velocity bins.

K_x is positively related to flow velocity (for a linear fit, $r^2 = 0.89$ when all measurements are considered; $r^2 = 0.999$ when only measurements <0.03 cm^2/cm^3 are considered; see Figure 5-17). Note that, because the dispersion constant cannot be negative, this linear fit can only be applied above a threshold of ~ 1 cm/s.

Note that the observed relationships may not hold up outside of the studied ranges. For very low velocities, dispersion will approach molecular diffusion. For much larger velocities, if they exist, the vegetation may bend out of the way and other processes may also become important. Similarly, different values of longitudinal dispersion may exist outside of this range of frontal area density. In particular, it is likely that K_x further increases as frontal area decreases and the vegetation begins to behave like a roughness layer on an otherwise logarithmic velocity profile.

Plotting spatial variance against the distance between release and measurement removes the influence of velocity on the measured variance. The mean spatial variance of field slug releases for the different velocity bins are plotted against distance in Figure 5-18. [Here, slugs released in all frontal area conditions are considered together; separating the data into different frontal area bins does not have a large effect on the results (data not shown)]. Within 150 cm of the release location, the rate of increase in variance is similar for all velocities. There is, however, considerably more variation in results at distances greater than 150 cm: the means of each bin are more separated, and the associated error bars are much larger.

These values for the longitudinal dispersion constant are consistent with those observed previously in natural systems. Hosokawa and Horie (1992) estimated K_x = 1-10 cm^2/s in a natural reed marsh in Japan. Saiers et al. (2003) reported that K_x = 0.42 cm^2/s for particles traveling through 6.8 m of grass in the Everglades.

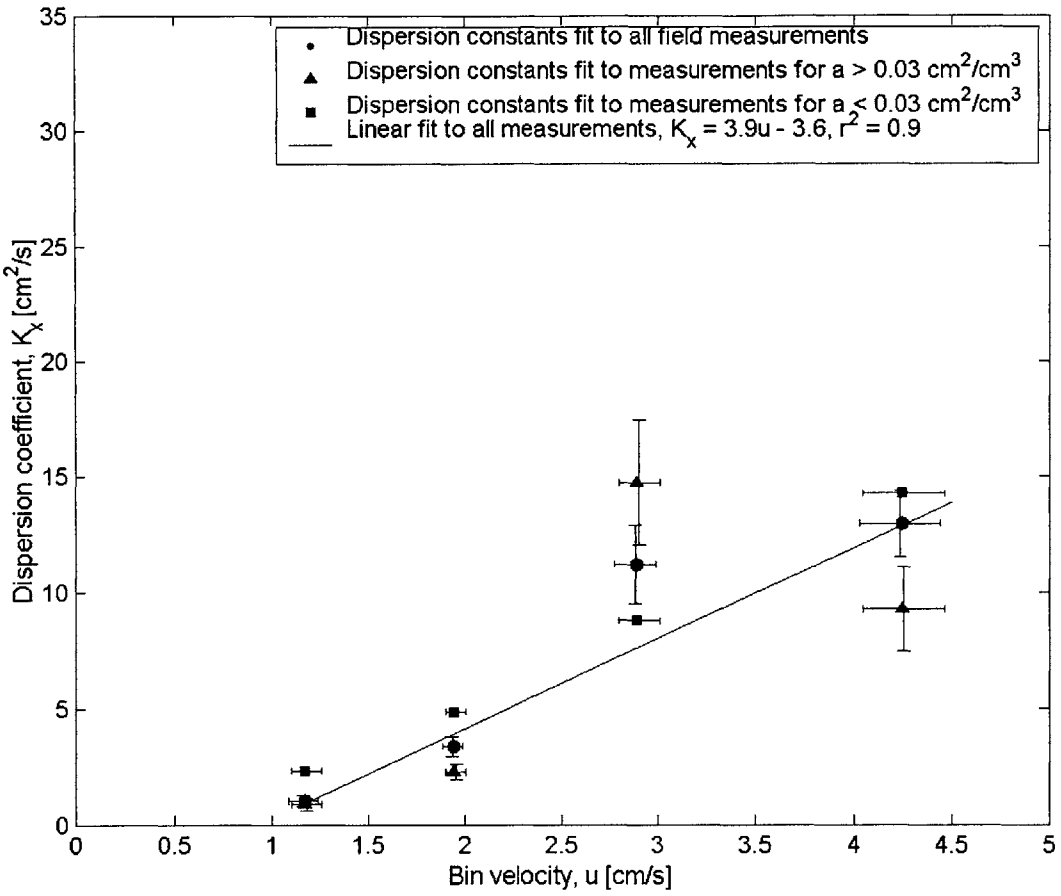

Figure 5-17. Dispersion constants for field measurements as a function of flow velocity. Flow velocity is calculated from the mean travel time (first temporal moment) for each cloud. Vertical bars indicate error in the dispersion constant fit. Horizontal bars indicate standard error of the mean velocity for each bin. Data points at the same velocity are offset slightly to distinguish error bars. Note that the dispersion constants increase linearly with velocity; the straight-line fit to all measurements is shown.

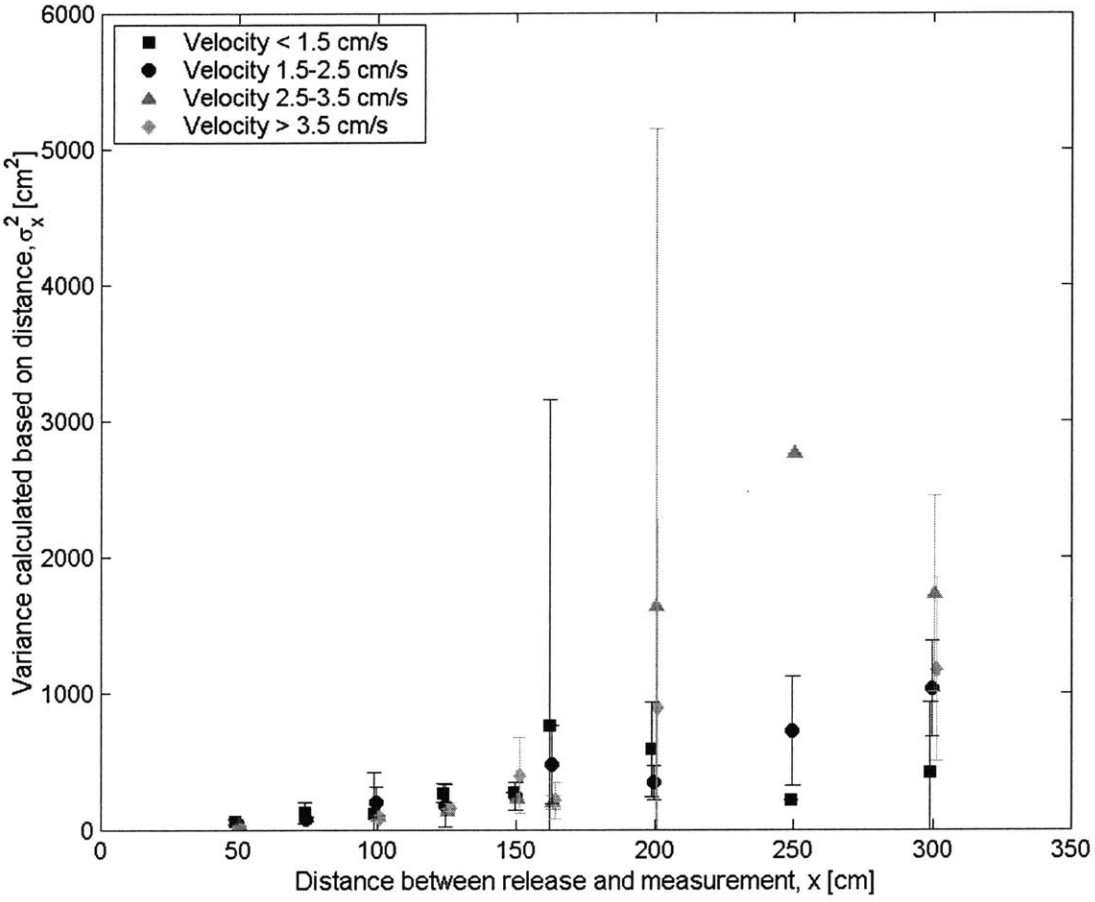

Figure 5-18. Dispersion of field measurements binned by velocity versus distance. Data points represent the mean variance for each velocity bin; error bars represent the standard error of the mean between different slug releases. Data points at the same distance are offset slightly to distinguish error bars. The point with no error bar is the variance calculated from a single slug release; repeated measurements at this distance downstream are expected to have an error comparable to that of nearby points.

Table 5-5. Skewness and patchiness of field slug releases at different distances downstream of release. Data are presented as mean ± standard error of the mean across slug releases.

Variable	Distance downstream								
	50 cm	75 cm	100 cm	125 cm	150 cm	163 cm	200 cm	250 cm	300 cm
Skewness, S	0.65 ± 0.39	0.52 ± 0.14	0.44 ± 0.15	0.50 ± 0.23	0.40 ± 0.28	0.35 ± 0.29	0.05 ± 0.28	0.00 ± 0.64	0.37 ± 0.14
Patchiness, C_{rms}/C_{avg}	2.2 ± 1.3	1.3 ± 0.3	1.5 ± 0.7	1.1 ± 0.4	0.6 ± 0.2	0.9 ± 0.4	0.4 ± 0.2	0.5 ± 0.6	1.2 ± 0.2

5.5 Skewness

The skewness of a concentration curve indicates whether it has reached its Fickian limit. Values of skewness for field slug releases are listed in Table 5-5. Although individual clouds do not appear Gaussian, the mean skewness approaches 0 after the dye cloud has traveled 250 cm and then increases to 0.4 by 300 cm (Figure 5-19). This progression suggests that the processes controlling dispersion at short distances become fully developed by 250 cm, and then other processes become important.

5.6 Patchiness

Individual concentration records taken at a single location downstream of an instantaneous release were not smooth Gaussian curves. Instead, they appeared much like releases in the laboratory (cf. Figure 4-16). Temporal averages over several curves, however, began to approximate a smooth Gaussian curve (Appendix B). Diffusion theory can therefore be used to predict the behavior of the center of mass, although, as noted by Finelli (2000), the behavior of individual clouds, and therefore the concentrations experienced by organisms, may differ drastically from this average.

The root mean square of the concentration deviation, C_{rms}, is a measure of the variability within each cloud. It is expected that the cloud variability decreases over distance, as more

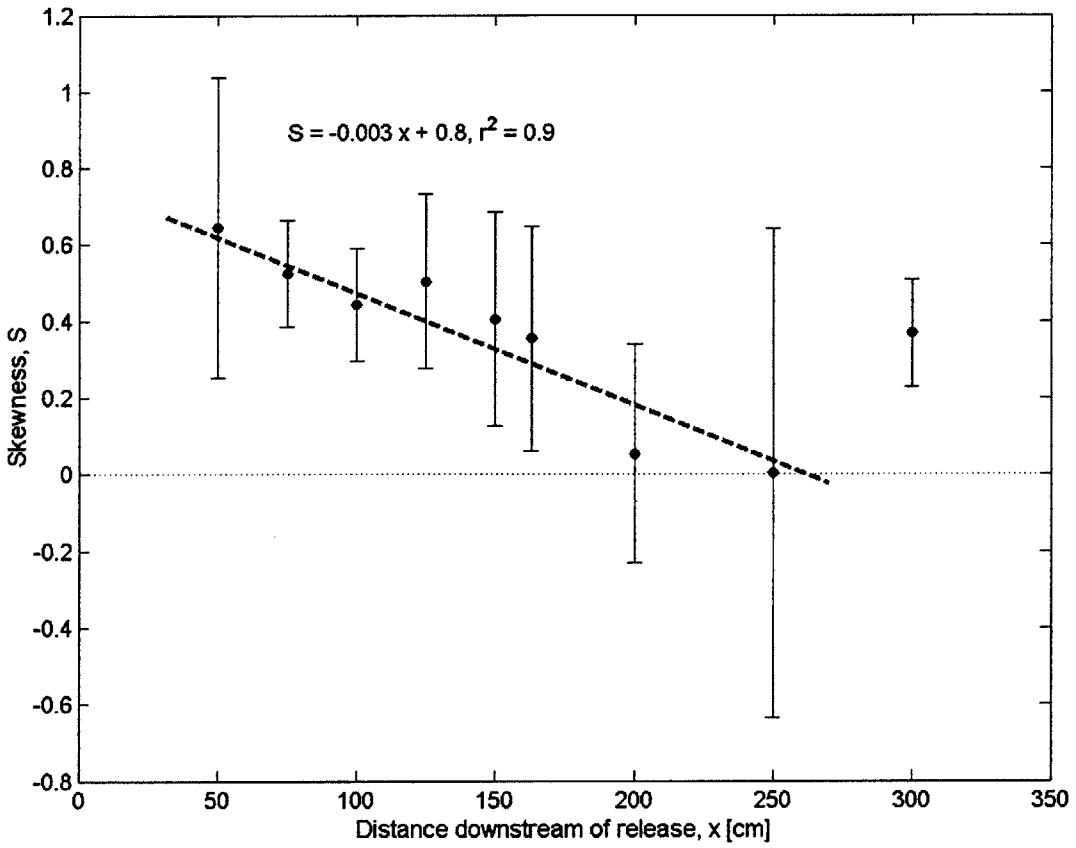

Figure 5-19. Skewness of slug releases in the field. Mean cloud skewness is shown, along with standard error in the mean, at various positions downstream of an instantaneous dye release. The data for all slugs measured $x \leq 250$ cm from their release are fit to a line.

turbulent eddies and stem-sized vortices have a chance to act on the cloud and mix out local heterogeneity. In particular, White and Nepf (2003) noted a smoothing of the cloud for large Reynolds number ($Re_d > 200$). Here, except for an anomalous measurement at 300 cm downstream, patchiness tends to decrease over distance (Table 5-5; Figure 5-20). (Note that it would be entropically unfavorable for dye filaments to re-form, so this observation is perhaps an artifact of the measurement technique.)

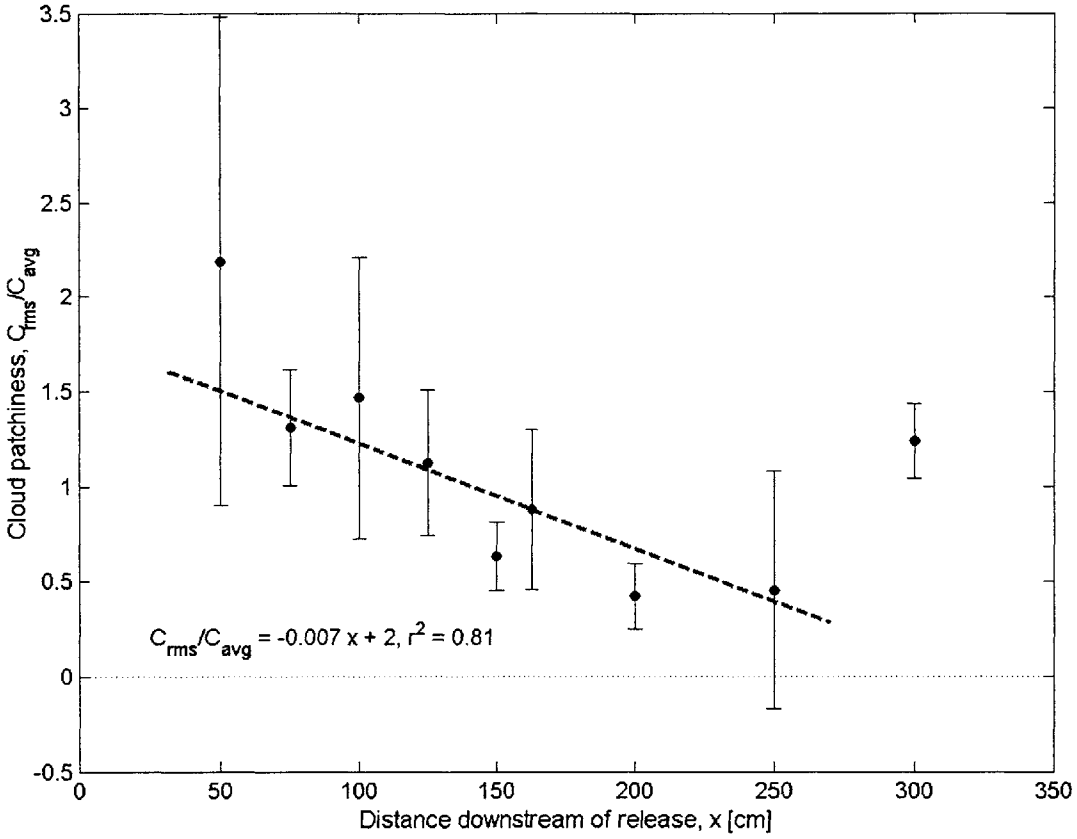

Figure 5-20. Patchiness of slug releases in the field. Mean patchiness is shown, along with standard error in the mean, at various positions downstream of an instantaneous dye release. The data for all slugs measured $\leq$ 250 cm from their release are fit to a line.

Chapter 6

Conclusions

6.1 Comparison of laboratory and field results

Despite the simplifications involved in approximating natural emergent vegetation by an array of wooden dowels in a laboratory flume, the laboratory and field canopies considered here appear to be governed by similar mechanisms over small to intermediate temporal and spatial scales. Over the velocity range of 1-4 cm/s, the stem density range ad = 0.004 - 0.100, and within 300 cm of a slug release, vertical diffusivity, longitudinal dispersion, turbulence intensities, and vertical variation in longitudinal velocity are on the same order of magnitude in both the laboratory and the field. Therefore, at short distances, emergent stands of *S. alterniflora* can be modeled as random arrays of thin circular cylinders.

6.1.1 Velocity

In both the laboratory and the field, the shape of the velocity profile was constant across different flow rates (although it different substantially between the laboratory and field). In the laboratory, velocity profiles were obtained only at the highest and lowest flow rates, but both profiles revealed a similar step profile with a 2-cm wide interface (Figure 4-1). This same step flow is therefore likely present in the intermediate flow rates. Vertical profiles in the field were obtained over a wider range of depth-averaged velocities, and within error they also were constant over flow rate (cf. Appendix A).

Also, in both the laboratory and the field, local longitudinal velocity, $u(z)$, is proportional to $1/\sqrt{C_d a(z)}$ over at least part of the canopy (Table 4-2; Figure 5-5). This relationship is expected for drag-dominated flow (equation 2-40), so its presence supports the assumption that drag balances pressure forcing at each distance from the bed in emergent canopies. In the field, it appears to be a good approximation for distances less than 40 cm from the bed, which is where $a > 0.015$ cm^2/cm^3 so $ad > 0.002$ (cf. Figures 5-4 and 5-5).

The value of the proportionality constant differs in the laboratory and field. In the field $|u|/u_{15} \approx \sqrt{a_{15}/a(z)}$, but in the laboratory $u_{top}/u_{bot} \approx 0.7\sqrt{a_{bot}/a_{top}}$. Including the predicted drag coefficient, the results are slightly closer: in the field $|u|/u_{15} \approx \sqrt{(C_d a)_{15}/C_d a(z)}$, and in the laboratory $u_{top}/u_{bot} \approx 0.8\sqrt{(C_d a)_{bot}/(C_d a)_{top}}$. The agreement between prediction and theory is thus quite good near the bed in the field. In the laboratory, it is possible that the strong shear layer affects the drag coefficient in the bottom and top layers in a nonlinear fashion.

If stem drag balances pressure forcing in the canopy (equation 2-10), the turbulent stress terms in equation 2-9 must be small compared to vegetative drag:

$$\frac{\partial}{\partial z}\left(\nu_t \frac{\partial u}{\partial z}\right) \approx \frac{\partial}{\partial z}\overline{u'w'} << \frac{1}{\rho}F_d = \frac{1}{2}C_d a u^2 \qquad (6\text{-}1)$$

The relative magnitude of these terms can be compared in the laboratory, where Reynolds stress was measured. For the lowest flow rate, the maximum value of $\overline{u'w'}$ occurs at the interface and is equal to -0.04 cm^2/s^2. The width of the shear layer is ~2 cm, so the maximum value of $\frac{\partial}{\partial z}\overline{u'w'} \approx 0.02$ cm/s^2. The drag force, $\frac{1}{2}C_d a u^2$, predicted in the upper canopy is 0.01 cm/s^2 and in the lower canopy is 0.02 cm/s^2. The stress terms are therefore not negligible at the interface, and the flow cannot be completely described as a balance between pressure and stem drag terms. It is therefore not surprising that u_{top}/u_{bot} does not equal $\sqrt{(C_d a)_{bot}/(C_d a)_{top}}$

The laboratory setup provides a bound on the amount of shear possible in an aquatic system; a step gradient in $ad(z)$, and hence $u(z)$, would be quite rare in real vegetation. In the field, if it is assumed that $\nu_t \sim D_t$, then $\frac{\partial}{\partial z}\left(\nu_t \frac{\partial u}{\partial z}\right) \approx \frac{\partial}{\partial z}\left(D_t \frac{\partial u}{\partial z}\right) \sim \frac{D_t \Delta u}{(\Delta h)^2}$, where Δh is the width of the shear layer. Assuming $D_z = 0.05$ cm^2/s, $\Delta u = 0.5$ cm/s, and $\Delta h = 3$ cm (the expected width of a cloud after 150 s), then $\frac{D_t \Delta u}{(\Delta h)^2} \approx 0.003$ cm/s^2. The drag force, $\frac{1}{2} C_d a u^2$, predicted for $u = 2$ cm/s at 20 cm from the bed is 0.3 cm/s^2. In the field, therefore, scale analysis confirms that drag dominates flow in the *S. alterniflora* canopy.

Water depths at the field site reached over 90 cm. If flow through the marsh is only dominated by drag within 35 cm of the bed, at first glance it appears that flow dominated by stem drag may not control much of the water column. It is likely to be important, however, in the bulk of the marsh. Because the field study site was deliberately chosen because it floods during every tide, its elevation is lower than the rest of the marsh, which may only flood on spring tides. In addition, the fastest tidal velocities occur soon after the platform is flooded and just before it is exposed, when the water level is at its lowest (cf. Shi et al., 2000), so most transport will occur during periods of fully emergent vegetation. Also note that suspended sediment concentrations are highest just after the platform is flooded (Christiansen et al., 2000), further supporting the idea that scalar transport occurs during periods when the stems play a large role in controlling water velocity. It is therefore likely that flow dominated by stem drag governs transport over the bulk of the marsh platform during most tides.

Flow in both the laboratory and field systems was at moderate Reynolds numbers, somewhere between the well-defined streamlines of Stokes flow and the large sweeping vortices and rapid small-scale mixing that characterize high Reynolds number flow. Despite Re_d reaching O(300), there was a lack of evidence of vortex structures in the laboratory: none were seen using dye visualization, there is no signal of vortex shedding on spectra, turbulent efficiency is low, the boundary layer thickness is roughly constant with increasing flow velocity, and complete small-scale mixing of dye plumes was absent. Time-averaged velocities up to 25 cm/s were recorded at individual locations in the field. Measurement constraints prevented vortex shedding and

turbulent efficiency from being measured directly in the field, but it is possible that vortices do form behind some stems at higher flow speeds. Dye visualization did not conclusively reveal the presence of any vortices, so if vortices do form in the field they are likely to do so only in part of the flow. Note that, if vortices form, the associated effects on dispersion will be highly nonlinear, so predictions based on the average velocity and average Reynolds number will not be adequate to describe average transport in the flow.

6.1.2 Vertical diffusivity

The vertical diffusion coefficient can be non-dimensionalized as K_z/ud, where u is the ambient flow velocity and d is the stem diameter. Within error the non-dimensionalized diffusivity D_z/Ud is constant for each stem density in both the laboratory and the field (Figure 6-1; Table 6-1). Normalized vertical diffusivity in the field ($D_z/Ud \approx 0.16$) was observed to be slightly greater than but on the same order of magnitude as the laboratory values in the upper canopy ($D_z/Ud \approx 0.08$) and the lower canopy ($D_z/Ud \approx 0.01$).

There is a fair amount of error associated with the calculation of the appropriate ad for the field data. The vertical diffusivity measurements in the field occurred between 10 and 20 cm from the bed, so $a = 0.03 - 0.09$ cm^2/cm^3 (including error). If the fact that d varies over depth is considered, then d = 0.06 – 0.25 cm. The resulting range for stem density is $ad = 0.002 - 0.022$. This large range makes it difficult to determine the relationship between ad and normalized vertical diffusion. In a vertically uniform canopy with a flow velocity of 3 cm/s, Sullivan (1996) found $D_z/Ud = 0.05 \pm 0.01$ for $ad = 0.018$ and $D_z/Ud = 0.09 \pm 0.01$ for $ad = 0.068$. Nepf et al. (1997b) also reported that D_z/Ud increases with stem density for 3.2 cm/s flow: from 0.04 ± 0.01 for $ad = 0.014$ to 0.09 ± 0.01 for $ad = 0.053$. Laboratory data from the present study suggest, however, that D_z/Ud is negatively correlated with ad, and field data are inconclusive.

The estimation of vertical transport is complicated by the presence of vertical secondary flows resulting from vertical pressure gradients behind each cylinder (Sullivan, 1996; Nepf et al., 1997b). For similar flow conditions to those considered here, Nepf et al. (1997b) estimated that the vertical advection timescale was nearly an order of magnitude larger than the diffusive

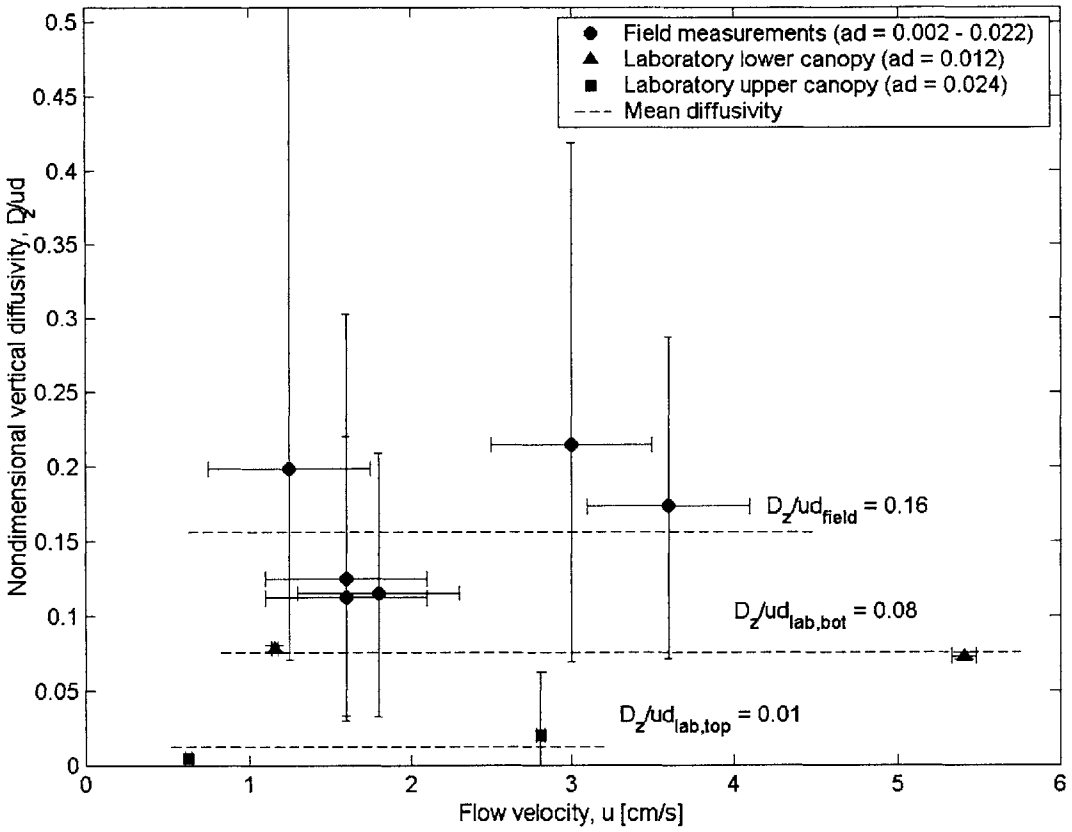

Figure 6-1. Nondimensional vertical diffusivity as a function of flow velocity. Vertical diffusion coefficients in the field (*ad* = 0.002-0.022) and laboratory (*ad* = 0.012 in the lower canopy and ad = 0.024 in the upper canopy) are normalized by stem diameter and the local velocity as determined by slug releases. Horizontal bars indicate error associated with velocity measurements. In the laboratory, this represents the standard error of the mean across slug releases; in the field, error was assumed to be 0.25 cm/s. Vertical bars indicate error associated with the value of D_z that produces a 5% change in the least-squares residuals for this fit. Horizontal dotted lines indicate the average nondimensional vertical diffusivity for each stem density. The D_z coefficient measured in the field 123 cm from the release at a flow velocity of 2.3 cm/s was an outlier and is not shown here or used in these calculations.

Table 6-1. Comparison of vertical diffusion in the laboratory and field. Diffusion constants are normalized by the local velocity as determined by slug releases. For field data, it was assumed that $a = 0.04$ cm^2/cm^3, $d = 0.15 \pm 0.07$ cm and that the error associated with each velocity measurement was 0.5 cm/s.

Location	Stem density, ad	Flow velocity, u [cm/s]	Vertical diffusion, D_z/ud
Field	0.002 – 0.022	1.25 ± 0.5	0.20 ± 0.24
		1.6 ± 0.5	0.12 ± 0.11
		1.8 ± 0.5	0.12 ± 0.09
		2.3 ± 0.5	2.0 ± 1.1
		3.0 ± 0.5	0.21 ± 0.17
		3.6 ± 0.5	0.17 ± 0.11
Laboratory lower canopy	0.012	1.16 ± 0.02	0.08 ± 0.03
		5.41 ± 0.07	0.07 ± 0.05
Laboratory upper canopy	0.024	0.63 ± 0.02	0.004 ± 0.001
		2.82 ± 0.03	0.02 ± 0.04

timescale. The contribution of secondary circulation to vertical transport is therefore not considered here.

In addition, not all stems in a natural system will be perfectly vertical. Valiela et al. (1978) noted that *S. alterniflora* leaves have an angle of $\theta = 5\text{-}10°$ to the vertical. Over a height h, leaves therefore tend to have a horizontal projection of $h \tan\theta = 0.09\text{-}0.15h$. Wetland plants with a more complicated morphology are likely to have even more horizontal protrusions. These horizontal objects could contribute a mechanical dispersion process similar to hold-up dispersion in the vertical, which would elevate vertical diffusion values over what is observed in the laboratory. Because *S. alterniflora* stems are nearly vertical, however, and vertical velocities are small, any possible effect will be small under the conditions considered here.

6.1.3 Longitudinal dispersion

The longitudinal dispersion coefficient can be non-dimensionalized as K_x/ud, where u is the ambient flow velocity and d is the stem diameter. Table 6-1 compares longitudinal dispersion constants in the laboratory and field. Field and laboratory values for longitudinal dispersion are on the same order of magnitude after normalization (Figure 6-2). It is therefore likely that they are affected by similar processes. There is no strong trend in the laboratory constants, but the field constants tend to increase with increasing velocity.

In the field, for all measured velocities, there was a difference between dispersion coefficients in the lower, denser region of the canopy ($a > 0.015$ cm^2/cm^3, so $ad > 0.002$) and the upper, less dense region ($ad < 0.002$). This observation suggests that there exists a threshold value above which vegetation becomes important. Similarly, Lopez and Garcia (2001) found that bed roughness was only dependent on vegetation above a critical plant density value of approximately 1.2 plants/m^2. Shi and Hughes (2002) reported that velocity profiles through submerged canopies of Hydrilla are similar when plant density > 27 stems/m2 but show differences below this critical density. When $ad < 0.002$, the vegetation does not exert sufficient drag to affect the flow, and other processes such as wind shear stresses may become important. The transition density where vegetation drag becomes important will depend on the exact magnitude of the drag force and shear stresses (cf. equation 6-1).

Table 6-2 also compares longitudinal dispersion observed in the field and laboratory with a variety of theoretical predictions: turbulent diffusion (equation 2-24), stem-wake dispersion (equation 2-27), hold-up dispersion (equation 2-31), shear dispersion in turbulent open channel flow (equation 2-37), shear dispersion for a step velocity gradient (equation 2-36), shear dispersion for a linear velocity gradient (equation 2-35), and shear dispersion calculated from the laboratory and field velocity profiles (equation 2-33).

Table 6-2. Comparison of normalized longitudinal dispersion constants in the laboratory and field with theory. Dispersion data are the mean over different slug releases (at the interface for laboratory data and for $a > 0.030$ cm^2/cm^3 ($ad > 0.005$) for field data) and are normalized by the local velocity. For purposes of comparison, all dispersion coefficients were normalized by d, even though the width of the velocity profile, Δh (assumed to equal 10 cm in all equations), is a more appropriate length scale for shear dispersion. All O(1) constants were assumed to equal 1. The estimated ranges for theoretical turbulent, hold-up dispersion, and open channel shear dispersion reflect $ad = 0.002$ - 0.024, $d = 0.15 - 0.64$, and $D_z = 0.002 - 0.025$ cm^2/s. The theoretical shear dispersion for a step gradient was calculated using laboratory values: $d = 0.64$ cm and, depending on flow rate, $u_1 = 1.16 - 5.41$ cm/s, $u_2 = 0.63 - 2.82$ cm/s, $U = 0.8 - 4.1$ cm/s, and $D_z = 0.08Ud$. The shear dispersion from the measured laboratory velocity profile was estimated from the portion of the profile between 5 and 15 cm from the bed. The theoretical shear dispersion for a linear gradient was calculated using field values: $U = 1$-4 cm/s, $D_z = 0.16Ud$, and $d = 0.15 \pm 0.07$ cm. The portion of the profile between 20 and 30 cm from the bed was used to estimate dispersion.

Method of calculating K_x/Ud	Flow velocity			
	1 cm/s	2 cm/s	3 cm/s	4 cm/s
Laboratory < 250 cm	3.6 ± 0.3	3.4 ± 0.2	3.9 ± 0.3	3.8 ± 0.2
Laboratory > 250 cm	24 ± 2	19 ± 3	22 ± 1	11 ± 1
Field for $a > 0.03$ cm^2/cm^3	5 ± 3	8 ± 4	34 ± 17	15 ± 7
Theoretical turbulent diffusion, $\frac{K_t}{Ud} = \sqrt[3]{C_d ad}$	0.1 - 0.4	0.1 - 0.4	0.1 - 0.4	0.1 - 0.3
Theoretical stem-wake dispersion, $\frac{K_w}{Ud} = \frac{\sqrt{C_d}^3 \mathrm{Re}_t}{8}$	5.2 - 6.1	4.9 - 5.6	4.8 - 5.3	4.7 - 5.2
Theoretical hold-up dispersion, $\frac{K_h}{Ud} = \frac{ad}{St}$	0.01 - 0.48	0.01 - 0.35	0.01 - 0.22	0.01 - 0.18
Theoretical shear dispersion for turbulent open channel flow, $\frac{K_s}{Ud} = 0.3\frac{\Delta h}{d}$	5 - 20	5 - 20	5 - 20	5 - 20
Theoretical shear dispersion for a step velocity gradient using laboratory values, $\frac{K_s}{Ud} = \frac{(u_1 - u_2)^2 \Delta h}{48\, UD_z}\frac{\Delta h}{d}$	20 - 45	20 - 45	20 - 45	20 - 45
Theoretical shear dispersion from the measured laboratory velocity profile, $\frac{K_s}{Ud} = -\frac{1}{Ud\Delta h}\int_0^h u' \int_0^z \frac{1}{D_z}\int_0^z u'\,dz\,dz\,dz$	310	-	-	20
Theoretical shear dispersion for a linear velocity gradient using field values, $\frac{K_s}{Ud} = \frac{U\Delta h}{120 D_z}\frac{\Delta h}{d}$	130 - 630	130 - 630	130 – 630	130 - 630
Theoretical shear dispersion from the measured field velocity profile, $\frac{K_s}{Ud} = -\frac{1}{Ud\Delta h}\int_0^h u' \int_0^z \frac{1}{D_z}\int_0^z u'\,dz\,dz\,dz$	8	11	12	13

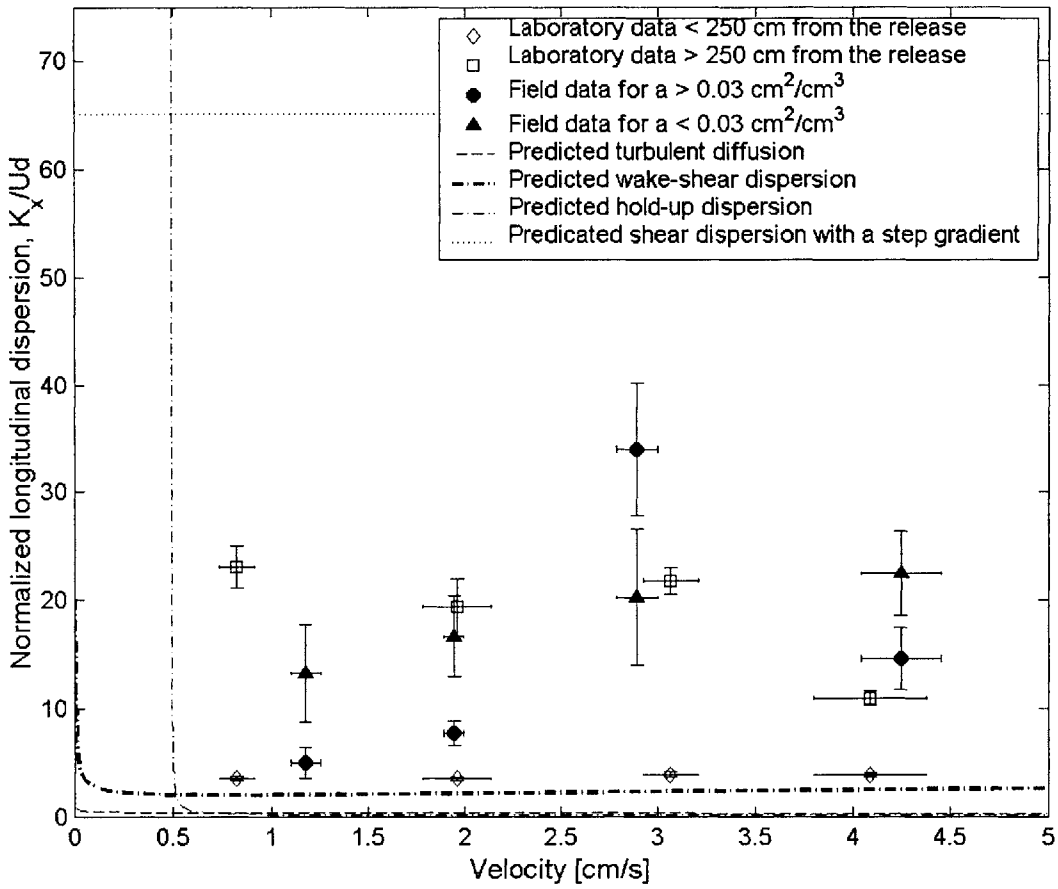

Figure 6-2. Comparison of longitudinal dispersion constants in the laboratory and field to theoretical predictions. Dispersion data are the mean over different slug releases (see Tables 4-5 and 5-4) and are normalized by the local velocity. For purposes of comparison, all dispersion coefficients were normalized by d, even though the width of the velocity profile, h, is a more appropriate length scale for shear dispersion. When predicting theoretical values, all O(1) constants were assumed to equal 1 (see Table 6-2 for equations used). The estimated values for theoretical turbulent, hold-up dispersion, and open channel shear dispersion were calculated assuming $ad = 0.02$, $d = 0.4$ cm, $h = 10$ cm, and $D_z = 0.04Ud$. The predicted shear dispersion assuming a linear velocity gradient is a constant function, $K_x/Ud = 105$, which is off the scale of this plot.

To facilitate comparisons among dispersion estimates, all estimates in Table 6-2 are normalized with respect to stem diameter, d. For shear dispersion, the relevant length scale is actually the width of the shear layer. In a canopy with continuously varying stem density over depth, this length scale is the height of the shear experienced by the tracer cloud, Δh. Predictions of shear dispersion should therefore be normalized as $K_x / U\Delta h$. Also note that the width of the clouds when sampled is somewhat ill-defined, although order of magnitude estimates based on vertical diffusivity (following equation 2-34) predict that the largest clouds will be $\sqrt{tD_z / 0.4}$ = $\sqrt{0.04xd / 0.4} \approx$ 10 cm wide 525 cm downstream a slug release. The predicted values in Table 6-2 are therefore all calculated with Δh = 10 cm.

The following example illustrates the method in which these estimates were calculated. Consider the calculation of shear dispersion for a step velocity gradient. This case is presented because of its similarity to the laboratory velocity profile, so values from the laboratory setup are used to estimate its magnitude. The theoretical expression for shear dispersion by a step profile (equation 2-36) can be rewritten as follows:

$$\frac{K_s}{Ud} = \frac{(u_1 - u_2)^2 \Delta h^2}{48 D_z} = \frac{1}{48}\left(\frac{\Delta u}{u}\right)^2 \left(\frac{Ud}{D_z}\right)\left(\frac{\Delta h}{d}\right)^2 \tag{6-2}$$

In the laboratory, it was found that $\Delta u / U \approx 0.6$ (Table 4-2). In drag-dominated flow, on the other hand, theory predicts that:

$$\frac{\Delta u}{u} = \frac{u_{bot} - u_{top}}{\frac{1}{2}(u_{bot} + u_{top})} = 2\left(\frac{1 - u_{top}/u_{bot}}{1 + u_{top}/u_{bot}}\right) = 2\left(\frac{1 - \sqrt{\frac{(C_d a)_{bot}}{(C_d a)_{top}}}}{1 + \sqrt{\frac{(C_d a)_{bot}}{(C_d a)_{top}}}}\right) \tag{6-3}$$

This ratio has a value of approximately 0.4 in the laboratory (Table 4-2). From laboratory data, $D_z/Ud \approx 0.04$ (Table 6-1). If Δh = 10 cm, then $\Delta h/d$ = 15.6. Therefore, K_s/Ud = 20 – 45. This

value is a rough estimate, but it is useful for comparing the order of magnitude of the various theoretical predictions.

A comparison of the order of magnitude of the observed and theoretical longitudinal dispersion constants makes it clear that turbulent diffusion and hold-up dispersion both have a minor role in this system. Hold-up dispersion is predicted to have the smallest dispersion constant of any process: $K/Ud \sim 0.1$, which is even smaller than the 0.1-0.4 predicted for turbulent diffusion. At a flow velocity of 1 cm/s, hold-up dispersion will require $t_h >> 100$ s (equation 2-31, with $\beta = \kappa = 1$, $St = 0.2$, and $a = 0.05$ cm^2/cm^3) to develop, so it will not become important until quite a bit downstream of the release. It is therefore not likely to be an important factor in this system because it takes longer to develop than other processes that have a much larger effect.

Turbulent diffusion, on the other hand, depends on eddies that exist in the flow before dye is released, so it will be a factor as soon as the slug enters the flow and may be important for the first few seconds after release. After this short time period, during which the dye has traveled only a few centimeters, turbulent diffusion is likely to be overwhelmed by other dispersive processes with a greater effect. However, it is likely to control dispersion at very short timescales and distances, < O(10 cm), before other processes have become important (cf. Figures 4-17 and 5-16, in which the straight-line fits do not intersect the origin, suggesting that there is another process controlling the flow at short timescales).

The measured dispersion constants within 250 cm of the release in both the field and the laboratory have the same order of magnitude as both stem-wake dispersion and shear dispersion in an open channel. The prediction for open channel flow, however, is based on a logarithmic velocity profile, which was not observed in either the field or the laboratory (Figures 4-1 and 5-5), so it is not an accurate description of this flow. It is also not large enough to explain the observed increase in the magnitude of longitudinal dispersion observed in the laboratory at distances greater than 250 cm downstream. Similarly, Nepf et al. (1997a) found that shear dispersion due to the bottom boundary layer was not large enough to explain the magnitude of observed dispersion in a model emergent canopy. In addition, shear dispersion will take a

certain amount of time to develop, since the slug releases must first spread across the shear layer. All of the slugs used to generate these constants were released at least 10 cm from the bed, which is the location of greatest shear in an open channel. Timescale analysis (equation 2-34) using Δh = 10 cm and $D_z = 0.04$ cm^2/s then predicts that the distance that these slugs need to develop shear dispersion from the bottom boundary layer is x = O(10 m), which is much farther downstream than was measured in either the laboratory or field.

The timescale over which stem-wake dispersion develops is much shorter. For example, 1 cm/s flow through a canopy of 0.64-cm-diameter cylinders for which $ad = 0.012$ will require $t_w >> 6$ s to become Fickian (equation 2-28). Dispersion due to the heterogeneous velocity field that results from secondary cylinder wakes is therefore likely to control the flow once it develops.

There is a large increase in the dispersion constant observed in the laboratory more than 250 cm downstream of slug releases. In addition, there is an increase in curve skewness at this distance (Figure 4-23), suggesting that another dispersive process, which has not yet reached its Fickian limit, has become important. The observed magnitude of the increase is comparable to the theoretical predictions for shear dispersion at all flow rates. The normalized longitudinal dispersion K_x/Ud increases from ~ 4 to ~23, a difference of ~20. Shear dispersion due to canopy-wide shear is the only factor considered here that can explain the size of this increase.

Two possible values are presented in Table 6.2 for comparison with the laboratory data: the theoretical value for a step velocity gradient (equation 2-36) and the value from the measured velocity profile (Figure 4-1). The value for the step gradient assumes a constant vertical diffusivity, an assumption that is clearly violated for this flow. An intermediate value of $D_z = 0.025$ cm^2/s was therefore used in the table. The result, $K_s/Ud = 20$ - 45, is within the range of $K_s/Ud = 20 - 310$ calculated from the velocity profile. Note that $K_s \sim 1/D_z$, so any error in the calculation of D_z will have a comparable effect on the prediction for K_s, which explains in part the large variation in the predicted dispersion values.

In the laboratory, the width of the velocity gradient between the upper and lower canopies remains constant at 2 cm as the flow increases (cf. Figure 4-1). The longitudinal distance necessary to develop shear dispersion is therefore the distance necessary to mix across it, $x = Ut_s = 0.4Uh^2/D_z \propto h^2$ if U/D_z is a constant. The fact that the transition distance is not a function of flow velocity is therefore consistent with the development of shear dispersion. In addition, if $D_z/U \approx 0.05$, the longitudinal distance necessary to mix across this distance is O(100 cm), which is on the same order of magnitude as the observed 250 cm. It is therefore possible that shear dispersion is the additional process experienced by the cloud as it travels past 250 cm.

The hypothesis that shear dispersion is responsible for the increased longitudinal dispersion observed at 250 cm downstream is further supported by the fact that slugs released away from the interface require a longer distance to transition to the higher dispersion value. Scale analysis suggests that the longitudinal distance necessary for the dye cloud to diffuse to the shear zone and back down again [$x = O(Uh^2/D_z) = O(7 - 250$ m), depending on vertical diffusivity] is greater than the length scales considered here. These slugs have limited contact with the shear zone and its processes. The interface is therefore instrumental in the transition to elevated dispersion.

Two possible values are also presented in Table 6.2 for comparison with the field data: the theoretical value for a linear gradient (equation 2-35) and the value from the measured velocity profile (Figure 5-5; Table 5-1). The field velocity profile increases approximately linearly between 20 and 30 cm from the bed, although it does not reach zero velocity at 20 cm. It therefore contains less variation in velocities and so is predicted to generate less dispersion than the theoretical distribution ($K_s/Ud = 8 - 12$, as opposed to $130 - 630$). Both of these calculated shear dispersion coefficients are similar to the observed dispersion in the field ($K_s/Ud = 5 - 34$), so shear dispersion may contribute to the observed dispersion in the field. Wake-shear dispersion may also play a role: its predicted order of magnitude is similar to that observed, so it may be important before a scalar cloud spreads across the shear layer.

It is not surprising that the abrupt onset of shear dispersion is not seen in the field results. It is not expected that any abrupt transition will ever be seen, since the shear is much more gradual. Moreover, the mean velocity profile is an average over many stems, and it is associated with large error bars, so the local shear may differ quite a bit from the spatial average. In addition, the larger dispersion in the laboratory was observed only downstream of 250 cm, which was close to the maximum longitudinal distance sampled in field. It will probably take an even longer distance for slugs in the field to spread across the shear layer, since the shear is more gradual (linear as opposed to step). In an unbounded shear flow, which is how slugs experience the dispersion in the field before significant cross-sectional mixing has occurred, it is expected that $\sigma_x^2 \sim t^2$ (Fischer et al., 1979). Within error, it is possible that this type of nonlinear behavior is seen (cf. the data for velocities between 1.5 and 2.5 cm/s in Figure 5-16). Shear dispersion may therefore be one of several processes contributing to the observed dispersion in the field.

The Peclet number (UL/K_x) compares the relative magnitude of longitudinal dispersion and advection in a system (equation 2-21). Length scales of $L = 50 - 525$ cm were considered in the laboratory. For $L < 250$ cm, $Pe \approx L/4d = 20 - 100$. For $L > 250$ cm, $Pe \approx L/20d = 20 - 50$. In the field for $ad > 0.005$, $Pe = 14 - 333$. Therefore, for all flows considered, $Pe >> 1$ and advection dominates dispersion. Tracer clouds should therefore not change appreciably while passing the fluorometer , justifying the method of calculating longitudinal dispersion from measurements of concentration as a function of time for a slug release.

The dispersive mechanisms that affect slugs released in field and laboratory therefore appear to be (a) turbulent diffusion for $x < O(10$ cm), (b) stem-wake dispersion for $x < O(100$ cm), and (c) shear dispersion for $x > O(100$ cm).

6.2 Predicting longitudinal dispersion

The dominant dispersive process, and thus the magnitude of the dispersion coefficient, is found to be a strong function of scale over the intermediate length scales studied here. Observations accord with the expectation that the scale of dispersion experienced by a cloud is related to the length scale of the cloud (see Section 1.3). As the cloud's length scale increases, it

is able to sample a wider range of velocities and therefore is acted upon by much larger dispersive forces.

Even though the largest process present will dominate dispersion, it is important to characterize the magnitude of dispersion acting at each length scale. Different applications occur on different scales and therefore require the application of a different dispersion coefficient. For example, when trying to understand the feeding behavior of benthic organisms (e.g., Finelli et al., 2002), it is important to use a value for the dispersion coefficient that reflects small-scale processes. When trying to model dispersion through an entire wetland (e.g., Wu and Tsanis, 1994), it is important to use a value that reflects large-scale processes. The dominant dispersive process will differ depending on the scale of interest, so the relevant length scale becomes important when trying to predict transport due to dispersion.

Over very short distances, O(10 cm) and less, turbulent diffusion appears to control transport. Normalized turbulent diffusion, D_t/Ud, is a weak function of C_d and ad (equation 2-24). Its contribution to dispersion in an aquatic canopy has been explored elsewhere (Nepf, 1999).

Over relatively short distances, O(10-100 cm), stem-wake dispersion will dominate transport. Normalized stem-wake dispersion (equation 2-27) is a weak function of ad and Re_d through the two variables γ and C_d, both of which are O(1) and neither of which is well characterized. It is therefore expected that for most flow conditions $K_w \approx 5Ud$ (Table 6-2).

Shear dispersion due to stem-density-generated vertical shear is the largest and most important longitudinal dispersion process in the wetland system considered here and will dominate as soon as the species of interest is mixed over the shear layer. In a natural wetland, mixing over depth may not even be necessary. Horizontal advection is typically much larger than vertical transport in a field canopy (Granata et al., 2001). Flow in the creek adjacent to the vegetation is likely to be well mixed, so scalars that enter the canopy from the creek will not need to mix across depth before experiencing shear dispersion. Instead, they will become

affected as soon as the velocity profile changes in response to stem drag, which occurs on O(1 m) from the edge of the canopy (Gambi et al., 1990).

Effectively predicting the magnitude of the shear dispersion a scalar cloud will experience requires relating a single measurement of velocity and a single measurement of frontal area to a predicted value of depth-averaged dispersion. Clearly, shear dispersion depends on the strength of the shear. Measuring velocities through a salt marsh canopy, however, is time-consuming and difficult. To be usable, predictions of longitudinal dispersion need to be linked with a depth-averaged velocity alone. If the shape of the velocity profile were known, then knowledge of the depth-averaged velocity would indeed be sufficient to derive the velocity profile. The problem of predicting shear dispersion thus becomes one of predicting the shape of the velocity profile.

The velocity profiles in the laboratory and for $ad > 0.002$ in the field have a constant shape at different flow rates (Figure 4-1 and Appendix A). Thus, u'/U is constant for a given flow. In addition, D_z/U is constant for a given stem density and diameter (Figure 6-1). Therefore, K_x/Uh should be a function of ad, such that for a given canopy shear dispersion should only depend on velocity and water depth. Normalizing equation 2-33 by U and assuming D_z is constant over depth,

$$K_x = -\frac{U^2}{hD_z}\int_0^h \frac{u'}{U}\int_0^z \int_0^z \frac{u'}{U} dz\, dz\, dz = \frac{U^2}{hD_z} I \tag{6-4}$$

where I (which has units of L^3) is the integral that provides the shape of the velocity shear (cf. Nepf et al., 1997a). Normalizing K_x by U and the water depth, h, which is the relevant length scale for transport across a vertical shear layer, and substituting in $D_z = \alpha U d$,

$$\frac{K_x}{Uh} = \frac{I}{\alpha h^2 d} \tag{6-5}$$

where $\alpha \approx 0.1$ and may be a function of ad (Table 6-1). K_x is thus shown to be a linear function of U, related through I and the easily measured parameters water depth and stem diameter.

Velocity through a drag-dominated canopy is related non-linearly to stem density, so characterizing the velocity fluctuations that contribute to I requires capturing ad as a function of depth. It may not be necessary to fully sample $ad(z)$ at each site, however. The ad curve in the present study agrees well with that developed for *S. alterniflora* canopies elsewhere (Leonard and Luther, 1995), and it may be possible to estimate the $ad(z)$ curve for each species or group of species with a common morphology. *S. alterniflora* has two main variants: a short form and a tall form, the relative heights of which may vary from marsh to marsh (Valiela et al., 1978). If the frontal area density curve is relatively invariant, it should be a function of total plant height, which is easy to measure. It may therefore be possible to estimate the magnitude of the resulting shear dispersion from simple information about the canopy. In addition, note that $u \sim 1/\sqrt{a}$ so is relatively insensitive to minor errors in $a(z)$.

There are a few other nuances that will affect the relationship between K_x and $ad(z)$. K_x is a strong function of vertical diffusivity, and D_z is a function of velocity and therefore not constant over depth. If D_z/Ud is constant, then this effect will not affect the normalized dispersion coefficient, K_x/Ud. It is likely, however that D_z/Ud is a function of frontal area density, which is not constant over depth (cf. equation 2-24 for turbulent diffusion, which predicts $D_t/ud \sim \sqrt[3]{C_d a}$, and Figure 6-1). Stem diameter and shape may also change over depth. Predicting the value of shear dispersion within more than an order of magnitude for a given canopy is thus still out of reach.

6.3 Implications for further research

This method of predicting dispersion constants can accommodate non-cylindrical obstructions in a relatively straightforward manner if the drag coefficient and frontal area of obstructions are known. To be confident in the use of $ad(z)$ to derive $u(z)$, the behavior of C_d must be better understood. The drag coefficient is likely to be highly dependent on the particular species in the canopy. *S. alterniflora* has stiff, roughly cylindrical leaves and stems Lopez and

Garcia, 2001; Nepf, 1999). Other common wetland species have more complicated morphology, which will make it more difficult to determine the velocity profile based only on stem density. *Phragmites australis* has abundant wrack, which will interfere with near-bed flow and may shift over time (Leonard and Reed, 2002). *Atriplex portuloides* is more vine-like and less rigid than *S. alterniflora*, so its position may change from one flooding cycle to the next. As a result, the vertical velocity profile associated with it is much more variable and much less regular than that of *S. alterniflora* (Leonard and Reed, 2002). Moreover, some vegetation, such as *Z. marina* and *Hydrilla* is truly flexible and bends in response to passing turbulence (Ackerman and Okubo, 1993; Ghisalberti and Nepf, 2002; Shi and Hughes, 2002). Predicting velocity profiles and dispersion in these types of vegetation will require more detailed study.

To predict the dispersion constant more exactly, several other relationships must be determined as well. D_z tends to decrease with ad in the present study but was observed to be directly proportional in other work (Zavistoski, 1994; Nepf et al., 1997b). In addition, there is a lot of uncertainty associated with the relationship between D_z and u and therefore the value of D_z/ud in the field. Moreover, the behavior of $d(z)$ and its effect on vertical diffusion and longitudinal dispersion has not been considered, even though preliminary observations suggest it varies considerably over depth. This model also assumes that $ad < 0.1$. If frontal area density is large, then modifications to this theory will be necessary.

In addition, other aspects of a real wetland system may have confounding effects. For example, whether or not the vegetation is emergent, free surface phenomena such as wind waves and boat wakes may be important. Shallow-water gravity waves create orbital motions that penetrate the water all the way to the bed (cf. Figure 5-6). Even though this produces little net transport, these waves can cause the cloud to interact with more stems and more shear than would otherwise be predicted. However, these waves may attenuate in the interior of the marsh canopy (Knutson et al., 1982; Yang, 1998; Vermaat et al., 2000), so this effect may only be relevant in the portions of a marsh or wetland bordering open water.

Turbulent shear stresses are important for predicting other processes, such as the ability of sediment and phytoplankton to remain in suspension (Gambi et al., 1990). Because there is a

threshold turbulence intensity below which inert particles may settle, differential velocity over depth will result in nonlinear settling behavior, with the possibility that particles will settle out of only part of the water column (Pethick et al., 1990). The observation that mean velocity and therefore the magnitude of turbulence at a certain distance from the bed will be related to local stem density may be a tool to estimate particle settling behavior, which is notoriously difficult to quantify (Shi et al., 1995; Nepf, 1999). This relationship should be explored in more detail if it is to become a useful method for the prediction of sedimentation.

Because $Pe >> 1$, this flow condition is closer to a plug flow than a stirred reactor. Most wetlands are similarly dominated by advection, which enhances their observed ability for contaminant removal (Kadlec, 1994). To the extent that K_x/Ud is a constant for these systems, decreasing d at a constant velocity will decrease K_x and make the system better approach plug flow. Thinner stems are therefore desirable for improving water quality. Reducing U will also have the effect of decreasing K_x, [which will also lengthen the residence time, thereby further increasing contaminant removal (Tilley and Brown, 1998; Werner and Kadlec, 1996)]. These effects should be incorporated into models and designs of constructed wetlands for water treatment.

In a typical salt marsh, stem densities and frontal areas change on a length scale of O(10 m) (Christiansen et al., 2000). When scalar clouds are larger than this length scale, they no longer experience a spatially homogenous canopy, and different stands of grasses will contribute spatial heterogeneity in drag (Granata et al., 2001). This differential stem density may introduce another form of mechanical dispersion into the system. When stem drag dominates the flow, a scalar parcel that enters a thick stand of vegetation will travel more slowly than scalar parcel that enters a less dense stand. The entire scalar cloud will therefore spread out over time as a result of this large-scale dispersion.

In addition, a salient feature of many coastal wetlands is a system of branching channels that cut through regions of dense vegetation. Since flow in the channels is much faster than through the vegetation [O(m/s) as opposed to O(cm/s)], these channels contribute yet another mechanism for shear dispersion. Most of the flow conveyance occurs in the channels, but most

of the biogeochemical processes occur within the vegetation. To understand the overall wetland function, we must be able to predict flow in the channels, flow in the vegetation, and communication between channels and vegetation. More work must be done to understand these relationships.

Finally, when large spatial scales are considered, the temporal scale also becomes large. A cloud advecting at a rate of 1 cm/s will require 1 hour to travel 36 m. The marsh is inundated only at high tide for 1-2 hours, over which time the tide comes in, slows to a halt, and reverses. Water depth, flow velocity, and flow direction therefore change considerably during the time in which a particle travels O(10 m), and transport can no longer be approximated as steady. Time-varying flow introduces another dimension over which velocity can vary in a wetland, potentially introducing even more dispersion into this inherently complex system.

References

Ackerman, J. D., and A. Okubo. 1993. Reduced mixing in a marine macrophyte canopy. Functional Ecology 7: 305-309.

Braskerud, B. C. 2002. Design considerations for increased sedimentation in small wetlands treating agricultural runoff. Water Science and Technology 45 (9): 77-85.

Burke, R., and K Stolzenbach. 1983. Free surface flow through salt marsh grass. Technical Report MITSTG 83-16, Massachusetts Institute of Technology, Cambridge, Massachusetts.

Butman, C. A. 1987. Larval settlement of soft-sediment invertebrates: the spatial scales of pattern explained by active habitat selection and the emerging role of hydrodynamical processes. Oceanography and Marine Biology: An Annual Review 25:113.

Chendorain, M., M. Yates, and F. Villegas. 1998. The fate and transport of viruses through surface water constructed wetlands. Journal of Environmental Quality 27: 1451-1458.

Christiansen, T., P. L. Wiberg, and T. G. Milligan. 2000. Flow and sediment transport on a tidal salt marsh surface. Estuarine, Coastal and Shelf Science 50: 315-331.

Darby, S. E. 1999. Effect of riparian vegetation on flow resistance and flood potential. Journal of Hydraulic Engineering 125(5): 443-454.

Duan, J., and S. Wiggins. 1997. Lagrangian transport and chaos in the near wake of the flow around an obstacle: a numerical implementation of lobe dynamics. Nonlinear Processes in Geophysics 4: 125-136.

Eames, I., and J. W. M. Bush. 1999. Longitudinal dispersion by bodies fixed in a potential flow. Proceedings of the Royal Society of London Series A 455(1990): 3665-3686.

Elder, J. W. 1959. The dispersion of marked fluid in turbulent shear flow. Journal of Fluid Mechanics 5: 544-560.

Fay, J. A. 1998. Introduction to Fluid Mechanics. Cambridge, Massachusetts: MIT Press.

Finelli, C. M. 2000. Velocity and concentration distributions in turbulent odor plumes in the presence of vegetation mimics: a flume study. Marine Ecology Progress Series 207: 297-309.

Finelli, C. M., D. D. Hart, and R. A. Merz. 2002. Stream insects as passive suspension feeders: effects of velocity and food concentration on feeding performance. Oecologia 131: 145-153.

Fischer, H. B., E. J. List, R. C. Y. Koh, J. Imberger, and N.H. Brooks. 1979. Mixing in Inland and Coastal Waters. San Diego: Academic Press.

Fischer-Antze, T., T. Stoesser, P. Bates, and N. R. B. Olsen. 2001. 3D numerical modelling of open-channel flow with submerged vegetation. Journal of Hydraulic Research 39(3): 303-310.

Fonseca, D. M., and D. D. Hart. 1996. Density-dependent dispersal of black fly neonates is mediated by flow. Oikos 75(1): 49-58.

Gambi, M. C., A. R. M. Nowell, and P. A. Jumars. 1990. Flume observations on flow dynamics in *Zostera marina* (eelgrass) beds. Marine Ecology Progress Series 61: 159-169.

Gerrard, J. H. 1978. The wakes of cylindrical bluff bodies at low Reynolds number. Philosophical Transactions of the Royal Society of London Series A – Mathematical Physical and Engineering Sciences (Philos T Roy Soc A) 288(1354): 351-382.

Ghisalberti, M., and H. M. Nepf. 2002. Mixing layers and coherent structures in vegetated aquatic flows. Journal of Geophysical Research 107(C2): Art. No. 3011.

Gleason, M. L., D. A. Elmer, N. C. Pien, and J. S. Fisher. 1979. Effects of stem density upon sediment retention by salt marsh cord grass, *Spartina alterniflora* Loisel. Estuaries 2(4): 271-273.

Granata, T. G., T. Serra, J. Colomer, X. Casamitjana, C. M. Duarte, and E. Gacia. 2001. Flow and particle distributions in a nearshore seagrass meadow before and after a storm. Marine Ecology Progress Series 218: 95-106.

Harvey, M., E. Bourget, and R. G. Ingram. 1995. Experimental evidence of passive accumulation of marine bivalve larvae on filamentous epibenthic structures. Limnology and Oceanography 40(1): 94-104.

Hosokawa, Y., and T. Horie. 1992. Flow and particulate nutrient removal by wetland with emergent macrophyte. Science of the Total Environment, Supplement: 1271-1282.

Jadhav, R. S., and S. G. Buchberger. 1995. Effects of vegetation on flow through free water surface wetlands. Ecological Engineering 5: 481-496.

Jenter, H. L., and M. P. Duff. 1999. Locally-forced wind effects on shallow water with emergent vegetation. Proceedings of the Third International Symposium on Ecohydraulics. IAHR, Salt Lake City, Utah.

Kadlec, R. H. 1990. Overland flow in wetlands: Vegetation resistance. Journal of Hydraulic Engineering 116 (5): 691-706.

Kadlec, R. H. 1994. Detention and mixing in free water wetlands. Ecological Engineering 3: 345-380.

Kadlec, R. H. 2000. The inadequacy of first-order treatment wetland models. Ecological Engineering 15: 105-119.

Kadlec, R. H., and R. L. Knight. 1996. Treatment Wetlands. Boca Raton, Florida: CRC Press, Inc.

Knutson, P., R. Brochu, W. Seelig, and M. Inskeep. 1982. Wave damping in *Spartina alterniflora* marshes. Wetlands 2: 87-104.

Koch, D. L., and J. F. Brady. 1985. Dispersion in fixed beds. Journal of Fluid Mechanics 154: 399-427.

Koch, D. L., and A. J. C. Ladd. 1997. Moderate Reynolds number flows through periodic and random arrays of aligned cylinders. Journal of Fluid Mechanics 349: 31-66.

Koskiaho, J. 2003. Flow velocity retardation and sediment retention in two constructed wetland-ponds. Ecological Engineering 19: 325-337.

Leonard, L. A., and M. E. Luther. 1995. Flow hydrodynamics in tidal marsh canopies. Limnology and Oceanography 40(8): 1474-1484.

Leonard, L. A., and D. J. Reed. 2002. Hydrodynamics and sediment transport through tidal marsh canopies. Journal of Coastal Research SI 36: 459-469.

Lopez, F., and M. H. Garcia. 2001. Mean flow and turbulence structure of open-channel flow through non-emergent vegetation. Journal of Hydraulic Engineering 127(5): 392-402.

Luo S. C., Y. T. Chew, and Y. T. Ng. 2003. Characteristics of square cylinder wake transition flows. Physics of Fluids. 15 (9): 2549-2559.

Middleton, B. 2000. Hydrochory, seed banks, and regeneration dynamics along the landscape boundaries of a forested wetland. Plant Ecology 146 (2): 169-184.

Mitsch, W. J., and J. G. Gosselink. 1986. Wetlands. New York: Van Nostrand Reinhold.

Nepf, H. M. 1999. Drag, turbulence, and diffusion in flow through emergent vegetation. Water Resources Research 35(2): 479-489.

Nepf, H. M., C. G. Mugnier, and R. A. Zavistoski. 1997a. The effects of vegetation on longitudinal dispersion. Estuarine, Coastal and Shelf Science 44: 675-684.

Nepf, H. M., J. A. Sullivan, and R. A. Zavistoski. 1997b. A model for diffusion within emergent vegetation. Limnology and Oceanography 42(8): 1735-1745.

Nepf, H. M., and E. R. Vivoni. 2000. Flow structure in depth-limited, vegetated flow. Journal of Geophysical Research 105(C12): 28,547-28,557.

Pearson, T. H., J. S. Gray, and P. J. Johannessen. 1983. Objective selection of sensitive species indicative of pollution-induced changes in benthic communities: data analysis. Marine Ecology Progress Series 12:237-255.

Persson, J., N. L. G. Somes, and T. H. F. Wong. 1999. Hydraulics efficiency of constructed wetlands and ponds. Water Science and Technology 40 (3): 291-300.

Peterson, C. G. 1996. Mechanisms of lotic microalgal colonization following space-clearing disturbances acting at different spatial scales. Oikos 77(3): 417-435.

Pethick, J., D. Leggett, and L. Husain. 1990. Boundary layers under salt marsh vegetation developed in tidal currents. In: J.B. Thornes (ed.). Vegetation and Erosion. New York: John Wiley & Sons Ltd., pp. 113-124.

Petryk, S., and G. Bosmajian III. 1975. Analysis of flow through vegetation. Journal of the Hydraulics Division – ASCE 101(7): 871-884.

Press, W. H., B. P. Flannery, S. A. Teukolsky, and W. T. Vetterling. 1992. Numerical Recipes in C: The Art of Scientific Computing. New York: Cambridge University Press.

Ramey, P. A, and P. V. R. Snelgrove. 2003. Spatial patterns in sedimentary macrofaunal communities on the south coast of Newfoundland in relation to surface oceanography and sediment characteristics. Marine Ecology Progress Series 262: 215-227.

Raupach, M. R., J. J. Finnigan, and Y. Brunet. 1996. Coherent eddies and turbulence in vegetation canopies: The mixing-layer analogy. Boundary-Layer Meteorology 78: 351-382.

Saiers, J. E., J. W. Jarvey, and S. E. Mylon. 2003. Surface-water transport of suspended matter though wetland vegetation of the Florida everglades. Geophysical Research Letters 30(19): Art. No. 1987.

Serra, T., H. J. S. Fernando, and R. V. Rodriguez. 2004. Effects of emergent vegetation on lateral diffusion in wetlands. Water Research 38: 139-147.

Shi, Z., J. S. Pethick, and K. Pye. 1995. Flow structure in and above the various heights of a saltmarsh canopy: A laboratory flume study. Journal of Coastal Research 11(4): 1204-1209.

Shi, Z., J. S. Pethick, F. Burd, and B. Murphy. 1996. Velocity profiles in a salt marsh canopy. Geo-Marine Letters 16: 319-323.

Shi, Z., L. J. Hamilton, and E. Wolanski. 2000. Near-bed currents and suspended sediment transport in saltmarsh canopies. Journal of Coastal Research 16(3): 909-914.

Shi, Z., and J. M. R. Hughes. 2002. Laboratory flume studies of microflow environments of aquatic plants. Hydrological Processes 16: 3279-3289.

Streeter, V. L., E. B. Wylie, and K. W. Bedford. 1998. Fluid Mechanics. 9th edition. Boston, Massachusetts: WCB McGraw-Hill.

Sullivan, J. A. 1996. Effects of marsh grass on diffusivity. MS thesis, Massachusetts Institute of Technology, Cambridge, Massachusetts.

Sundaravadivel, M., and S. Vigneswaran. 2001. Constructed wetlands for wastewater treatment. Critical Reviews in Environmental Science and Technology 31 (4): 351-409.

Taylor, J. R. 1997. An Introduction to Error Analysis: The Study of Uncertainty in Physical Measurements. 2nd Ed. Sausalito, California: University Science Books.

Tilley, D. R., and M. T. Brown. 1998. Wetland networks for stormwater management in subtropical urban watersheds. Ecological Engineering 10: 131-158.

Valiela, I., J. M. Teal, and W. G. Deuser. 1978. The nature of growth forms in the salt marsh grass *Spartina alterniflora*. The American Naturalist 112: 461-470.

Vermaat, J. E., L. Santamaria, and P. J. Roos. 2000. Water flow across and sediment trapping in submerged macrophyte beds of contrasting growth form. Archiv fur Hydrobiologie 148(4): 549-562.

Webster, D. R., S. Rahman, and L. P. Dasi. 2003. Laser-induced fluorescence measurements of a turbulent plume. Journal of Engineering Mechanics 129 (10): 1130-1137.

Wei, C.-Y., and J.-R. Chang. 2002. Wake and base-bleed flow downstream of bluff bodies with different geometry. Experimental Thermal and Fluid Science 26: 39-52.

Werner, T. M., and R. H. Kadlec. 1996. Application of residence time distributions to stormwater treatment systems. Ecological Engineering 7: 213-234.

White, B. L. 2002. Transport in random cylinder arrays: A model for aquatic canopies. MS thesis, Massachusetts Institute of Technology, Cambridge, Massachusetts.

White, B. L., and H. M. Nepf. 2003. Scalar transport in random cylinder arrays. Journal of Fluid Mechanics 487: 43-79.

White, F. M. 1991. Viscous Fluid Flow. New York, McGraw-Hill.

Wu, J. and I. K. Tsanis. 1994. Pollutant transport and residence time in a distorted scale model and a numerical model. Journal of Hydraulic Research 32 (4): 583-598.

Yang, S. L. 1998. The role of *Scirpus* marsh in attenuation of hydrodynamics and retention of fine sediment in the Yangtze estuary. Estuarine, Coastal and Shelf Science 47: 227-233.

Zavistoski, R. A. 1994. Hydrodynamic effects of surface piercing plants. MS thesis, Massachusetts Institute of Technology, Cambridge, Massachusetts.

Appendix A. Field velocity profiles taken using the Flowtracker sideways-looking 2D ADV. Because the flow was tidally produced, the free-stream velocity changed during the ~20 minutes of each profile. When two readings were taken at one distance from the bed during a single profile, all measurements were corrected by linear interpolation using the percentage change between these two measurements. Each profile is marked with its identifying number. The first number indicates the month, the second the day, and the third which profile from that date. Also shown are the corrected velocity at 15 cm from the bed (which is used to normalize the profile) and the water levels at the beginning and the end of the profile.

Appendix A

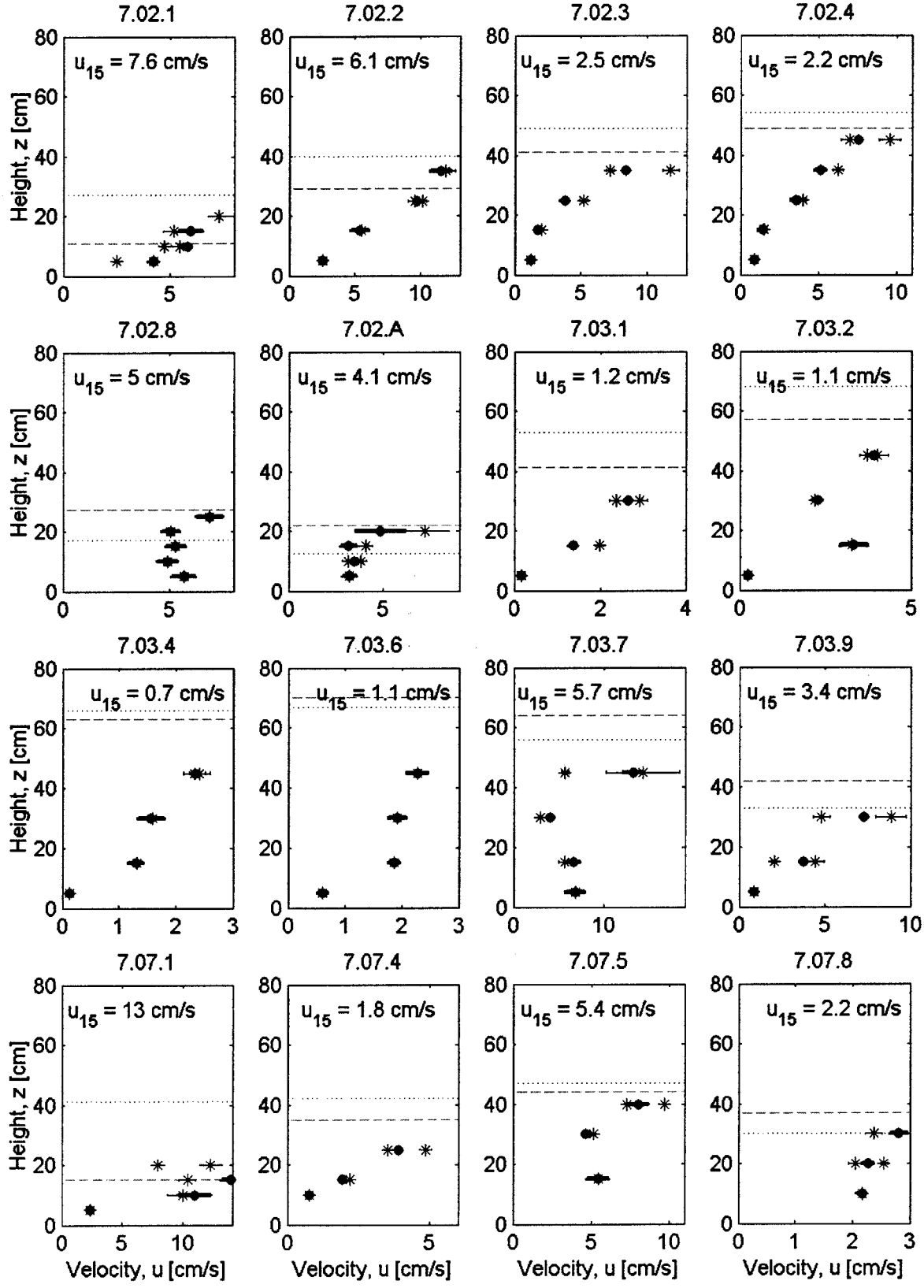
7.02.1
u_{15} = 7.6 cm/s
7.02.2
u_{15} = 6.1 cm/s
7.02.3
u_{15} = 2.5 cm/s
7.02.4
u_{15} = 2.2 cm/s
7.02.8
u_{15} = 5 cm/s
7.02.A
u_{15} = 4.1 cm/s
7.03.1
u_{15} = 1.2 cm/s
7.03.2
u_{15} = 1.1 cm/s
7.03.4
u_{15} = 0.7 cm/s
7.03.6
u_{15} = 1.1 cm/s
7.03.7
u_{15} = 5.7 cm/s
7.03.9
u_{15} = 3.4 cm/s
7.07.1
u_{15} = 13 cm/s
7.07.4
u_{15} = 1.8 cm/s
7.07.5
u_{15} = 5.4 cm/s
7.07.8
u_{15} = 2.2 cm/s
Height, z [cm]
Velocity, u [cm/s]

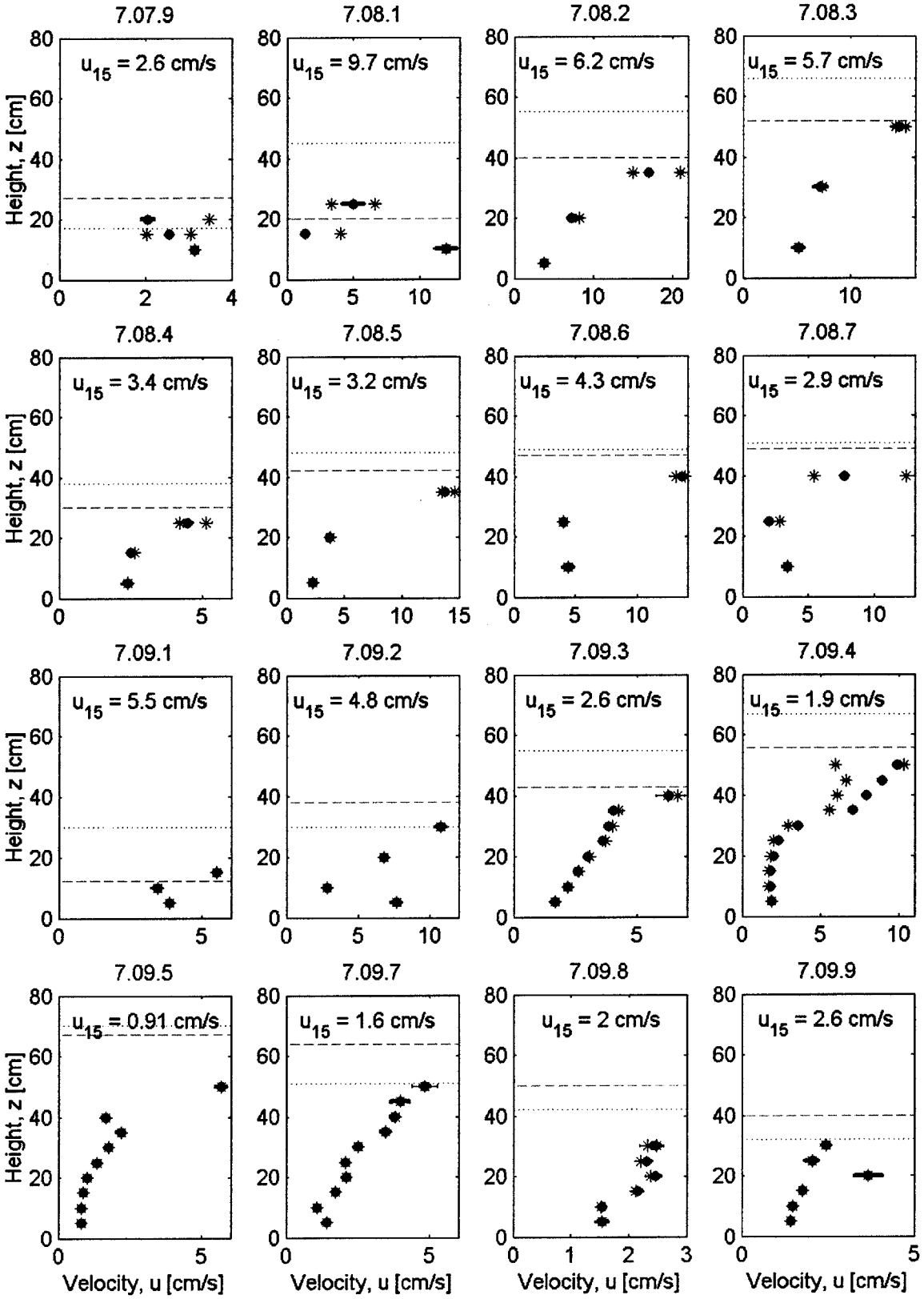
7.07.9
u_{15} = 2.6 cm/s
7.08.1
u_{15} = 9.7 cm/s
7.08.2
u_{15} = 6.2 cm/s
7.08.3
u_{15} = 5.7 cm/s
7.08.4
u_{15} = 3.4 cm/s
7.08.5
u_{15} = 3.2 cm/s
7.08.6
u_{15} = 4.3 cm/s
7.08.7
u_{15} = 2.9 cm/s
7.09.1
u_{15} = 5.5 cm/s
7.09.2
u_{15} = 4.8 cm/s
7.09.3
u_{15} = 2.6 cm/s
7.09.4
u_{15} = 1.9 cm/s
7.09.5
u_{15} = 0.91 cm/s
7.09.7
u_{15} = 1.6 cm/s
7.09.8
u_{15} = 2 cm/s
7.09.9
u_{15} = 2.6 cm/s
Height, z [cm]
Velocity, u [cm/s]

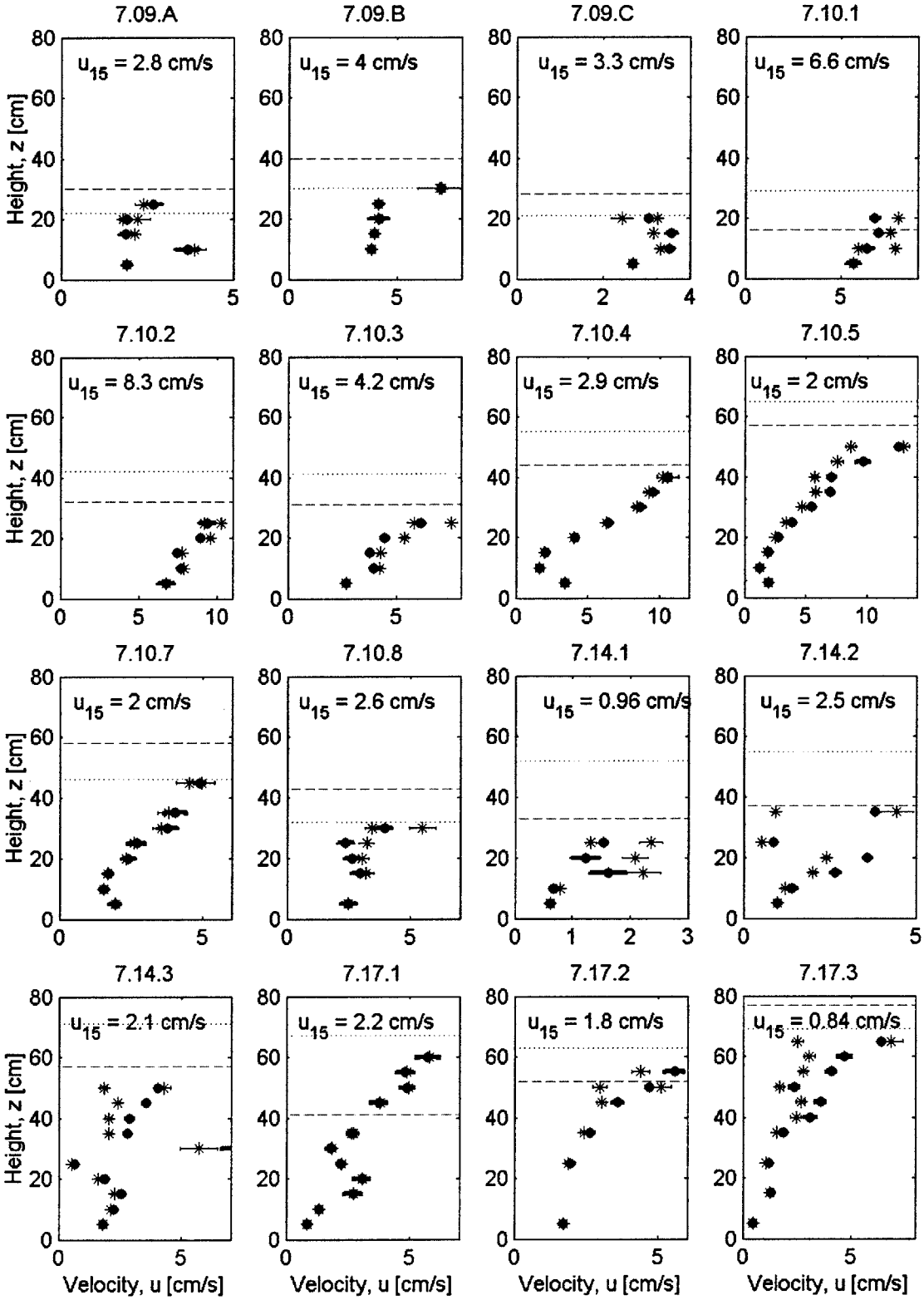
7.09.A
u_{15} = 2.8 cm/s
7.09.B
u_{15} = 4 cm/s
7.09.C
u_{15} = 3.3 cm/s
7.10.1
u_{15} = 6.6 cm/s
7.10.2
u_{15} = 8.3 cm/s
7.10.3
u_{15} = 4.2 cm/s
7.10.4
u_{15} = 2.9 cm/s
7.10.5
u_{15} = 2 cm/s
7.10.7
u_{15} = 2 cm/s
7.10.8
u_{15} = 2.6 cm/s
7.14.1
u_{15} = 0.96 cm/s
7.14.2
u_{15} = 2.5 cm/s
7.14.3
u_{15} = 2.1 cm/s
7.17.1
u_{15} = 2.2 cm/s
7.17.2
u_{15} = 1.8 cm/s
7.17.3
u_{15} = 0.84 cm/s
Height, z [cm]
Velocity, u [cm/s]

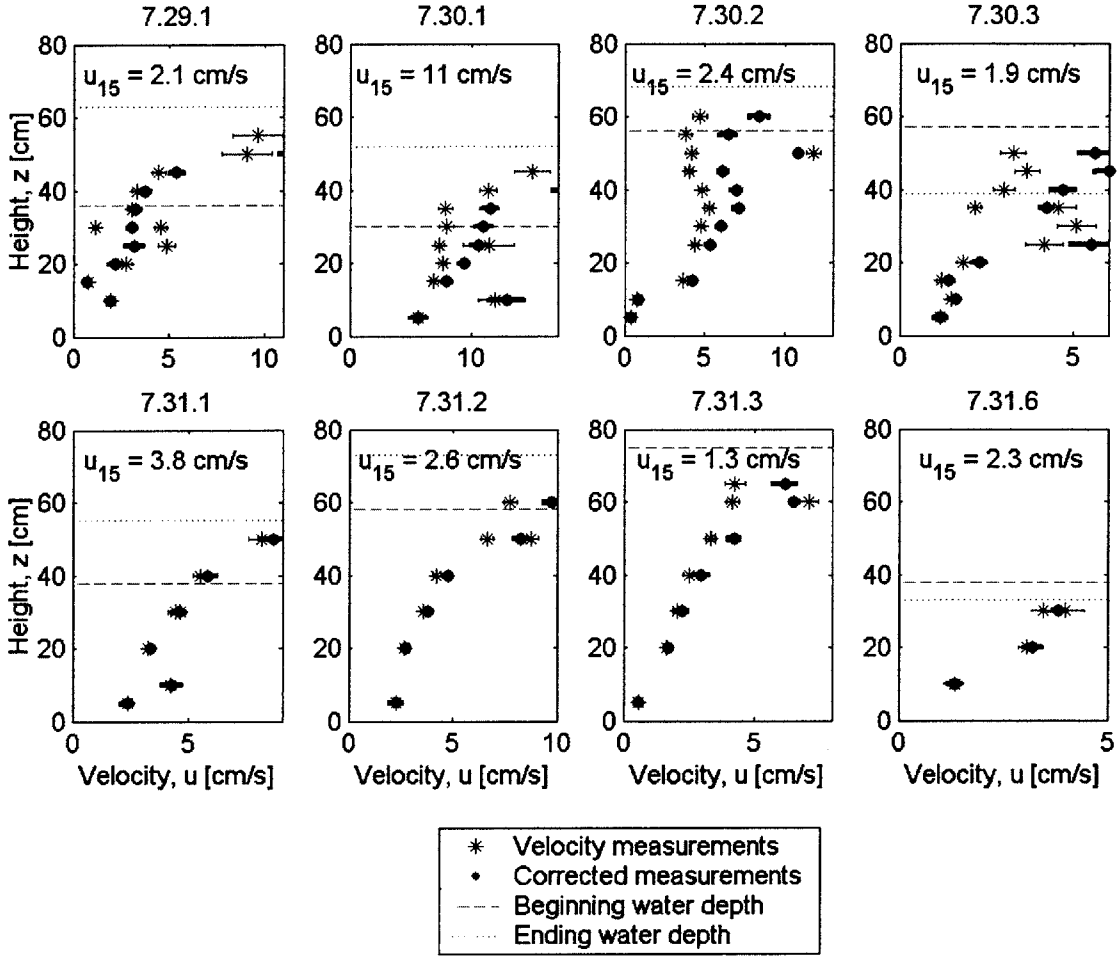
7.29.1
u_{15} = 2.1 cm/s
7.30.1
u_{15} = 11 cm/s
7.30.2
u_{15} = 2.4 cm/s
7.30.3
u_{15} = 1.9 cm/s
7.31.1
u_{15} = 3.8 cm/s
7.31.2
u_{15} = 2.6 cm/s
7.31.3
u_{15} = 1.3 cm/s
7.31.6
u_{15} = 2.3 cm/s
Height, z [cm]
Velocity, u [cm/s]
Velocity measurements
Corrected measurements
Beginning water depth
Ending water depth

Appendix B. Average nondimensional concentration curves for slug releases in the laboratory and field. Concentration recorded by a fluorometer as a function of time at various locations downstream of slug dye releases in the laboratory at the junction between two different vegetation different densities at a mean flow speed of approximately 1 cm/s. Concentration is nondimensionalized by the total mass recovered, M_0; time is nondimensionalized by the average travel time, $t_{avg} = M_1/M_0$. Each curve is the average of several individual records, aligned by their centers of mass; the number of records used to construct each average is indicated on each plot. (a)-(i) Field releases. (j)-(q) Laboratory releases at 10 cm from the bed with an observed velocity of 0.8 cm/s. (r)-(v) Laboratory releases at 10 cm from the bed with an observed velocity of 2.0 cm/s. (w)-(aa) Laboratory releases at 10 cm from the bed with an observed velocity of 3.0 cm/s. (ab)-(af) Laboratory releases at 10 cm from the bed with an observed velocity of 4.1 cm/s. (ag)-(aj) Laboratory releases at 4 from the bed with an observed velocity of 0.8 cm/s. (ak)-(an) Laboratory releases at 16 cm from the bed with an observed velocity of 0.8 cm/s.

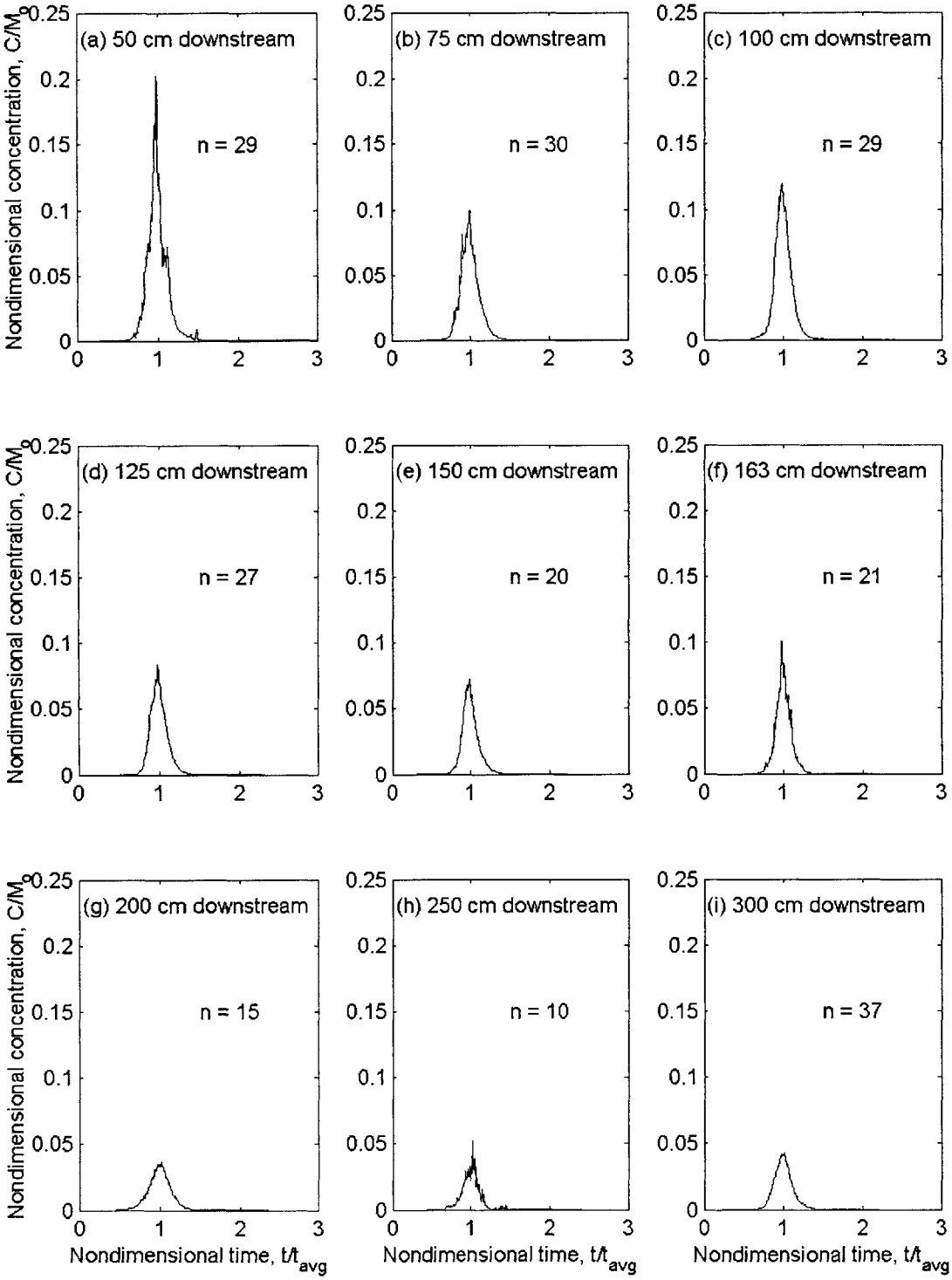
(a) 50 cm downstream
n = 29
(b) 75 cm downstream
n = 30
(c) 100 cm downstream
n = 29
(d) 125 cm downstream
n = 27
(e) 150 cm downstream
n = 20
(f) 163 cm downstream
n = 21
(g) 200 cm downstream
n = 15
(h) 250 cm downstream
n = 10
(i) 300 cm downstream
n = 37
Nondimensional concentration, C/M0
Nondimensional time, t/tavg
0
0.05
0.1
0.15
0.2
0.25
1
2
3

Appendix B (cont.): Laboratory measurements, 0.8 cm/s flow

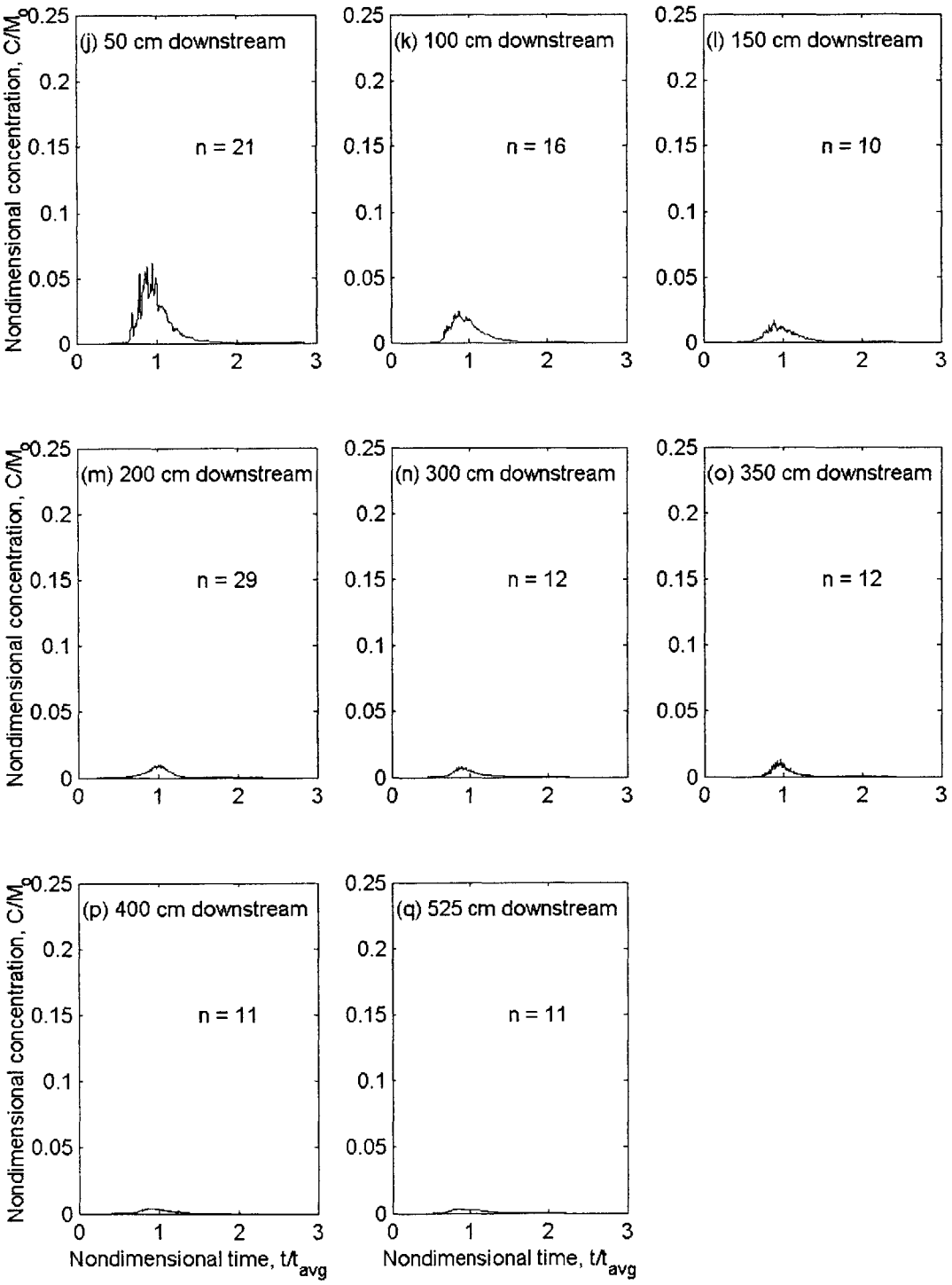

Appendix B (cont.): Laboratory measurements, 2 cm/s flow

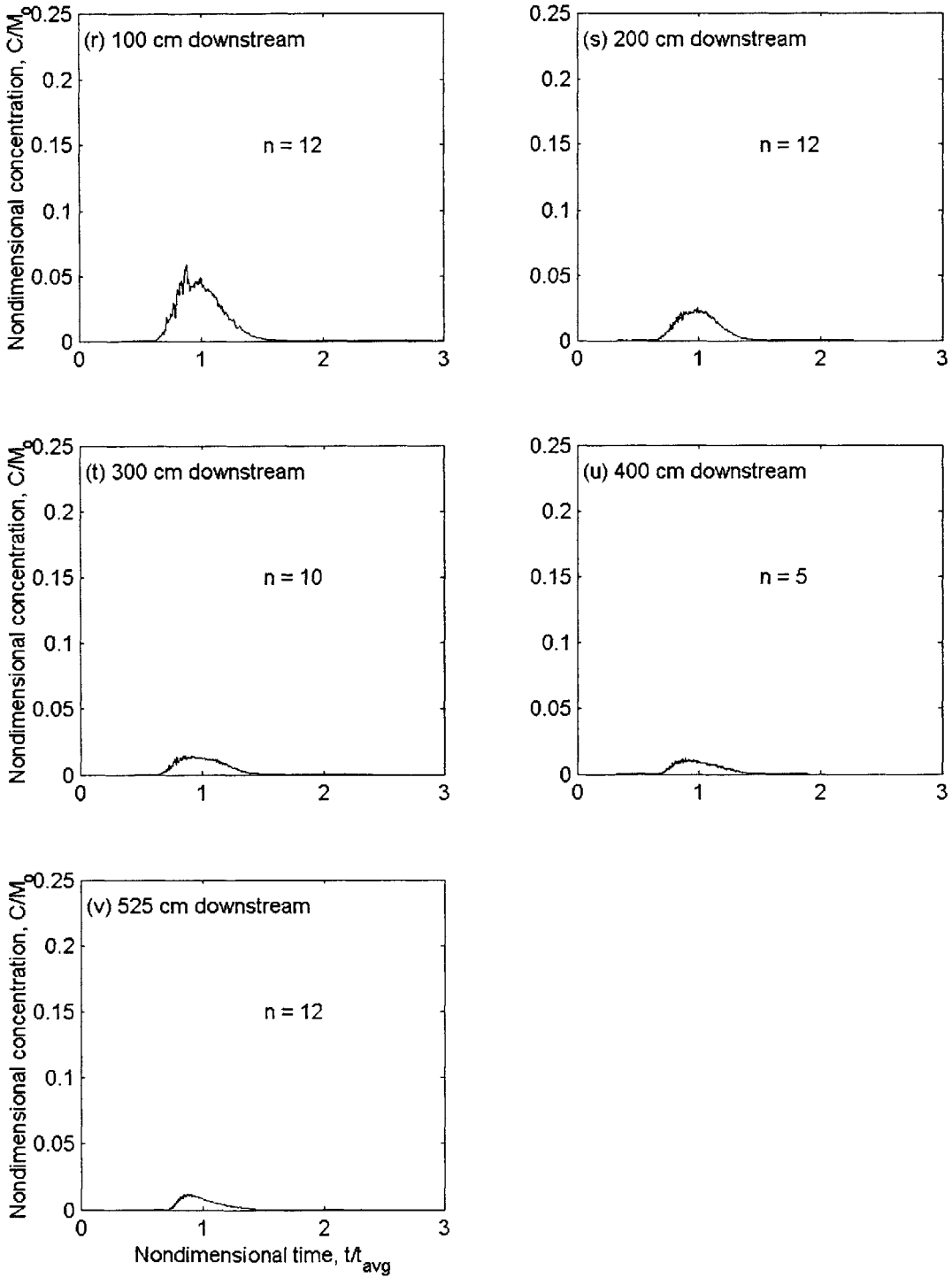

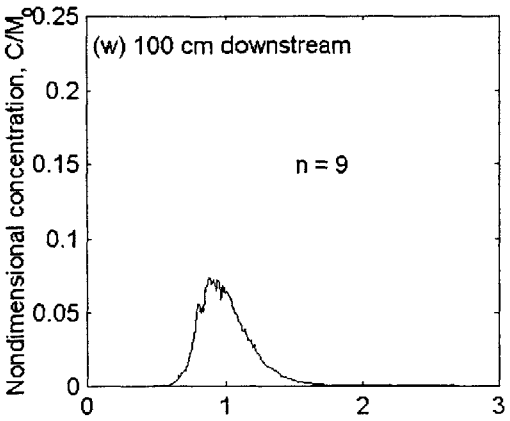
(w) 100 cm downstream
n = 9
Nondimensional concentration, C/M
0.25
0.2
0.15
0.1
0.05
0
0
1
2
3

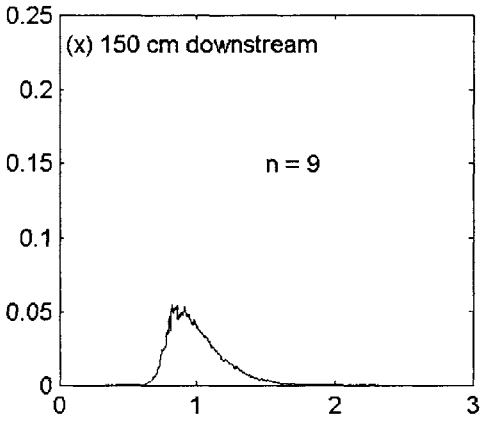
(x) 150 cm downstream
n = 9
0.25
0.2
0.15
0.1
0.05
0
0
1
2
3

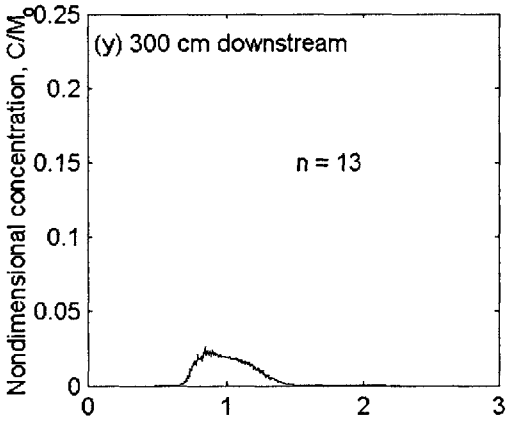
(y) 300 cm downstream
n = 13
Nondimensional concentration, C/M
0.25
0.2
0.15
0.1
0.05
0
0
1
2
3

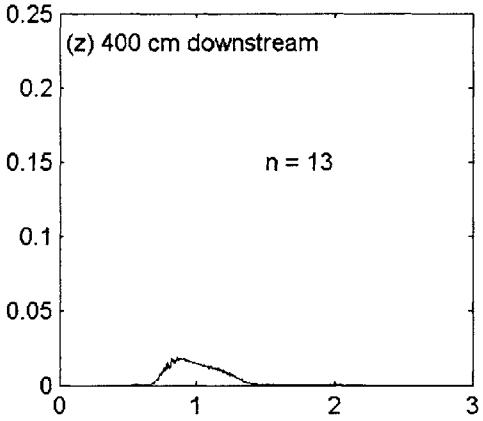
(z) 400 cm downstream
n = 13
0.25
0.2
0.15
0.1
0.05
0
0
1
2
3

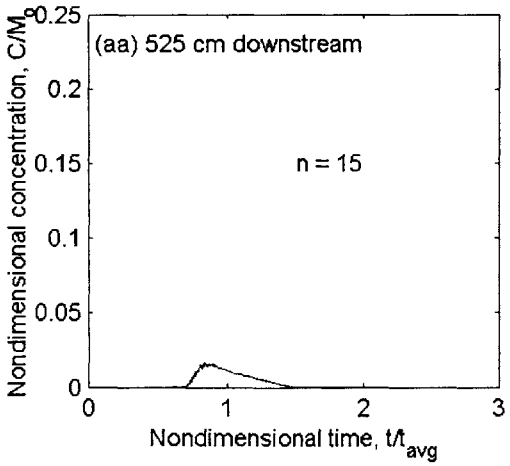
(aa) 525 cm downstream
n = 15
Nondimensional concentration, C/M
0.25
0.2
0.15
0.1
0.05
0
0
1
2
3
Nondimensional time, t/t avg

Appendix B (cont.): Laboratory measurements, 4.1 cm/s flow

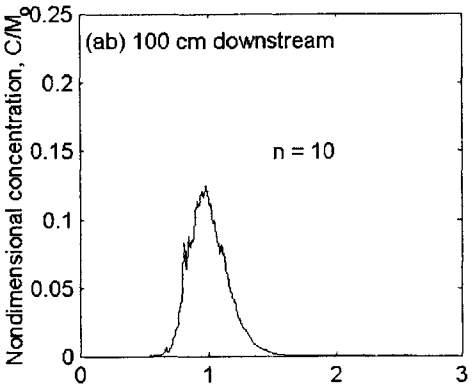

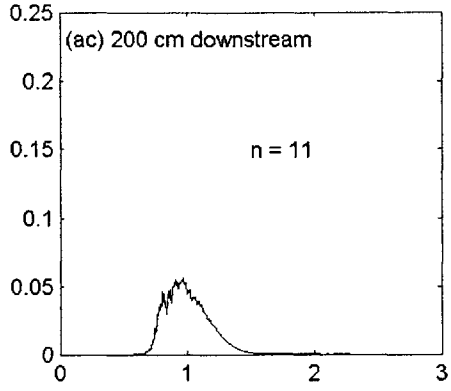

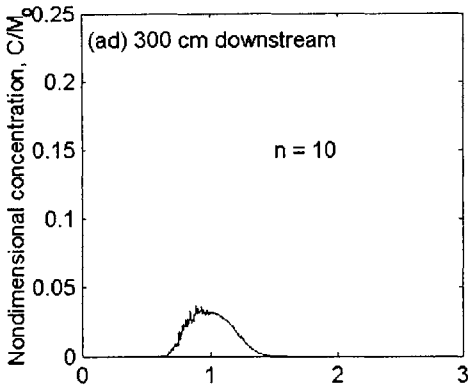

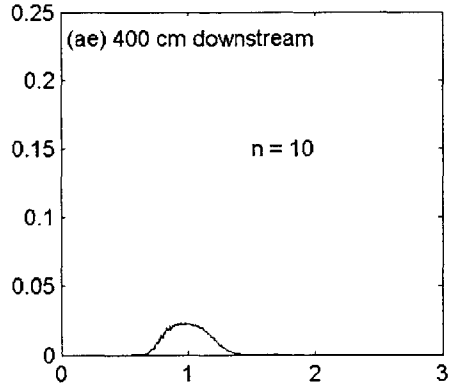

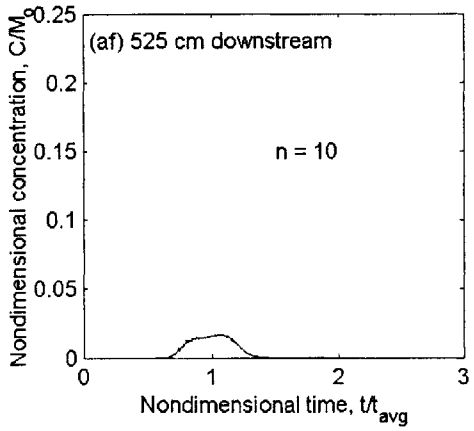

Appendix B (cont.): Laboratory measurements, 0.8 cm/s flow, release at 4 cm from the bed

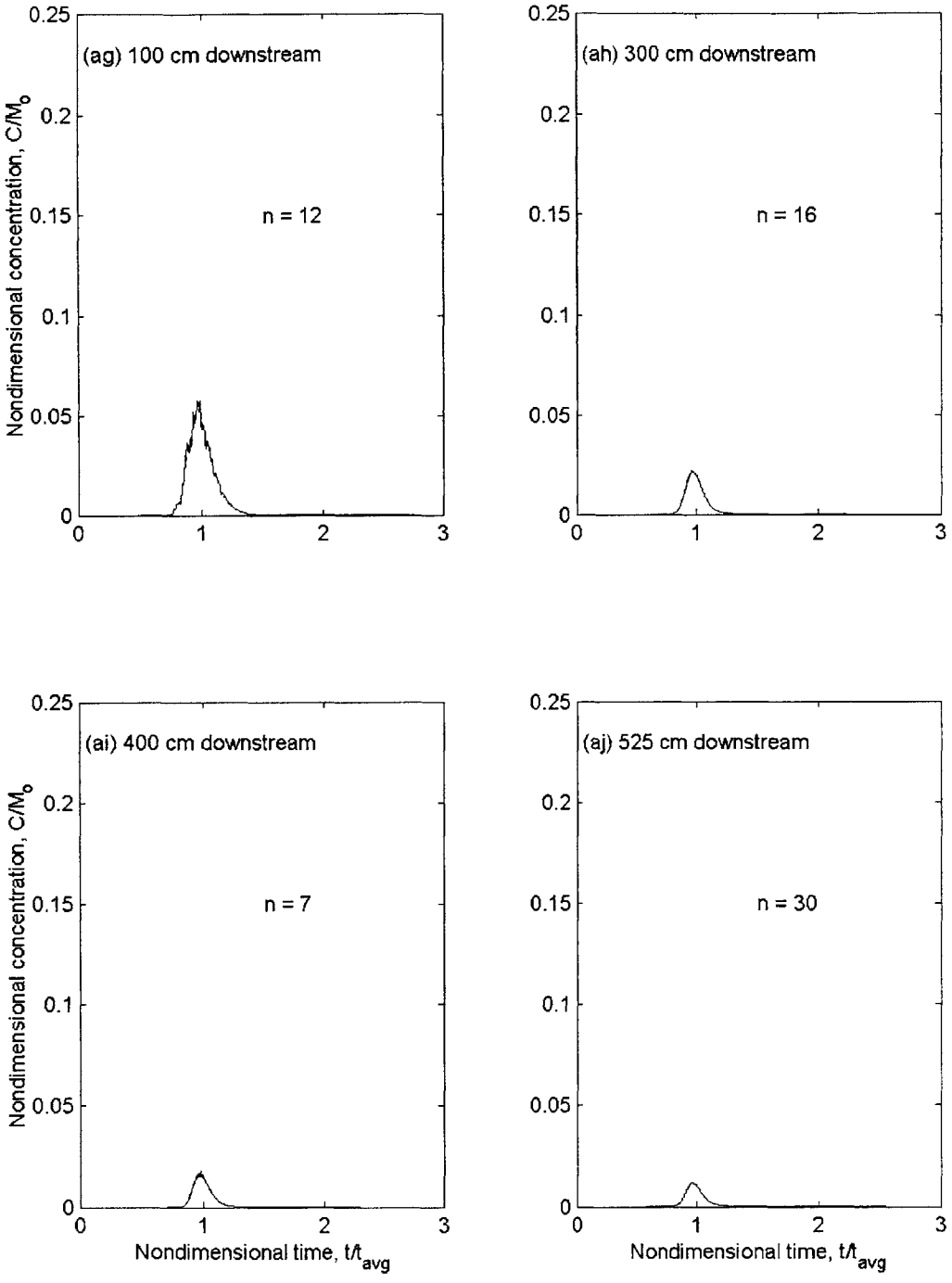

Appendix B (cont.): Laboratory measurements, 0.8 cm/s flow, release at 16 cm from the bed